AD-A089 296 PRATT AND WHITNEY AIRCRAFT GROUP WEST PALM BEACH FL G--ETC F/G 11/6
EVALUATION OF CRACK GROWTH IN ADVANCED P/M ALLOYS.(U)
MAR 80 D L SIMS, F K HAAKE F33615-77-C-5093
UNCLASSIFIED PWA-FR-12126 AFML-TR-79-4160 NL

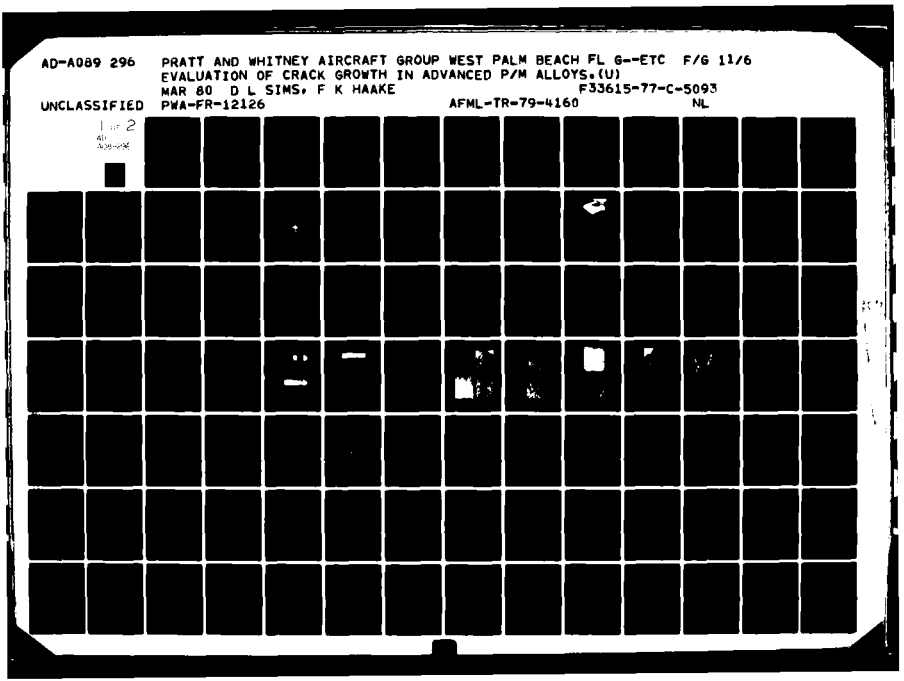

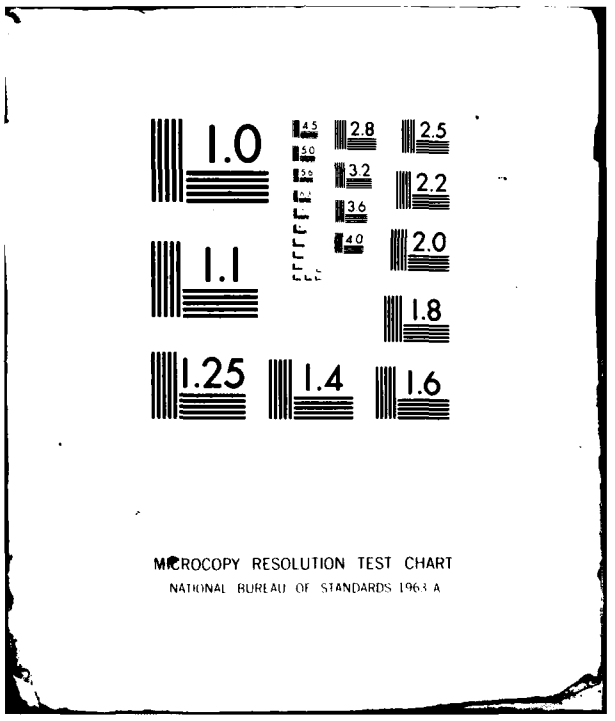
1.0
1.1
1.25
1.4
1.6
1.8
2.0
2.2
2.5
2.8
3.2
3.6
4.0
4.5
5.0
MICROCOPY RESOLUTION TEST CHART
NATIONAL BUREAU OF STANDARDS 1963 A

AFML-TR-79-4160

EVALUATION OF CRACK GROWTH IN ADVANCED P/M ALLOYS

David L. Sims, F. Konrad Haake
Pratt & Whitney Aircraft Group
Government Products Division
Box 2691, West Palm Beach, Florida 33402

March 1980

Technical Report AFML-TR-79-4160
for Period 1 September 1977 through 30 June 1979

Approved for public release; distribution unlimited

AIR FORCE MATERIALS LABORATORY
AIR FORCE WRIGHT AERONAUTICAL LABORATORIES
AIR FORCE SYSTEMS COMMAND
WRIGHT-PATTERSON AIR FORCE BASE, OHIO 45433

NOTICE

When Government drawings, specifications, or other data are used for any purpose other than in connection with a definitely related Government procurement operation, the United States Government thereby incurs no responsibility nor any obligation whatsoever; and the fact that the government may have formulated, furnished, or in any way supplied the said drawings, specifications, or other data, is not to be regarded by implication or otherwise as in any manner licensing the holder or any other person or corporation, or conveying any rights or permission to manufacture, use, or sell any patented invention that may in any way be related thereto.

This report has been reviewed by the Information Office (IO) and is releasable to the National Technical Information Service (NTIS). At NTIS, it will be available to the general public, including foreign nations.

This technical report has been reviewed and is approved for publication.

W. REIMANN, Project Engineer
Metals Behavior Branch
Metals and Ceramics Division

NATHAN G. TEPPER, Chief
Metals Behavior Branch
Metals and Ceramics Division

If your address has changed, if you wish to be removed from our mailing list, or if the addressee is no longer employed by your organization please notify, AFWAL/MLLN, W-PAFB, OH 45433 to help us maintain a current mailing list.

Copies of this report should not be returned unless return is required by security considerations, contractual obligations, or notice on a specific document.

AIR FORCE/56780/26 August 1980 — 430

UNCLASSIFIED

SECURITY CLASSIFICATION OF THIS PAGE (When Data Entered)

REPORT DOCUMENTATION PAGE

READ INSTRUCTIONS BEFORE COMPLETING FORM

1. REPORT NUMBER: AFML-TR-79-4160	2. GOVT ACCESSION NO.: AD-A089296
3. RECIPIENT'S CATALOG NUMBER:	
4. TITLE (and Subtitle): EVALUATION OF CRACK GROWTH IN ADVANCED P/M ALLOYS	5. TYPE OF REPORT & PERIOD COVERED: Final Report, 1 Sept 1977-30 June 1979
6. PERFORMING ORG. REPORT NUMBER: PWA-FR-12126	
7. AUTHOR(s): David L. Sims F. Konrad Haake	8. CONTRACT OR GRANT NUMBER(s): F33615-77-C-5093
9. PERFORMING ORGANIZATION NAME AND ADDRESS: Pratt & Whitney Aircraft Group, Government Products Division, P. O. Box 2691, West Palm Beach, Florida 33402	10. PROGRAM ELEMENT, PROJECT, TASK AREA & WORK UNIT NUMBERS: Project 2420 01 04
11. CONTROLLING OFFICE NAME AND ADDRESS: Air Force Materials Laboratory, AFSC Aeronautics Systems Division, Wright-Patterson AFB, Ohio 45433	12. REPORT DATE: March 1980 13. NUMBER OF PAGES: 97
14. MONITORING AGENCY NAME & ADDRESS (if different from Controlling Office)	15. SECURITY CLASS. (of this report): Unclassified 15a. DECLASSIFICATION/DOWNGRADING SCHEDULE

16. DISTRIBUTION STATEMENT (of this Report)

Approved for public release; distribution unlimited.

17. DISTRIBUTION STATEMENT (of the abstract entered in Block 20, if different from Report)

18. SUPPLEMENTARY NOTES

19. KEY WORDS (Continue on reverse side if necessary and identify by block number)

Fatigue, Crack Propagation, Hyperbolic Sine Model, AF2-1DA, P/M Alloys

20. ABSTRACT (Continue on reverse side if necessary and identify by block number)

This program evaluates the crack growth characteristics of the advanced P/M alloy AF2-1DA. An interpolative model, developed in an earlier program (Reference AFML-TR-76-176, Part I), based on the hyperbolic sine equation:

$$\log (da/dN) = C_1 \sinh (C_2(\log(\Delta K) + C_3)) + C_4$$

DD FORM 1 JAN 73 1473 EDITION OF 1 NOV 65 IS OBSOLETE

UNCLASSIFIED

SECURITY CLASSIFICATION OF THIS PAGE (When Data Entered)

392887

is used to describe crack growth properties at various conditions. Results are presented, including applicability of linear elastic fracture mechanics (LEFM) and the effects of frequency, stress ratio, and temperature on crack propagation rates.

FOREWORD

This report is submitted in accordance with the requirements of Contract F33615-77-C-5093 and represents the final technical report covering the period of 1 September 1977 to 30 June 1979. The program was conducted under the cognizance of M. C. Van Wanderham, General Supervisor of the Mechanics of Materials and Structures section of the Material Engineering and Technology Department at the Pratt & Whitney Aircraft Group, Government Products Division (P&WA/Florida). Capt. J. Hyzak, AFML/LLN, was the Air Force Project Engineer, and D. L. Sims the P&WA program manager and principal investigator.

The author gratefully acknowledges the technical contributions of several individuals in the Material Engineering and Technology Department whose support was vital to this program: C. G. Annis (Group Leader of the Experimental Life Analysis Group), B. A. Cowles, J. M. Larsen, B. J. Schwartz, and V. De La Torre contributed significantly to the program effort.

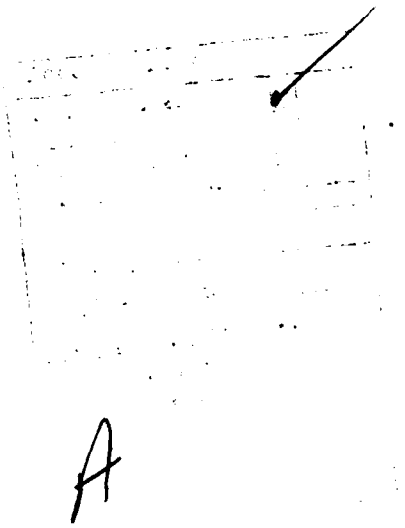

TABLE OF CONTENTS

LIST OF ILLUSTRATIONS

LIST OF ILLUSTRATIONS (Continued)

LIST OF ILLUSTRATIONS (Continued)

LIST OF ILLUSTRATIONS (Continued)

SUMMARY

This final report for Contract F33615-77-C-5093 summarizes the work performed during the period 1 September 1977 to 30 June 1979.

The fatigue crack growth behavior of an advanced powder metallurgy (P/M) superalloy (AF2-1DA) was characterized, and an interpolative mathematical model was put into computer code to permit accurate predictions of crack propagation rates under different stress-temperature-time conditions. The Interpolative Hyperbolic Sine Model (References 1, 2 and 3) having the general equation

$$\log (da/dN) = C_1 \sinh (C_2(\log (\Delta K) + C_3)) + C_4 \quad (1)$$

was the basis for model development.

Interpolative crack growth rate models are presented showing the effects of frequency, stress ratio, temperature, and dwell time at maximum tensile stress. The effect of specimen thickness on crack growth rates is also shown.

Verification testing to check the model demonstrated the model's capability of predicting crack growth rates where no data exist. Crack growth rates, calculated using the interpolative model before testing, were used to predict specimen cyclic lives. The results of these predictions (Figures 70 through 75) show that the interpolative hyperbolic sine (SINH) model accurately predicts crack propagation life of AF2-1DA at elevated temperatures.

SECTION I

INTRODUCTION

The presence of a crack in a stressed component necessitates redistribution of stresses around the crack. The stress intensity factor is a parameter that reflects this redistribution and is a function of nominal stress, flaw size, and specimen and crack geometries. The concept of stress intensity factor was originally defined for an infinitely sharp crack in a perfectly elastic medium. In most engineering materials, localized plastic deformation occurs due to high stresses at the crack tip, and it is this deformation that gives the material resistance to crack propagation. In a completely brittle material, crack tip stress relaxation is so small that simple reinitiation of a stopped crack is sufficient to promote complete fracture.

The degree of brittleness of a material (and the limit to the applicability of linear elastic fracture mechanics) is directly related to the type of relaxation process that occurs at the crack tip. In the high temperature fatigue process, this relaxation is expected to depend on the relative degree of elastic, plastic, creep, and chemical work expended at the crack tip. In this program, linear elastic fracture mechanics is investigated only to the extent required to determine specimen thickness needed for thickness-independent data. This is adequate because only the compact specimen is being used and anomalies associated with high net section stresses and geometric variations are avoided.

The technical approach of this program consists of (1) isolation, testing and modeling the effects of stress, time and temperature on the crack growth rate of the advanced P/M superalloy AF2-1DA; (2) synthesis and testing of models that accurately reflect parametric interactions; and (3) demonstration of the models for a simple crack geometry subjected to a typical stress-time-temperature history.

The technical program consists of four phases: The first phase determines the effect of specimen thickness on crack growth rates for AF2-1DA material and characterizes the effects of stress ratio, cyclic frequency, and temperature. Phase II consists of generalized interpolative model development based on the hyperbolic sine equation

$$\log (da/dN) = C_1 \sinh (C_2 (\log (\Delta K) + C_3)) + C_4 \quad (1)$$

and Phase III provides for demonstration of the predictive model. Phase IV encompasses the reporting requirements.

SECTION II

TECHNICAL PROGRESS

MATERIAL PROCUREMENT

This program examined the crack growth behavior of an advanced powder metallurgy (P/M) superalloy, AF2-1DA. This alloy was developed as a turbine disk material for use at 1400°F, a temperature at which time dependent deformation is a major concern. The material was processed by the GATORIZING® technique of superplastic forming, creating the microstructure of a typical disk forging. All testing was performed on a single heat of material. Low-cycle fatigue (LCF), creep, tensile, and combination stress rupture tests were performed to qualify the material. The specimens are shown in Figures 1 through 4.

The first forging developed a maze of cracks during heat treatment to AMS 5881. It was determined that this specification contained an error in the heat treatment procedure. The solution heat treatment calls for an oil quench and it should require rapid air cooling. The material used in this program was heat-treated by taking exception to AMS 5881 and the microstructure compared favorably to a good full-scale component forging, an F100 3rd-stage turbine disk (S/N 455-B2) developed under AFML Contract F33615-74-C-5108. Figure 5 shows the structures to be identical in all important respects. Comparison of the size and distribution of γ' reveals that the heat treatment developed under AFML Contract F33615-74-C-5108 (reference 4) was duplicated. The grain sizes of the components were also similar, ranging from ASTM 0 to 3, predominantly 0 and 1.

The qualification testing for the three forgings is summarized in Table 1. AMS 5881 requires the stress rupture *specimen* to rupture in not less than 23.0 hr, but the test specimen lasted between 15.7 and 19.3 hr (except for the first BAUD-3 specimen that failed early in the notch). Out of six disks tested for AFML Contract F33615-74-C-5108, on*ly one* would have met the AMS 5881 stress rupture requirements for time to rupture. Data from the six disks show an average stress-rupture life of 18.9 hr and a 97.5% lower bound of 11.5 hr based on 12 data points and an assumed log-normal distribution of life. Tests performed on the AF2-1DA forgings resulted in stress-rupture lives near the 18.9 hr mean life. This indicates material behavior similar to the results reported in the referenced contract.

The tensile properties recommended in AFML-TR-76-101 are also reduced from AMS 5881. Table I summarizes the tensile requirements of both specifications in addition to the test results.

Four (4) isothermal, axial strain-controlled LCF tests were performed to provide a comparison of the LCF capability of the forging used for test material in this program with previously tested AF2-1DA. All tests were conducted at 760°C (1400°F) at a cyclic frequency of 0.17 Hz (10 cpm) using a sawtooth strain vs time waveform. The strain cycle was all tensile such that the mean strain was equal to one-half the maximum strain ($R_\epsilon = 0$).

The AF2-1DA material used in this program exhibited LCF lives comparable to previously tested AF2-1DA. The test results are presented in Table 2 and plotted in Figure 6 for comparison. The total strain range, elastic and inelastic strain components, stress range, and mean stress were determined at specimen half-life ($N_f/2$) and are presented in Table 2. All four specimens exhibited stable cyclic stress-strain behavior. Failure origins for specimens tested at the higher total strain ranges (1.1% and 0.9%) were surface connected; the failure origin in the specimen tested at 0.82% strain range was subsurface and at a probable nonmetallic inclusion. The test specimen cycled at 0.6% total strain range was discontinued after 182,000 cycles with no indications of failure.

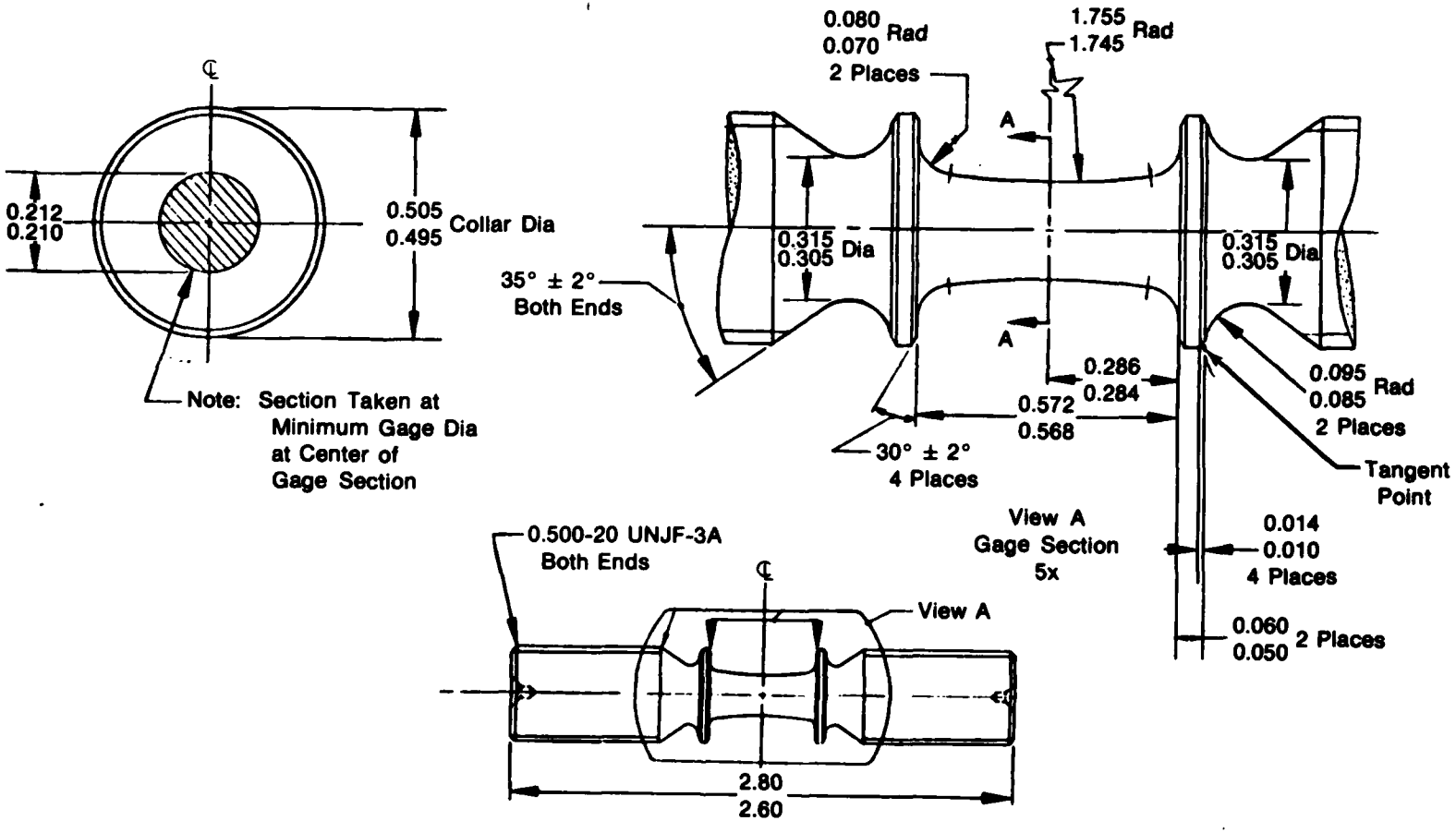

Figure 1. Strain-Controlled Low-Cycle Fatigue Specimen

FD 139896

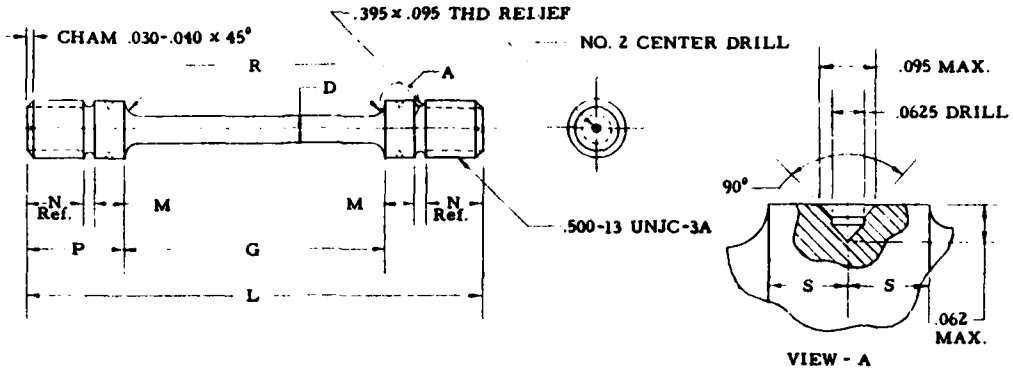

DRILL & C'SK 2 HOLES 180° APART BOTH ENDS

RADIAL ALIGNMENT ± 00°30'
AXIAL ALIGNMENT ± .0015

NOTES

1. All dim. in inches
2. Tolerances ± .010 unless noted.
3. All dia. to be conc. to within .0005 F.I.R.
4. Reduced section to be 16 ± 3 microinch AA grind finish using 320 grit wheel. NOT TO BE POLISHED.
5. Identification markings permitted only on specimen ends.

SPEC. NO.	±.0005 D	G	L	M	N	P	R	S
1	.252	2.250	3.940	.250	.500	.845	.125	.125
2*	.178	1.062	2.375	.187	.375	.657	.156	.093

*NON-STANDARD SPECIMEN

FD 158145

Figure 2. Creep Specimen

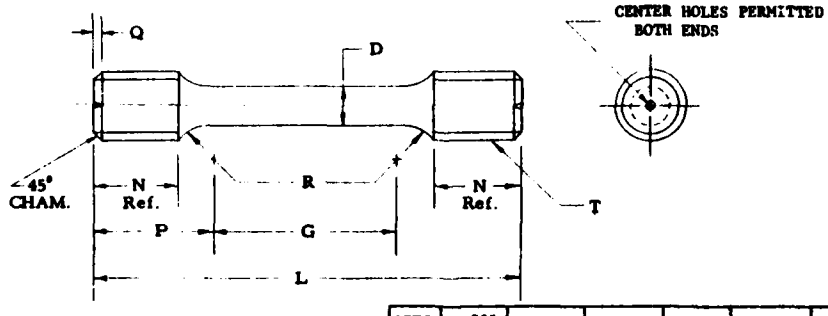

NOTES

1. All dim. in inches.
2. Tolerances ± .010 unless noted.
3. All dia. to be conc. to within .001 F.I.R.
4. Reduced section to be 16 ± 3 μinch AA grind finish using 320 grit wheel.
5. Dia. of reduced section to be slightly smaller at center than at ends (approx. .0015), but not to exceed 1% of larger dia.
6. Identification markings permitted only on specimen ends.

SPEC NO.	±.001 D	G	L	N	P	Q	R	T
1	.095	0.562	1.000	.156	0.219	.025	.062	8 -32 UNJC-3A
2	.095	1.062	2.000	.375	0.469	.035	.125	10 -32 UNJF-3A
3	.125	1.062	2.000	.375	0.469	.035	.125	.250 -28 UNJF-3A
4	.188	1.062	2.000	.375	0.469	.035	.175	.375 -16 UNJC-3A
5	.188	1.062	2.375	.500	0.656	.045	.190	.375 -16 UNJC-3A
6*	.252	1.062	2.750	.625	0.844	.055	.250	.500 -13 UNJC-3A
7	.313	1.562	3.500	.750	0.969	.055	.325	.500 -13 UNJC-3A
8	.375	1.812	3.812	.750	1.000	.065	.375	.5625-12 UNJC-3A
9	.438	2.062	4.125	.750	1.031	.065	.450	.625 -11 UNJC-3A
10	.500	2.062	4.500	.812	1.219	.075	.500	.750 -10 UNJC-3A

*MDL Preferred Standard Specimen

FD 158146

Figure 3. Tensile Specimen

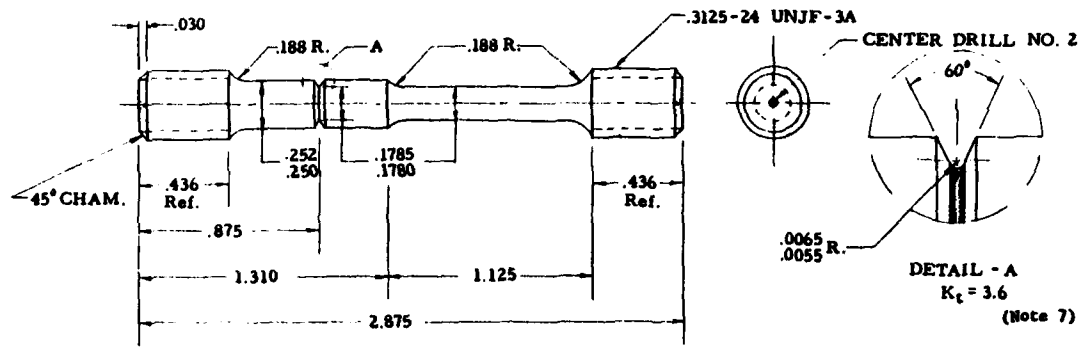

NOTES:

1. All dimensions in inches.
2. Tolerances ± .010 unless noted.
3. All dia. to be conc. to within .0005 F.I.R.
4. Reduced section to be 16 ± 3 microinch AA grind finish (notch 8 ± 3) using 320 grit wheel.
5. Ends to be square with center line and parallel to each other to within .0005.
6. Identification markings permitted only on specimen ends.
7. K_t per Peterson, "Stress Concentration Factors".

FD 158147

Figure 4. Combination Stress Rupture Specimen

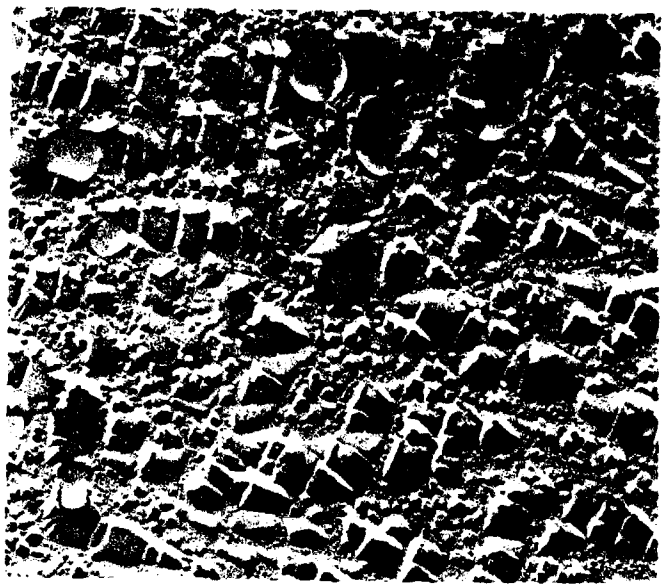

Mag: 10,000X

A. Microstructure of AF2-1DA Pancake

Mag: 10,000X

B. Microstructure of F100 3rd-Stage Turbine Disk Developed Under AFML Contract F33615-74-C-5108

FD 158101

Figure 5. Comparison of AF2-1DA Pancake Microstructure to the Microstructure of F100 3rd-Stage Turbine Disk from AFML Contract F33615-74-C-5108

TABLE 1.
QUALIFICATION TEST RESULTS

Tensile Properties

	Temp. (°C)	0.2% Y.S. (MPa)	Tensile Strength (MPa)	El %	Ra %
AMS 5881†	R.T.	965	1310	10.0	12.0
AFML-TR-76-101†	R.T.	931	1310	10.0	12.0
BAUD-3	R.T.	981	1517	14.5	15.6
BAUD-4	R.T.	960	1480	14.5	16.3
BAUD-5	R.T.	983	1488	16.0	17.5
AMS 5881†	816	862	1034	10.0	12.0
AFML-TR-76-101†	816	1000	827	10.0	12.0
BAUD-3	816	861	985	20.0	28.7
BAUD-4	816	907	1056	18.0	29.0
BAUD-5	816	848	994	19.0	24.4

Creep Properties

Heat Code	Temp. (°C)	Stress (MPa)	Rupture Time (Hours)	Hours To Creep 0.1%	Hours To Creep 0.2%	% at 100 Hrs
BAUD-3	760	483	>100	12.0	55.6	.312
BAUD-4	760	483	>100	53.0	68.7	.273
BAUD-5	760	483	>100	31.6	90.6	.215

Stress Rupture Properties

Heat Code	Temp. (°C)	Stress (MPa)	Rupture Time (Hours)	El %	RA %
BAUD-3	816	552	9.0*	—	—
BAUD-3	816	552	15.7	8.1	12.4
BAUD-3	816	552	19.3	7.7	11.6
BAUD-4	816	552	17.5	7.6	10.8
BAUD-5	816	552	16.5	6.9	8.0

†Requirements of this specification

* Failed in notch after 9.0 hr, continued to test smooth section with failure after 19.4 hr.

TABLE 2.

AXIAL CONTROLLED STRAIN LOW-CYCLE FATIGUE RESULTS OF AF2-1DA TESTED IN AIR 760°C (1400°F), 0.17 Hz (10 cpm), R_ϵ = 0.

Spec. S/N	Strain (m/m at $N_f/2$) Range	Elastic	Inelastic	Creep	Mean Stress at $N_f/2$	Stress Range Cycle 1	Stress Range $N_f/2$	Cyclic Stability	Cycles To Failure N_f
1*	0.0112	0.0106	0.0006	0	119 MPa (17.3 ksi)	1737 MPa (252.0 ksi)	1726 MPa (250.4 ksi)	Stable	1,037
2*	0.0090	0.0088	0.0002	0	148 MPa (21.4 ksi)	1476 MPa (214.1 ksi)	1442 MPa (209.2 ksi)	Stable	5,282
3**	0.0082	0.0081	0.0001	0	267 MPa (38.7 ksi)	1306 MPa (189.4 ksi)	1317 MPa (191.0 ksi)	Stable	6,623
4***	0.0060	0.0060	<0.0001	0	108 MPa (15.7 ksi)	988 MPa (143.3 ksi)	966 MPa (140.1 ksi)	Stable	182,460

*Surface origin.
**Origin approximately 0.4 mm from specimen surface at possible inclusion.
***Test discontinued. Did not fail.

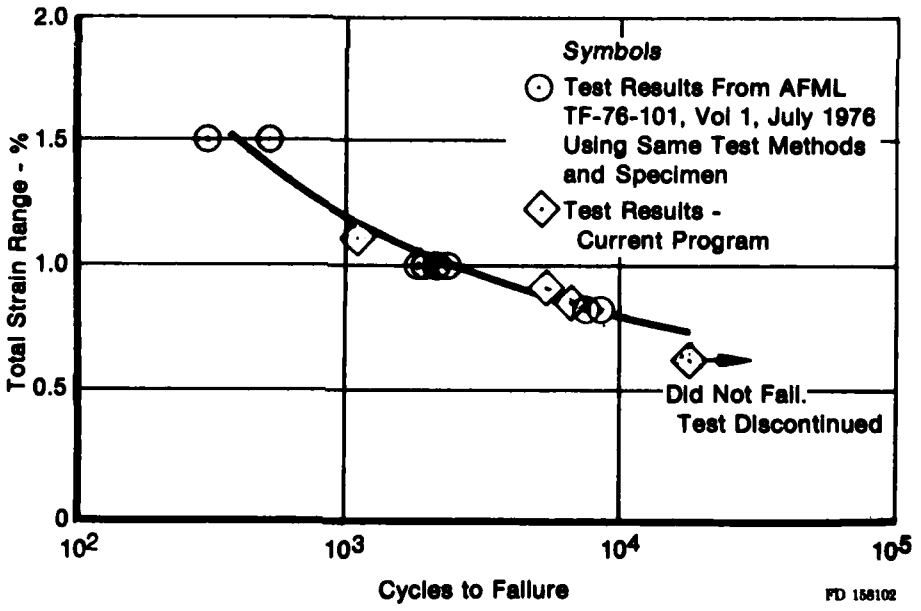

Figure 6. Axial Controlled Strain Low-Cycle Fatigue Crack Initiation Results for AF2-1DA Tested in Air at 760°C (1400°F), 0.17 Hz (10 cpm), R_ϵ = 0

Figure 7 compares the results of a 12.7 mm (0.500 in.) thick compact specimen tested at 650°C (1200°F), R = 0.1, 10 cpm with data from previous experience. The excellent agreement of the data with previous experience removes all doubt as to whether this heat of material is typical of other AF2-1DA material.

TEST SPECIMEN AND PROCEDURES

Figure 8 shows the compact specimen used to obtain crack propagation data. Testing was conducted on servohydraulic, closed-loop, load-controlled testing machines. Specimens were precracked using procedures outlined in ASTM E-399. Crack lengths were measured directly with a Gaertner traveling microscope without cooling the specimen. The intervals between crack growth measurements were selected to obtain crack growth increments of approximately 0.5 mm (0.02 in.), which normally results in an average of 40 to 50 readings per specimen. The crack propagation tests were conducted with a triangular loading wave form or a triangle wave with a hold time at the tensile peak with all portions of the cycle under tensile load-controlled conditions. Table 3 lists all crack propagation test specimens for AF2-1DA.

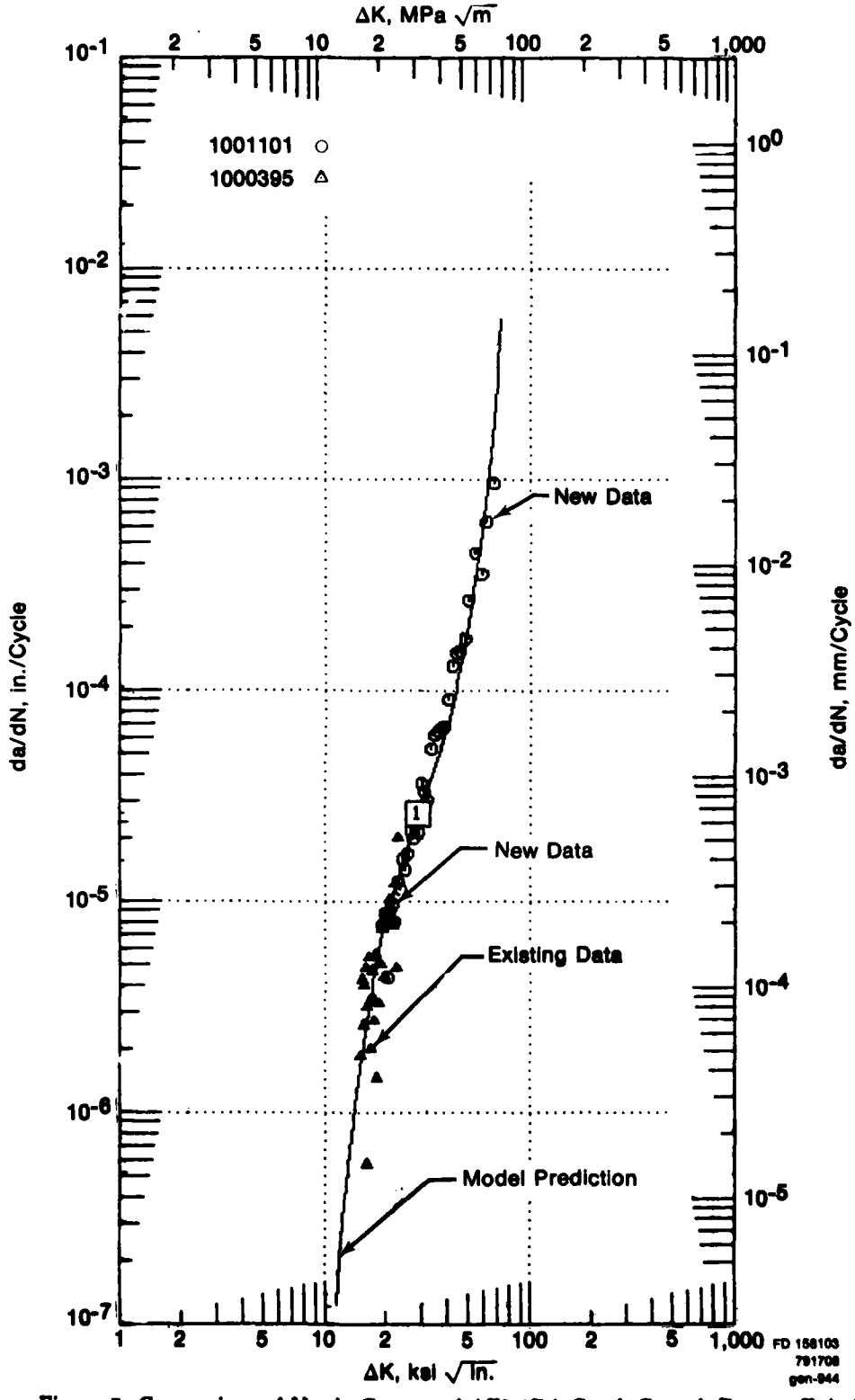

Figure 7 Comparison of Newly Generated AF2-1DA Crack Growth Data to Existing Data for 10 cpm, R = 0.1, 650°C (1200°F)

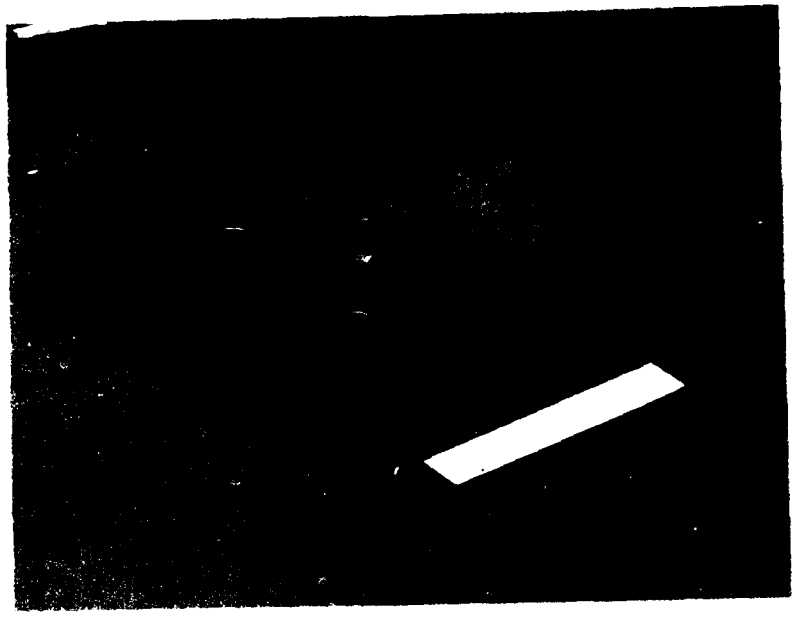

(a)

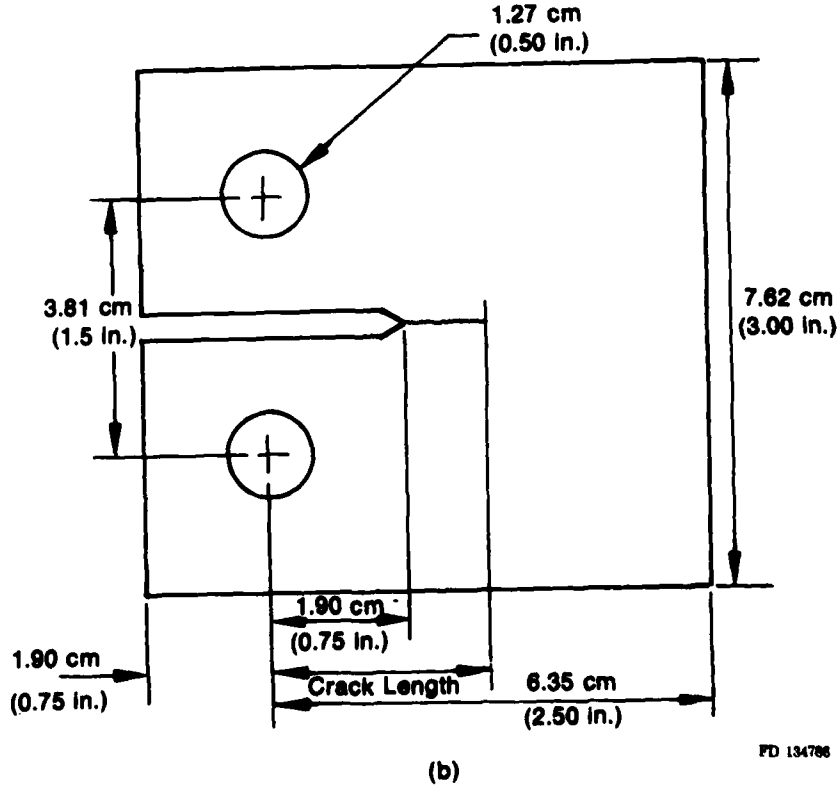

(b)

Figure 8. Compact Specimen

TABLE 3.
CRACK PROPAGATION TEST SPECIMENS FOR AF2-1DA

Specimen Number	Temperature (°C)	Temperature (°F)	Cyclic Frequency	Stress Ratio	Thickness (in.)	Remarks
1101	649	1200	0.17 Hz (10 cpm)	0.10	0.500	
1102	427	800	0.17 Hz (10 cpm)	0.10	0.503	
1103	649	1200	120 Sec. Dwell	0.10	0.502	
1104	649	1200	0.0083 Hz (0.5 cpm)	0.10	0.500	
1106	649	1200	0.17 Hz (10 cpm)	0.50	0.468	
1107	427	800	0.0083 Hz (0.5 cpm)	0.10	0.500	No data
1108	649	1200	120 Sec. Dwell	0.10	0.500	No data
1109	427	800	20 Hz	0.10	0.487	
1110	760	1400	0.0083 Hz (0.5 cpm)	0.10	0.501	Overstress failure
1111	760	1400	120 Sec. Dwell	0.10	0.501	
1112	427	800	0.17 Hz (10 cpm)	0.50	0.250	
1114	760	1400	600 Sec. Dwell	0.10	0.498	Excessive Curvature
1115	649	1200	0.0083 Hz (0.5 cpm)	0.50	0.500	
1117	760	1400	120 Sec. Dwell	0.10	0.124	Equipment
1118	649	1200	0.17 Hz (10 cpm)	0.10	0.125	
1119	427	800	0.17 Hz (10 cpm)	0.10	0.124	Equipment Failure
1120	427	800	0.17 Hz (10 cpm)	0.10	0.250	
1122	760	1400	120 Sec. Dwell	0.10	0.124	
1124	649	1200	600 Sec. Dwell	0.10	0.452	
1125	649	1200	20 Hz	0.10	0.249	
1126	649	1200	0.17 Hz (10 cpm)	0.10	0.249	
1128	649	1200	120 Sec. Dwell	0.10	0.130	
1129	760	1400	0.17 Hz (10 cpm)	0.10	0.124	
1130	649	1200	120 Sec. Dwell	0.10	0.254	
1131	427	800	0.17 Hz (10 cpm)	0.10	0.126	
1132	427	800	20 Hz	0.10	0.253	Equipment Failure
1134	427	800	20 Hz	0.10	0.243	
1135	649	1200	20 Hz	0.50	0.244	
1136	760	1400	20 Hz	0.50	0.244	
1137	427	800	0.0083 Hz (0.5 cpm)	0.50	0.244	
1138	427	800	20 Hz	0.10	0.257	
1139	427	800	20 Hz	0.80	0.254	
1140	649	1200	0.17 Hz (10 cpm)	0.80	0.250	
1142	649	1200	20 Hz	0.80	0.249	
1143	760	1400	0.0083 Hz (0.5 cpm)	0.50	0.248	
1144	649	1200	0.0083 Hz (0.5 cpm)	0.80	0.249	
1145	760	1400	120 Sec. Dwell	0.10	0.250	
1146	427	800	20 Hz	0.50	0.250	
1147	760	1400	0.0083 Hz (0.5 cpm)	0.80	0.249	
1148	760	1400	120 Sec. Dwell	0.10	0.500	
1149	760	1400	0.17 Hz (10 cpm)	0.10	0.501	
1150	649	1200	Sustained Load	1.00	0.500	
1151	760	1400	Sustained Load	1.00	0.498	
1152	649	1200	300 Sec. Dwell	0.10	0.499	
1153	718	1325	15 Sec. Dwell	0.10	0.499	Verification Test
1154	718	1325	15 Sec. Dwell	0.10	0.500	Verification Test
1156	760	1400	20 Hz	0.10	0.250	
1157	760	1400	0.0083 Hz (0.5 cpm)	0.10	0.252	
1160	760	1400	0.17 Hz (10 cpm)	0.80	0.251	
1162	649	1200	0.17 Hz (10 cpm)	0.80	0.250	
1165	649	1200	30 Sec. Dwell	0.10	0.300	
1167	538	1000	0.017 Hz (1 cpm)	0.65	0.242	Verification Test
1168	538	1000	0.017 Hz (1 cpm)	0.65	0.251	Verification Test
1173	760	1400	600 Sec. Dwell	0.10	0.750	

DATA ANALYSIS PROCEDURES

The reduction of crack length, a, versus cycles, N, data is accomplished by using the incremental polynomial method (Reference 5). This method for computing da/dN involves fitting a second-order polynomial (parabola) to sets of seven successive data points. The equation for the local fit takes the form:

$$\hat{a}_4 = b_0 + b_1 \left[\frac{N_4 - \xi_1}{\xi_2} \right] + b_2 \left[\frac{N_4 - \xi_1}{\xi_2} \right]^2 \tag{2}$$

where:

$$-1 \leq \left[\frac{N_4 - \xi_1}{\xi_2} \right] \leq +1$$

and b_0, b_1 and b_2 are the regression parameters which are determined by the least squares method (that is, minimization of the square of the deviations between observed and fitted values of crack length) over the range a_1 to a_7. The value $\hat{a}_4$ is the fitted value of crack length at N_4. The parameters, $\xi_1 = \frac{1}{2}(N_1 + N_7)$ and $\xi_2 = \frac{1}{2}(N_7 - N_1)$, are used to scale the input data. The crack growth rate at N_4 is obtained directly from the derivative of equation 2 as follows:

$$(da/dN)\ \hat{a}_4 = \frac{b_1}{\xi_2} + 2\, b_2\, (N_4 - \xi_1) / \xi_2^2 \tag{3}$$

The ΔK associated with this da/dN is calculated using the fitted crack length $\hat{a}_4$.

After calculation of da/dN and ΔK using the first seven a versus N data points, another da/dN versus ΔK value is calculated using actual a versus N data points 2 through 8 (renumbered 1 through 7 for use in the equations). The local fit is moved along the data one point at a time until the last seven points are used in the calculation. A computer-drawn plot of actual crack length versus cycles is produced when the da/dN and ΔK calculations are made to allow the actual data to be scrutinized by the engineer.

The da/dN versus ΔK calculations from the seven-point incremental polynomial computer program are modeled using the hyperbolic sine equation, and the final da/dN versus ΔK computer-drawn plots are produced on log-log scale. Families of da/dN versus ΔK curves are then related by the SINH coefficients, C_1 through C_4, to provide frequency, stress ratio, and temperature models.

The final interpolative models are presented using data reduced by the incremental polynomial method; however, many of the preliminary models presented data evaluated by the direct secant method. Discrete values of Δa and ΔN were computed from raw laboratory data. By not smoothing (regressing) the a, N data, the actual local $\Delta a/\Delta N$ perturbations are observable in the final da/dN versus ΔK curves. Figures 9 through 15 compare the direct secant and incremental polynomial methods, and the only significant difference for these well-behaved data is three additional data points at each extreme for the direct secant method.

Crack propagation under constant amplitude loading conditions is a function of the applied stress intensity range (within the limits of applicability of linear elastic fracture mechanics). The applied stress intensity range, ΔK, is the driving force for crack propagation. Many relationships have been developed to correlate observed crack growth rate and stress intensity. Paris presented the simple relationship (Reference 6):

$$da/dN = C\,(\Delta K)^n \tag{4}$$

where C and n are material constants. At elevated temperatures, however, the crack growth process is a complicated function of stress ratio, temperature, load history, and environment. These dependencies make the general use of equations, such as equation (4), more difficult. A model developed at P&WA/Florida (References 1, 2 and 3) was used to describe the effects of cyclic frequency, stress ratio, and temperature on the crack growth rate of AF2-1DA. The model is based on the hyperbolic sine equation:

$$\log(da/dN) = C_1 \sinh (C_2(\log (\Delta K) + C_3)) + C_4, \quad (1)$$

where the coefficients have been shown to be functions of test frequency, stress ratio, and temperature:

C_1 = material constant
$C_2 = f_2 (R, \nu, T)$
$C_3 = f_3 (C_4, \nu, R)$
$C_4 = f_4 (\nu, R, T)$.

The hyperbolic sine equation was selected as the model for the following reasons:

- It exhibits the overall shape of typical da/dN vs ΔK plots obtained over several decades of crack growth rates.
- All or part of the equation may be used to fit data since the hyperbolic sine has both a concave and a convex half and a nearly linear portion near inflection. Also, the slope at inflection can vary with the fitting constants. (By comparison, the slope of an x^3 model is always zero at inflection.)
- The *sinh* is not periodic (*e.g.*, trigonometric tangent) nor asymptotic (e.g., tangent, or inverse hyperbolic tangent); therefore, when extrapolation becomes necessary, the sinh behaves well at distances removed from the data, quite unlike most polynomials, periodic, or asymptotic functions.
- This model requires no information other than a, N data. By comparison, some other models in current use require both K_{th} and K_{IC}, in addition to a, N data, to model crack growth behavior. Both K_{th} and K_{IC} are difficult to obtain experimentally; K_{th} because of the extremely small crack growth measurements necessary, and K_{IC} because of gross plasticity at the crack tip encountered in fracture-toughness testing at elevated temperatures.

The hyperbolic sine is defined as:

$$y = \sinh x = \frac{e^x - e^{-x}}{2} \quad (5)$$

and when presented on Cartesian coordinates, it appears as shown in Figure 16. The function is zero at $x = 0$ and has its inflection there.

The introduction of the four regression coefficients, C_1 through C_4, permits relocation of the point of inflection and scaling of both axes. In the equation,

$$(y - C_4) = \sinh (x + C_3), \quad (6)$$

C_3 establishes the horizontal location of the hyperbolic sine point of inflection and C_4 locates its vertical position.

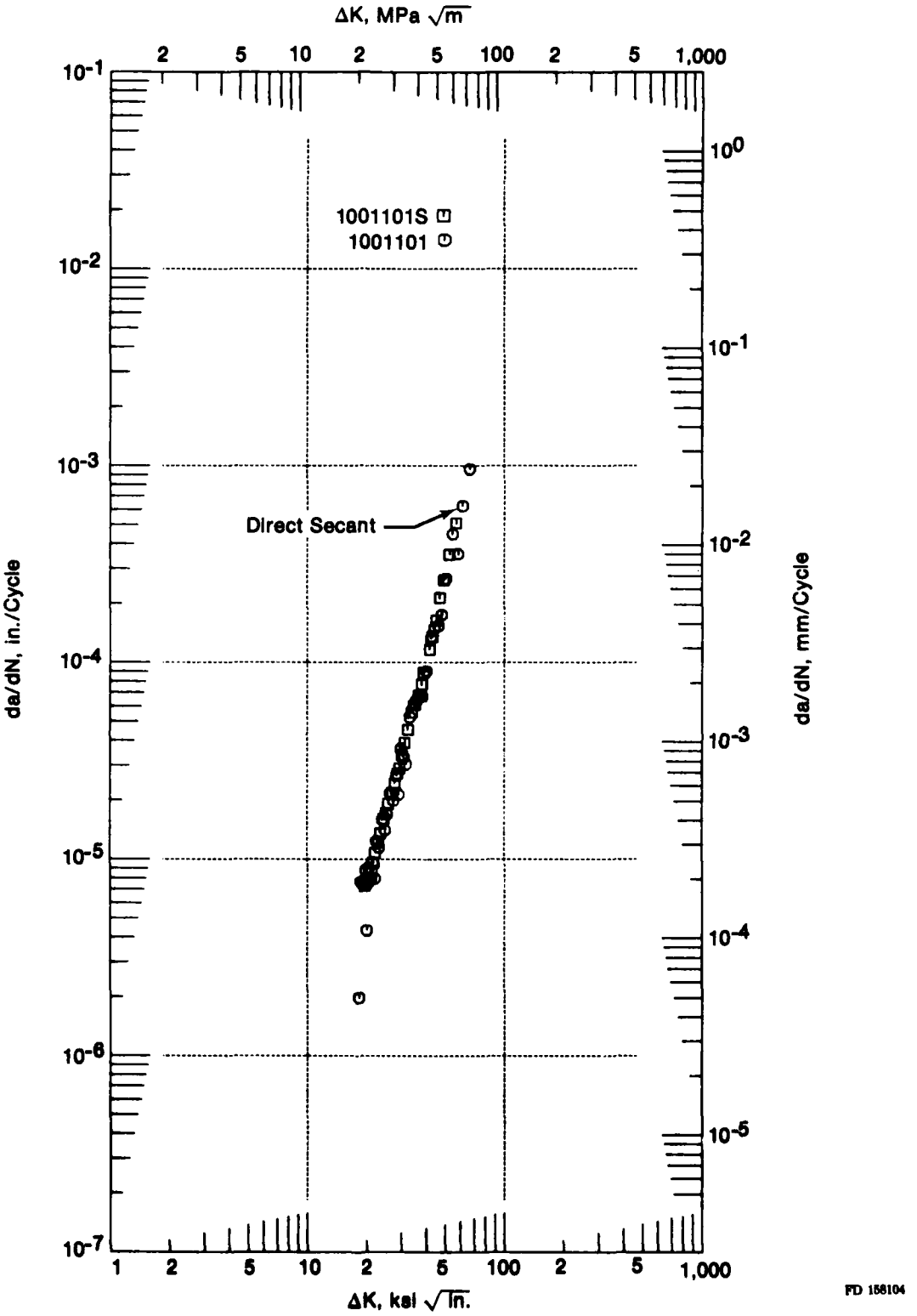

Figure 9. Comparison of Direct Secant and Incremental Polynomial Data Reduction Methods for Specimen 1101

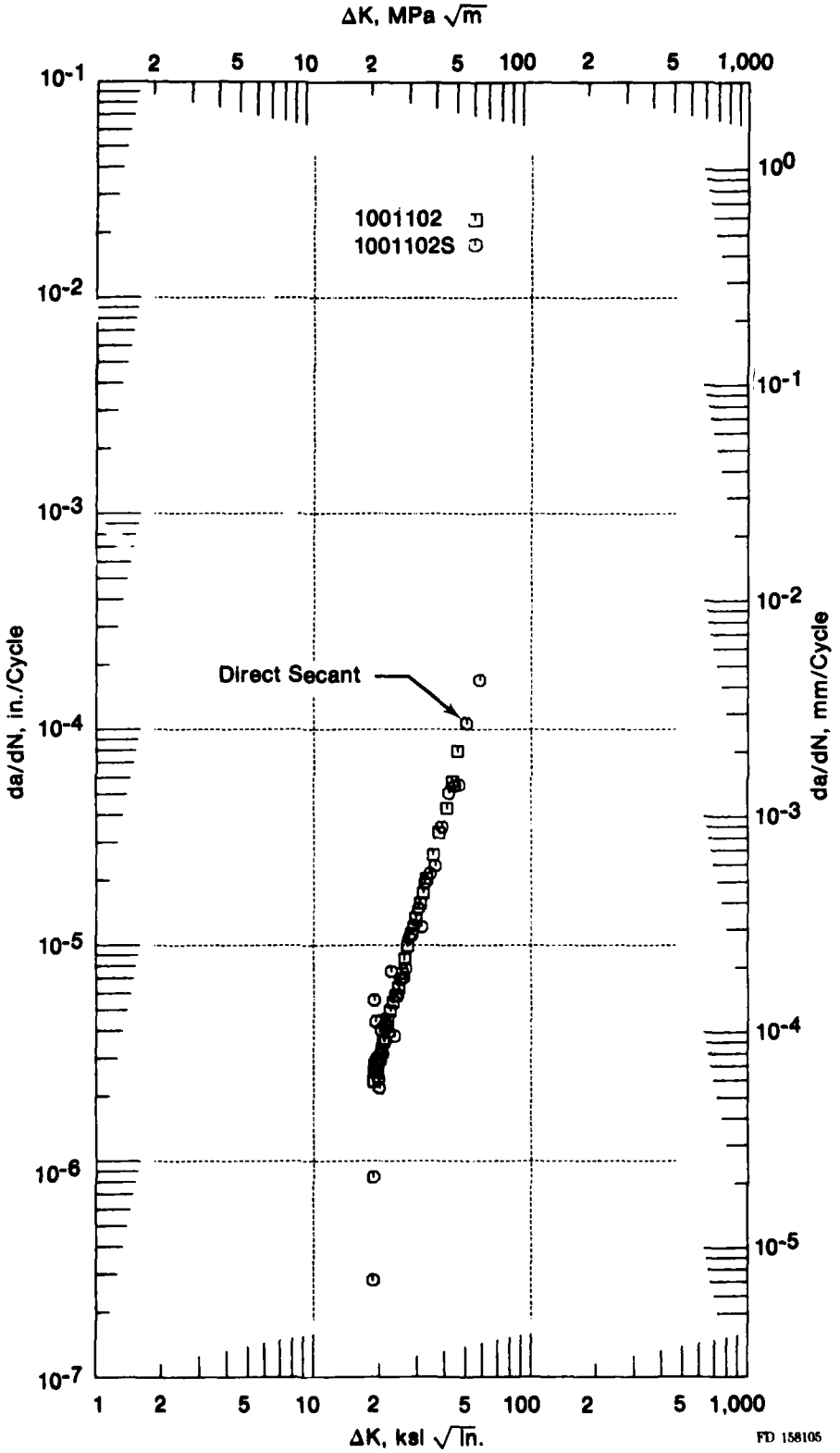

Figure 10. Comparison of Direct Secant and Incremental Polynomial Data Reduction Methods for Specimen 1102

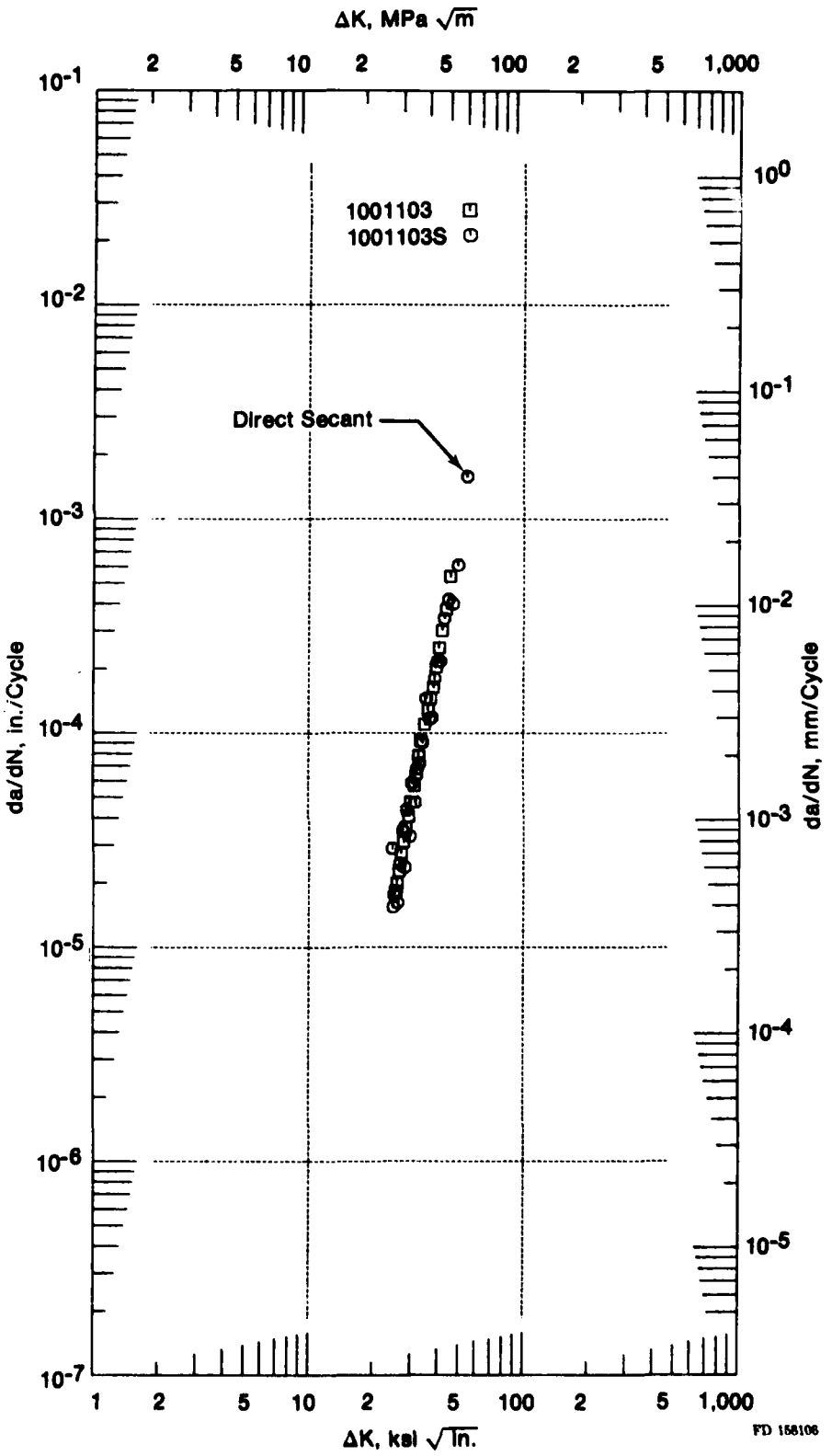

Figure 11. Comparison of Direct Secant and Incremental Polynomial Data Reduction Methods for Specimen 1103

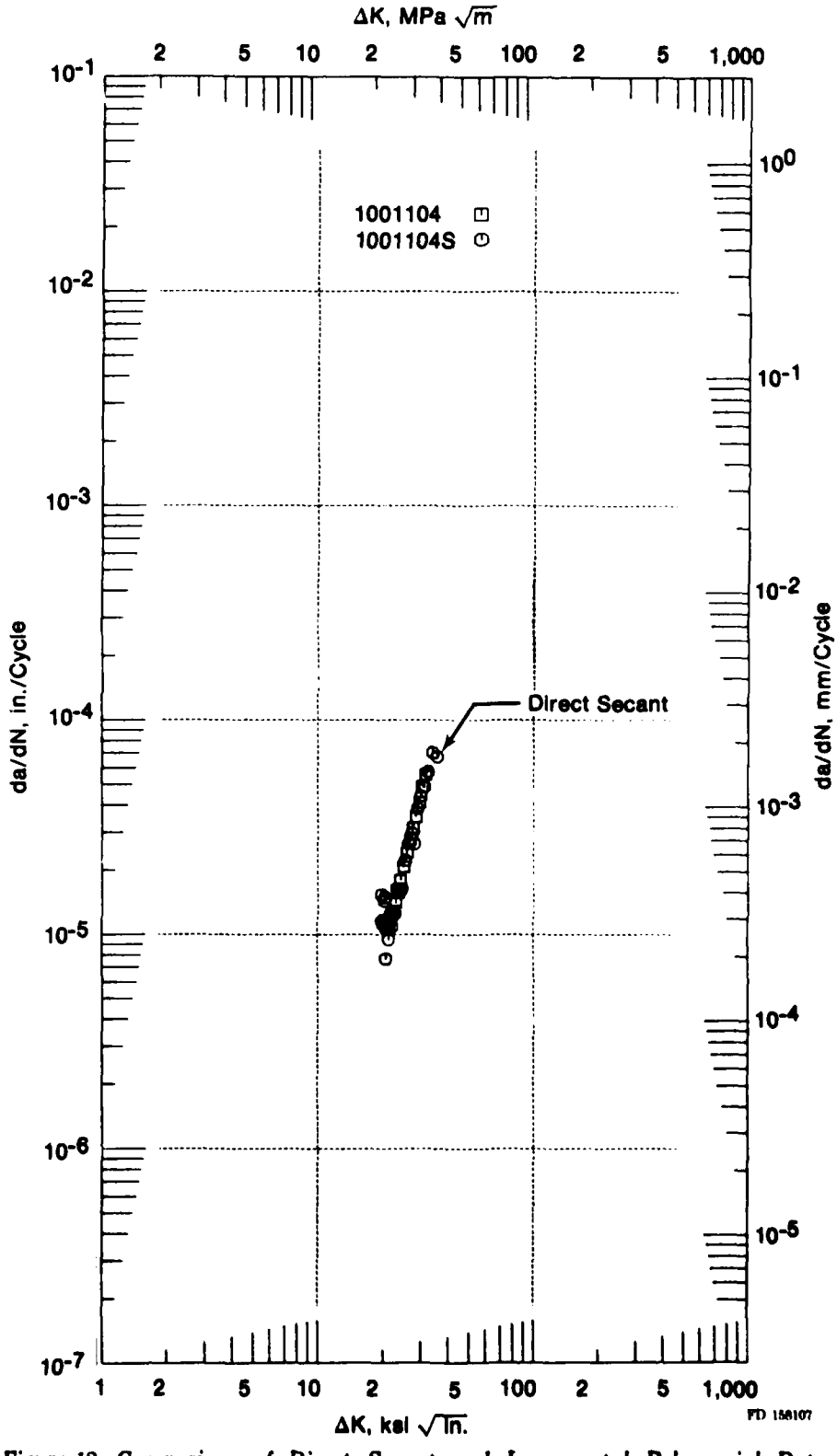

Figure 12. Comparison of Direct Secant and Incremental Polynomial Data Reduction Methods for Specimen 1104

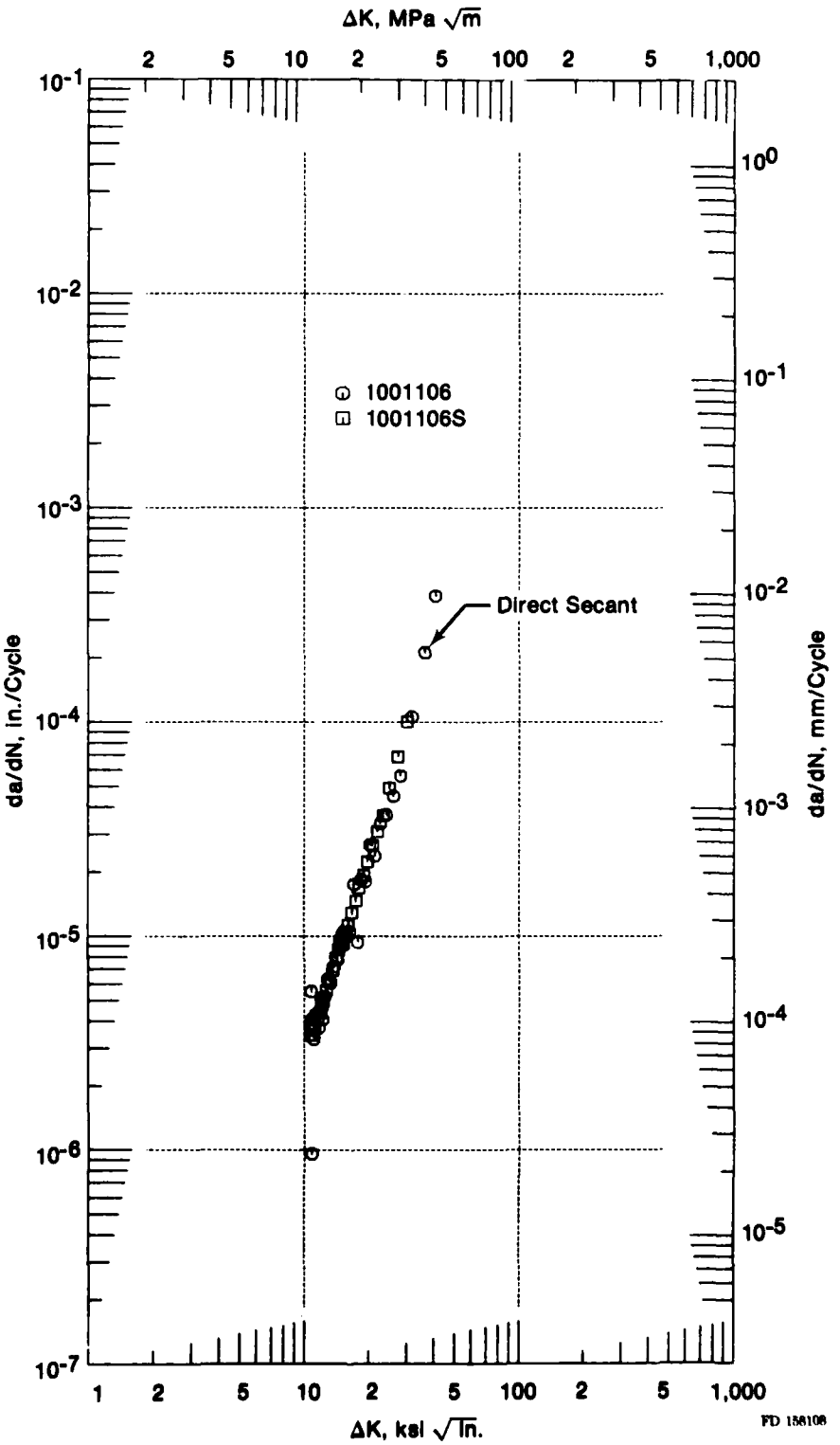

Figure 13. Comparison of Direct Secant and Incremental Polynomial Data Reduction Methods for Specimen 1106

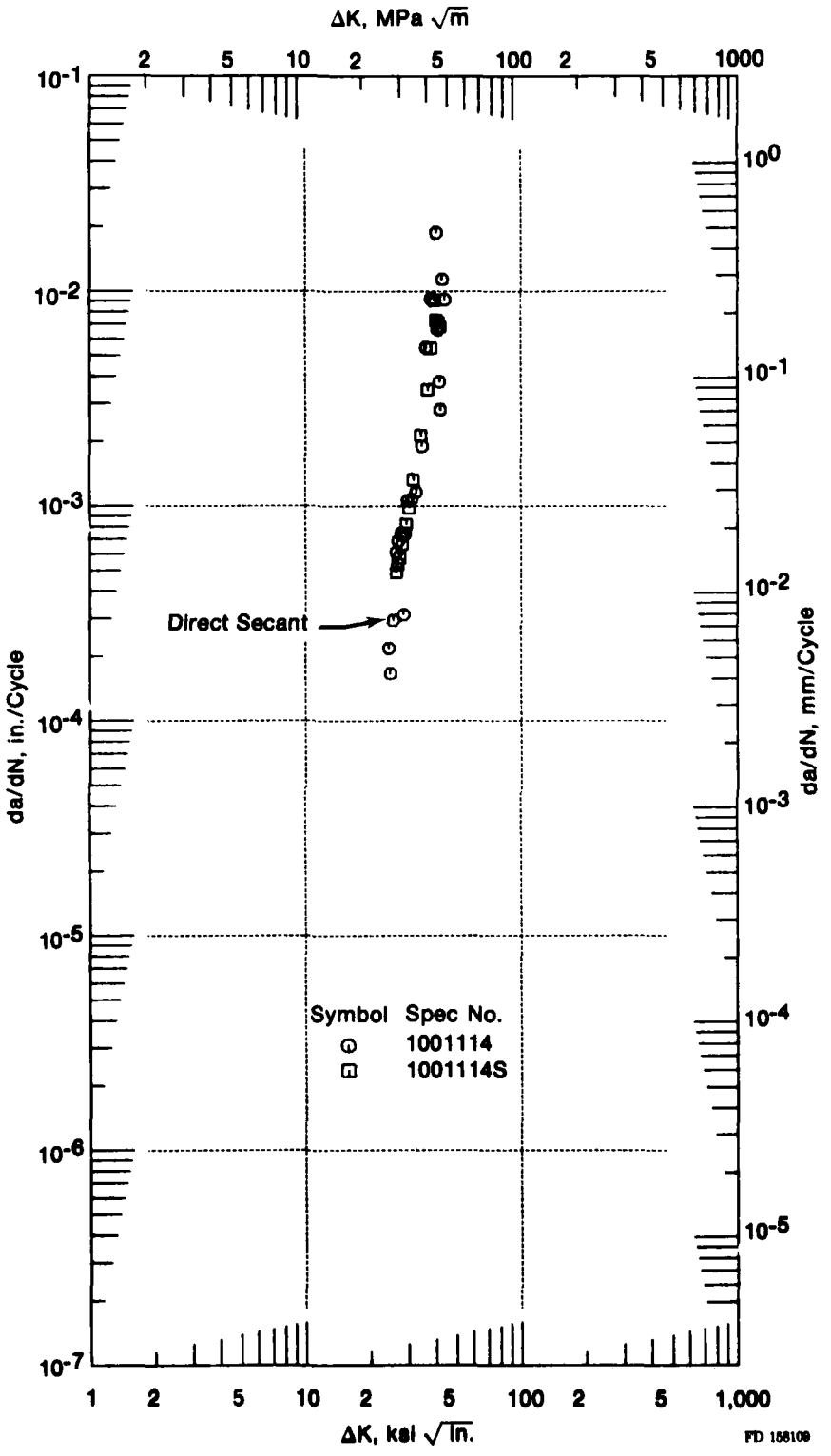

Figure 14. Comparison of Direct Secant and Incremental Polynomial Data Reduction Methods for Specimen 1114

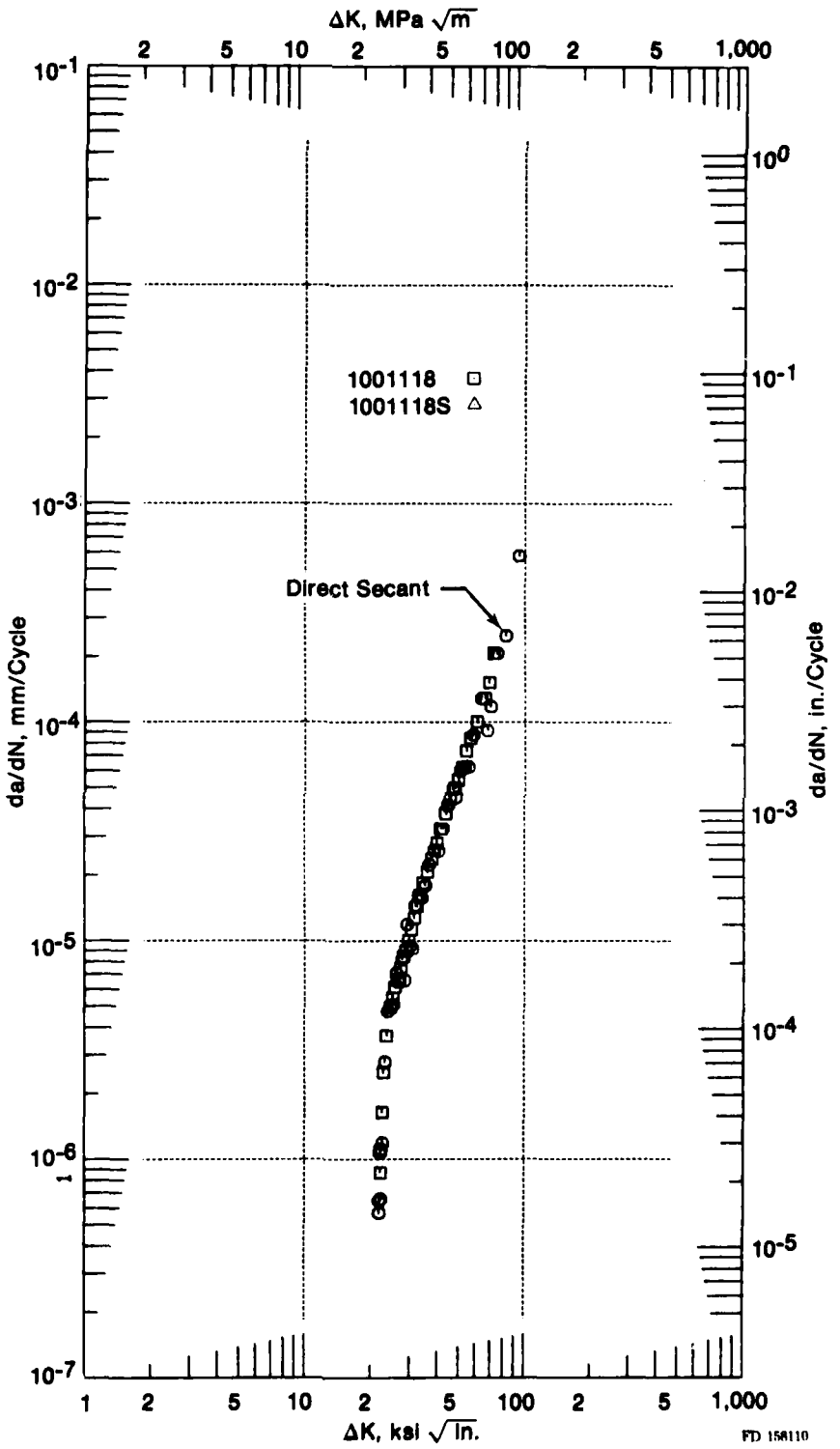

Figure 15. Comparison of Direct Secant and Incremental Polynomial Data Reduction Methods for Specimen 1118

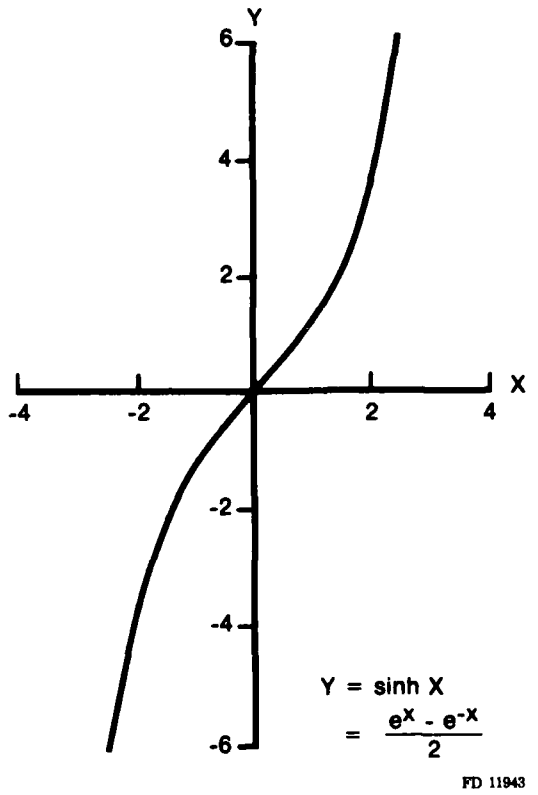

Figure 16. Hyperbolic Sine on Cartesian Coordinates

To scale the axes, C_1 and C_2 are introduced

$$\frac{(y - C_4)}{C_1} = \sinh (C_2 (x + C_3)) \tag{7}$$

which can be rewritten as

$$y = C_1 \sinh (C_2 (x + C_3)) + C_4 \tag{8}$$

of which equation (2) is a special case where $y = \log(da/dN)$ and $x = \log(\Delta K)$. Note that C_3 has units of log (ΔK) and C_4 has units of log (da/dN); C_1 and C_2 are dimensionless and can be conceptualized as stretching the curve vertically and horizontally, respectively. Experience indicates that for a given material, C_1 can be fixed without adversely affecting model flexibility (Reference 3).

The hyperbolic sine model is easily adapted to describe the fundamental parametric effects of stress ratio, frequency, and temperature on crack growth rate. Experience with turbine disk alloys indicates that changing test frequency, while holding stress ratio and temperature constant, produces crack growth curves similar in shape, but shifted along a nearly vertical line passing through the points of inflection. The location of these inflection points is related to test frequency. Similar results can be obtained with stress ratio and temperature. Figure 17 schematically depicts the qualitative effects of frequency, stress ratio, and temperature on crack growth rates.

Because of the simple relationships observed between the coefficients of the SINH model and the fundamental propagation-controlling parameters, interpolations are straightforward. It is here that the model demonstrates its great usefulness: the Hyperbolic Sine Model provides descriptions of crack propagation characteristics even where data are unavailable. The interpolation algorithm is described in Reference 7, and the four SINH model coefficients can be determined as follows:

C_1 = material constant (0.5 for AF2-1DA)
$C_2 = m_2 \log (\nu) + b_2$
$C_3 = m_3 C_4 + b_3$
$C_4 = m_4 \log (\nu) + b_4$.

Computation of a crack growth rate equation for any given frequency (with stress ratio and temperature held constant) is a straightforward calculation, once the above linear relationships have been established.

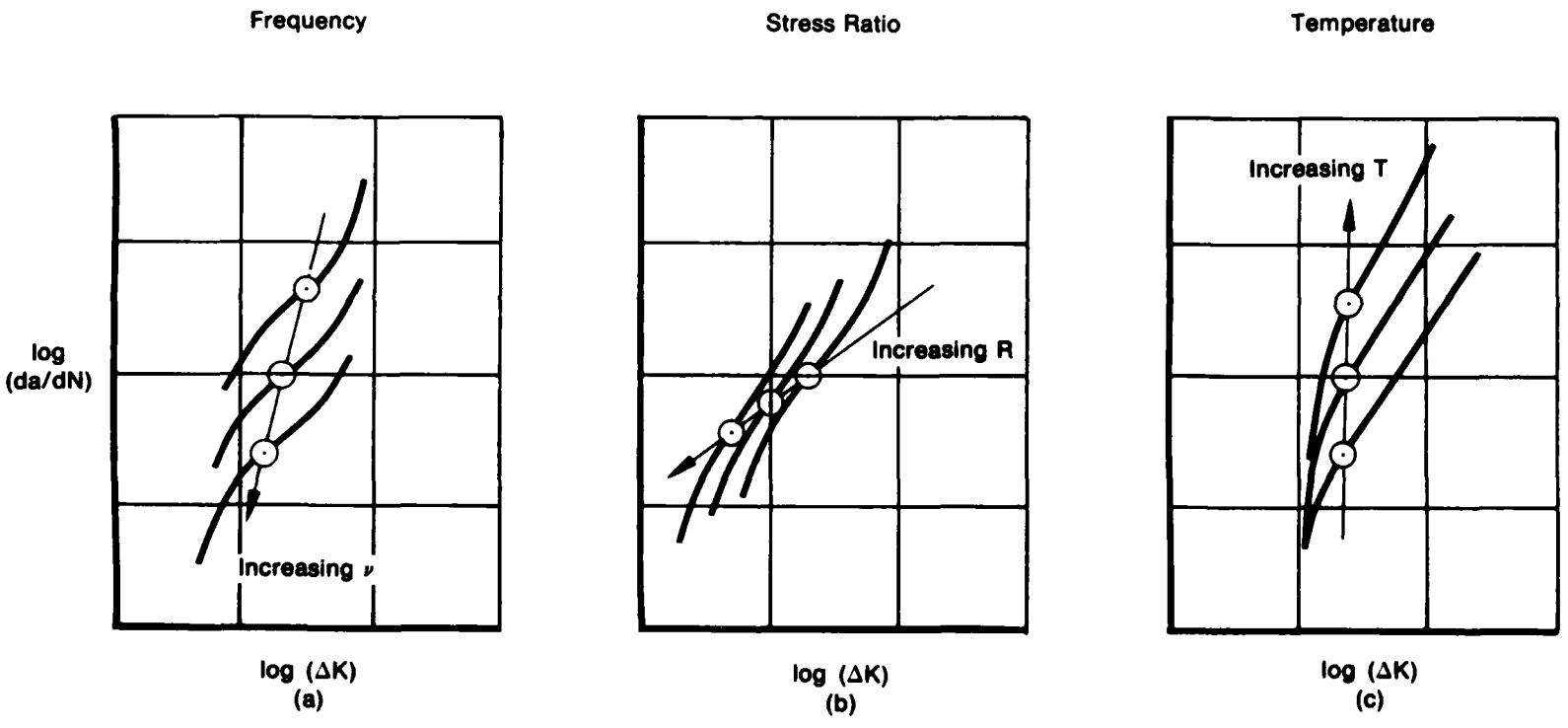

Figure 17. Crack Propagation is Influenced by Frequency (a), Stress Ratio (b), and Temperature (c)

TEST PROGRAM

Phase I: Crack Growth Data Generation

The objectives of Phase I are to determine the effects of specimen thickness on crack growth rates for AF2-1DA material and characterize the effects of stress ratio, cyclic frequency, and temperature.

The effects of thickness on crack propagation were determined by testing 3.17 mm, 6.35 mm, and 12.70 mm thick specimens. Thickness effects were determined at 427°C, 649°C, and 760°C for both cyclic and cyclic/dwell stress-time waveforms.

The modeling of frequency effects on subcritical crack growth is accomplished using 20 Hz, 0.17 Hz, and 0.0083 Hz as the test points, and the effects of stress ratio are modeled using data generated at R=0.1, R=0.5, and R=0.8. The temperature effects are characterized at isothermal conditions, and the modeling of these effects is based on test data at 427°C, 649°C, and 760°C.

Applicability of Linear Elastic Fracture Mechanics

The usefuless of linear elastic fracture mechanics (LEFM) depends on a uniparametrical relationship between crack growth rate and the stress intensity factor. Crack tip inelasticity, due to material response at elevated temperatures, can preclude general utility of K as the correlative parameter. Tests were conducted to ensure sufficient geometric constraint and/or environment embrittlement at the crack tip as to render crack growth rate — ΔK relationships independent of specimen geometry (e.g., only thickness in this case). Universal applicability of LEFM is not determined in this program.

In advanced P/M alloys, crack tip inelasticity increases with increasing applied stress intensity. When the plastic zone size becomes comparable to the specimen thickness, the model of crack propagation changes from pure Mode I (i.e., opening mode) to mixed mode (MODE I and MODE III, tearing mode) and LEFM is invalid. For a constant applied stress intensity range, mixed mode propagation rates are slower than those for plane strain constraint at the crack tip. Only compact specimens were used in this program, alleviating problems with differing geometry and net section stress; therefore, the only requirement was that a specimen produce thickness-independent data (i.e., a thicker specimen will not produce a different propagation rate).

Figure 18 shows the effect of thickness on crack growth rates for 3.18 mm (0.125 in.), 6.35 mm (0.250 in.), and 12.70 mm (0.500 in.) thick specimens. All specimens were tested at 427°C (800°F), 10 cpm, R=0.1. To ensure thickness-independent crack growth data, a minimum specimen thickness of 6.35 mm is needed.

The cyclic (0.17 Hz) crack growth rates at 649°C (1200°F), R=0.1 are shown in Figure 19 for three thicknesses (3.18 mm, 6.35 mm and 12.70 mm). A comparison of these rates shows that 6.35 mm is the minimum thickness needed for thickness-independent data at these conditions.

At 760°C (1400°F), 10 cpm, and R=0.1, the 3.18 mm thick specimen produced nearly the same crack growth rate (Figure 20) as the 12.70 mm thick specimen. Since the two extremes in thickness produce nearly equal data, 6.35 mm thick specimens are probably adequate to produce thickness-independent data.

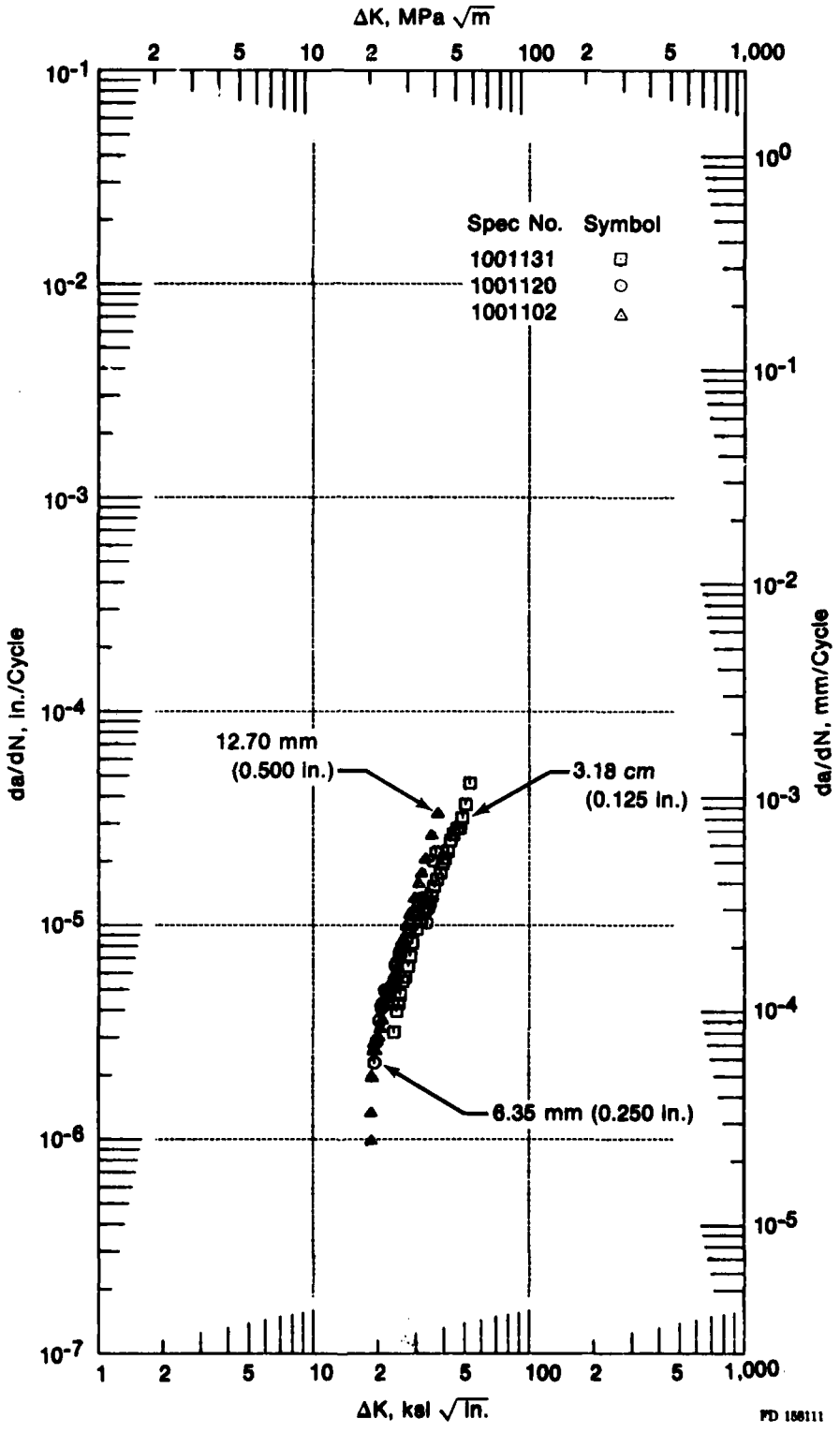

Figure 18. Thickness Comparison at 427°C (800°F), 10 cpm, R = 0.1

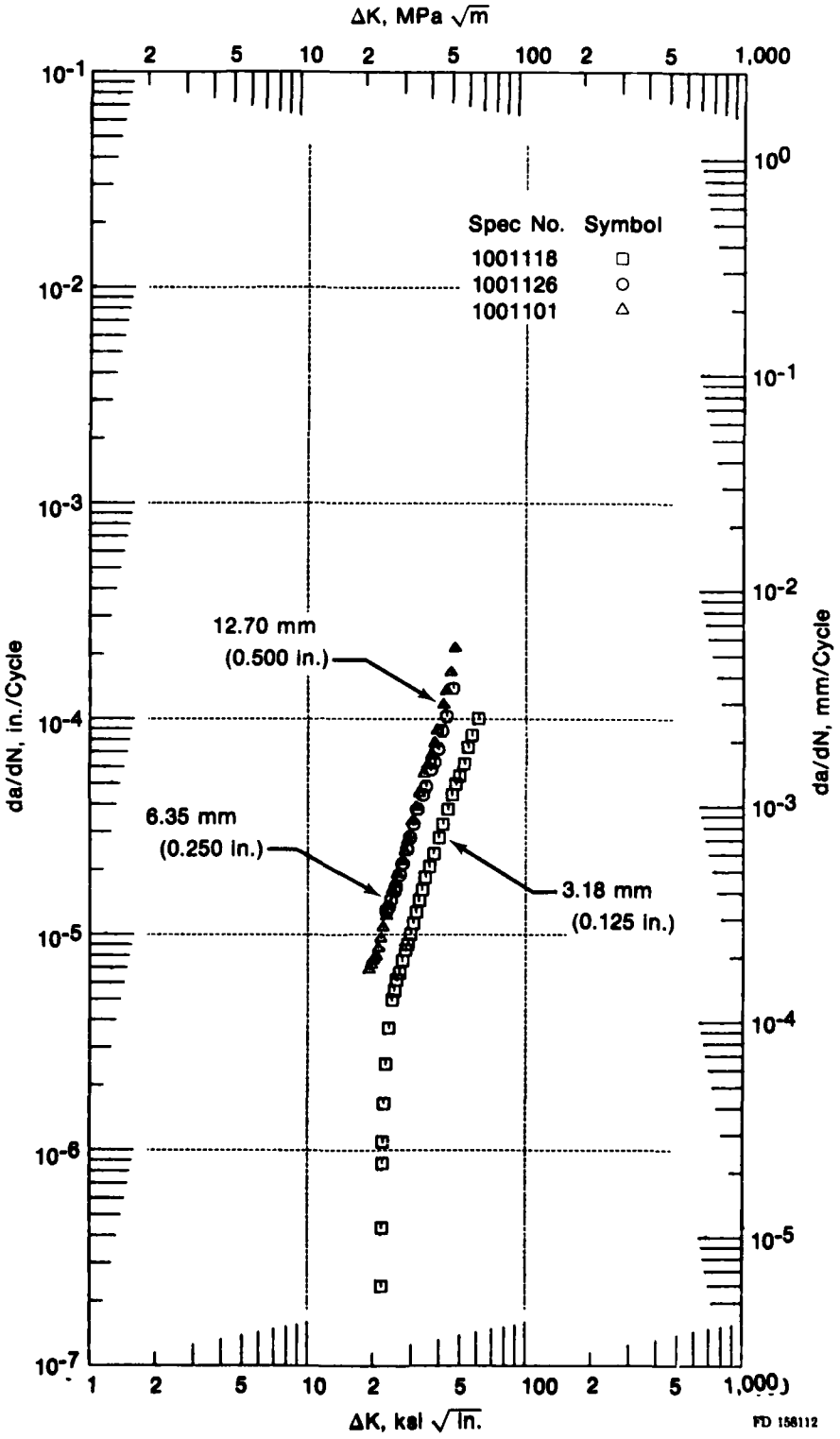

Figure 19. Thickness Comparison at 649°C (1200°F), 10 cpm, R = 0.1

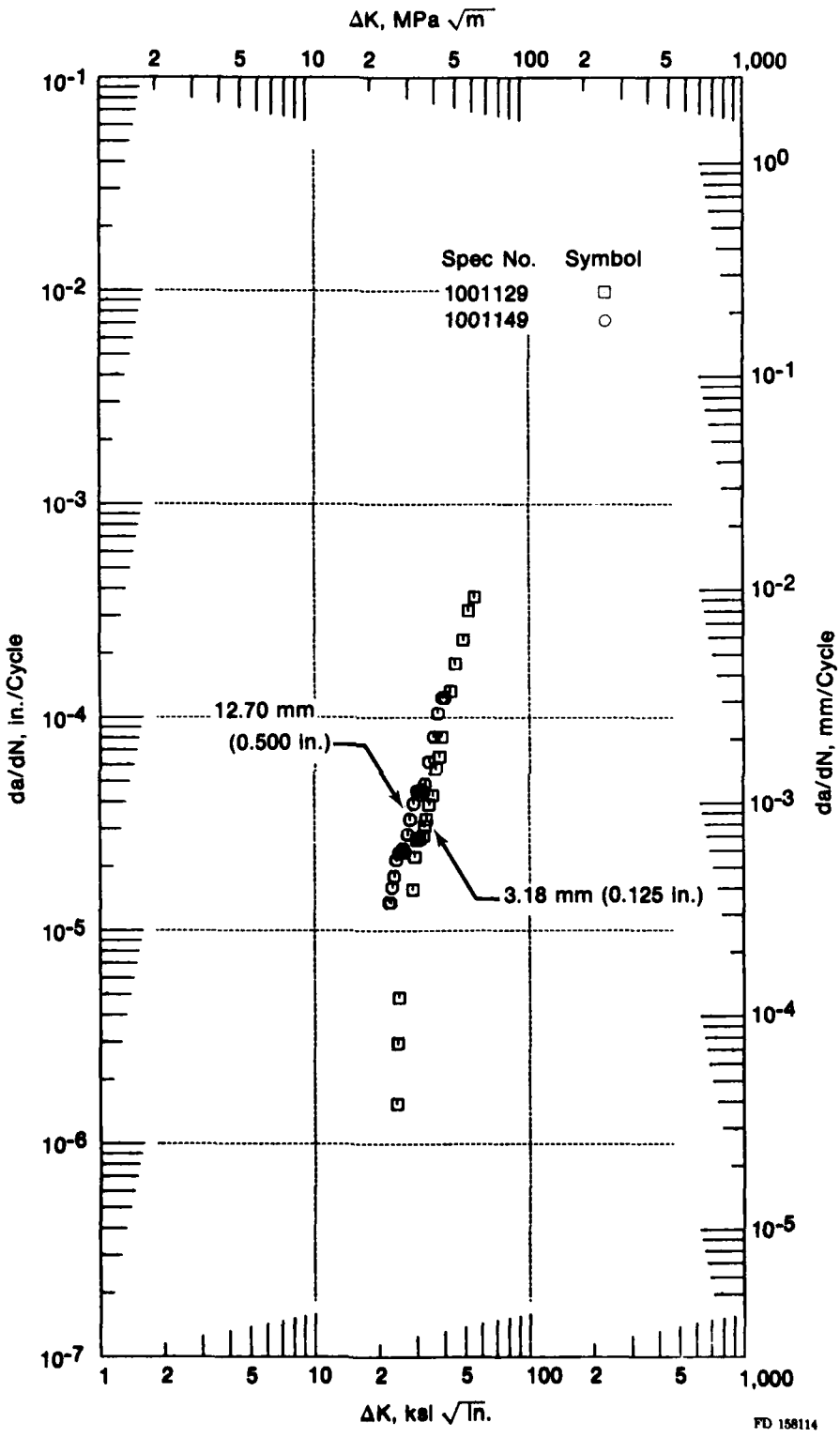

Figure 20. Thickness Comparison at 760°C (1400°F), 10 cpm, R = 0.1

A comparison at 649°C, R=0.1, with a 120 sec dwell at maximum tensile load (using the same ramp as a 0.17 Hz cycle) shows that even the 12.70 mm thick specimen may not produce thickness-independent data. However, since the difference between the 6.35 mm and the 12.70 mm specimen data shown in Figure 21 is small, it is likely that a thicker specimen would not produce higher crack growth rates than the 12.70 mm thick specimen, indicating that thickness-independent data is probably provided by the 12.70 mm thick specimen.

Figure 22 shows the comparison of the crack growth rates for 6.35 mm and 12.70 mm thick specimens. Both tests were conducted at 760°C (1400°F), 120 sec dwell, R = 0.1. The crack growth data from the thin specimen is nearly equal to the thick specimen data. Therefore, a 12.70 mm thick specimen should be thick enough to give thickness-independent data.

To confirm the conclusion that 12.70 mm thick specimens produce thickness-independent data for dwell tests, a 19.05 mm thick specimen was tested at 760°C, R = 0.1, 600 sec dwell at maximum tensile load. The comparison of the data with data from a 12.70 mm thick specimen tested at the same conditions shown in Figure 23 indicates that 12.70 mm thick specimens produce thickness-independent data.

Note that the thickness required at 649°C to assure plane strain constraint at the crack tip increases from 6.35 mm for cyclic tests to 12.70 mm (or possibly greater) for tests containing dwells at maximum tensile load. One explanation of this behavior can be obtained by considering the environmental influences (oxidation) on crack tip elasticity. Environmental degradation promotes crack tip embrittlement, which in turn acts to discourage through-thickness strain. Therefore, thinner sections will exhibit more enhanced plane strain conditions in an oxidizing atmosphere than in an unoxidized condition. During sustained load, or long dwell, tests, a protective oxide layer can form which prevents further oxygen diffusion into the material. As this prophylactic effect reduces the oxidation rate, the thickness required for plane strain constraint at the crack tip increases.

Constant load amplitude fatigue testing to determine the effects of thickness on crack propagation indicates that all cyclic tests should be performed on 6.35 mm (0.250 in.) thick specimens, and cyclic/dwell (and sustained load) tests should be performed on 12.70 mm (0.500 in.) thick specimens for thickness-independent data at the temperatures tested (427°C, 649°C, 760°C). These represent minimum thicknesses.

Fractography

The fracture surfaces of specimens 1102 (427°C, cyclic), 1101 (649°C, cyclic), and 1106 (649°C, cyclic) were examined using the transmission electron microscope (TEM). Five areas of each fracture surface were scrutinized to determine the fracture mechanism at different stress intensity (K) levels as shown in Figures 24, 25 and 26. A more in-depth study coupled with a scanning electron microscope evaluation might be more conclusive, but is not within the scope of this program. The following conclusions were determined from inspection of representative areas.

All specimens had a heavy oxide on the fracture surface, which obscured most fracture features. Specimen 1101 showed faint oxidized river markings in area 1 (Figure 27), but the other areas were too oxidized to see any significant features. In general the fracture face was flat and showed no signs of intergranular propagation.

There was also evidence of oxidized river markings in areas 1 and 2 of specimen 1106 (Figure 28). Area 3 (Figure 29) appeared to have remnant striations, but the heavy oxide prevented definite identification. This fracture surface also was flat and showed no evidence of intergranular propagation.

Specimen 1102 (427°C) showed definite fatigue striations in area 3 (Figure 30) with an average spacing of 6.9×10^{-4} mm ($\Delta K = 36$) which correlates well with the da/dN plot. Area 4 was suggestive of remnant coarse striations but no real conclusion could be made from what little was observed. Figures 31 and 32 show that areas 1 and 2 were relatively flat and oxidized, and like the other two specimens, showed no evidence of intergranular propagation.

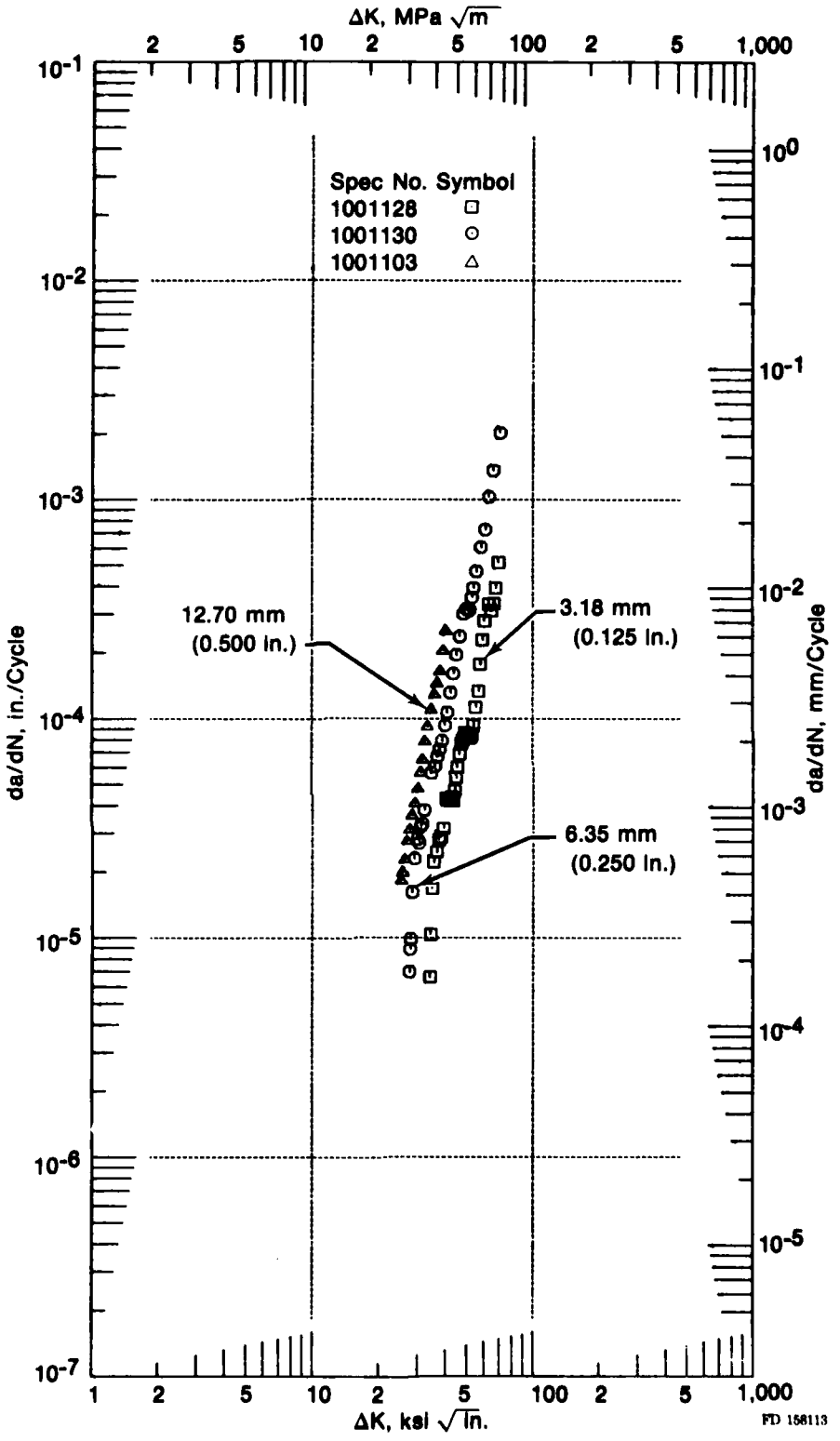

Figure 21. Thickness Comparison at 649°C (1200°F), 120 sec Dwell, R = 0.1

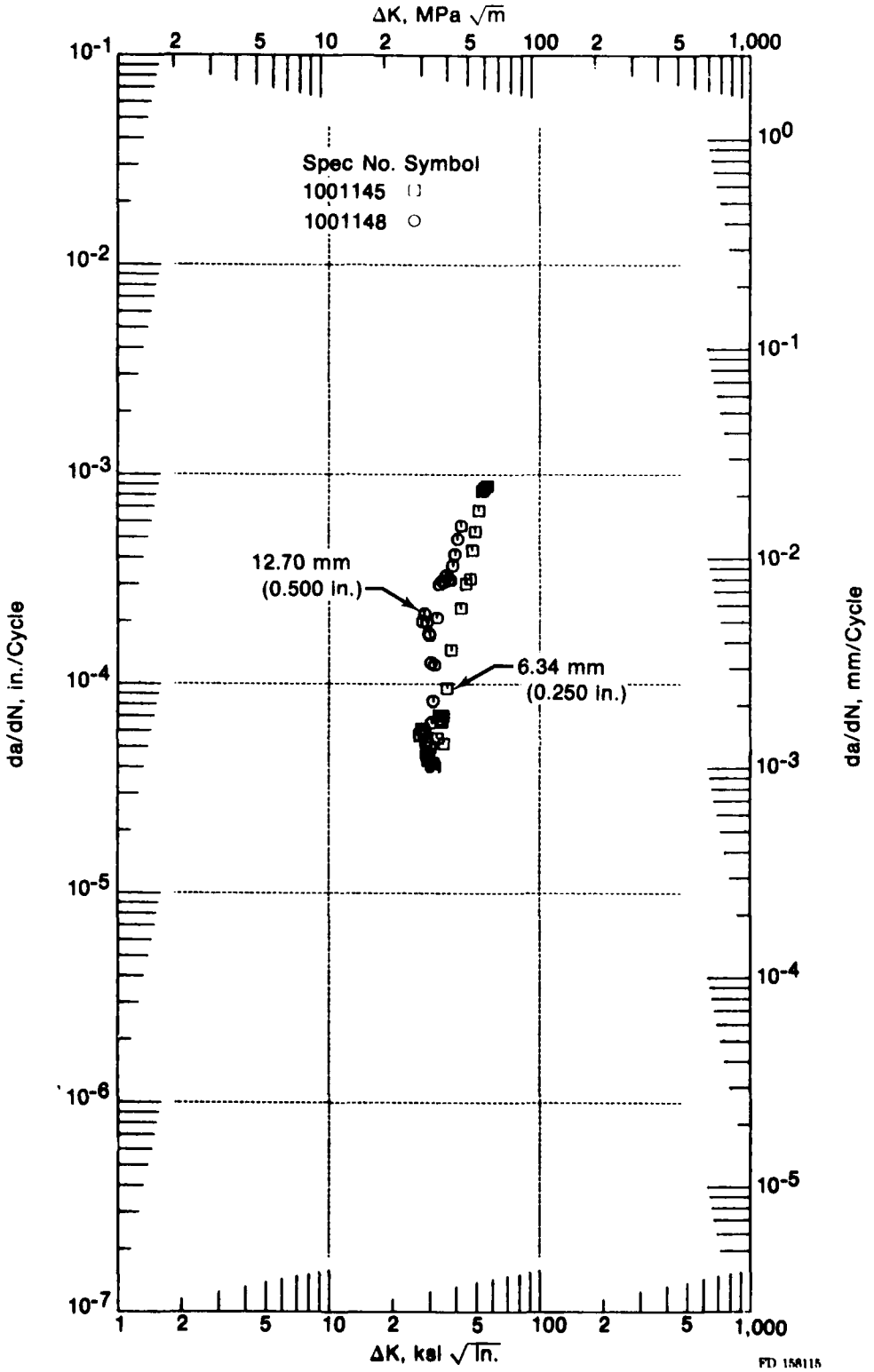

Figure 22. Thickness Comparison at 760°C (1400°F), 120 sec Dwell, R = 0.1

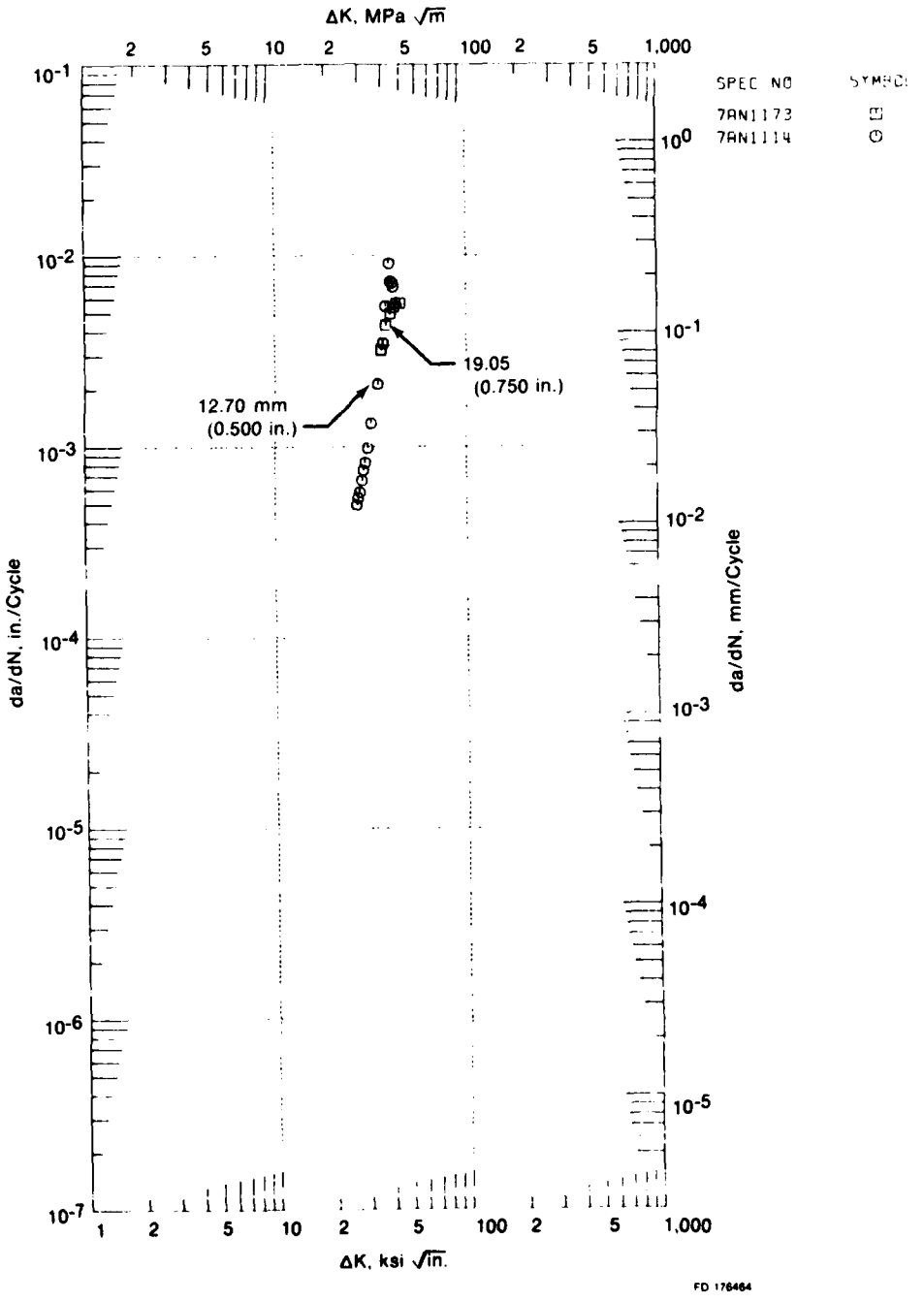

Figure 23. Effect of Thickness on Crack Growth Rates at 760°C, 600 sec Dwell, R = 0.1

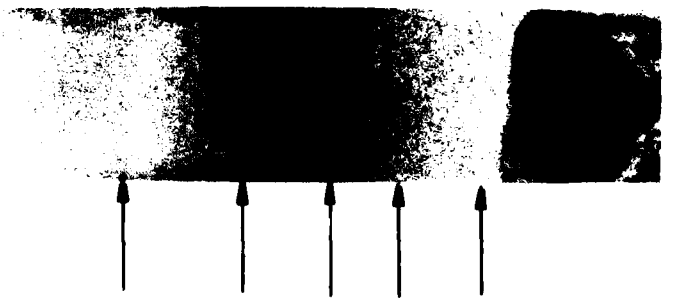

Figure 24. Macrofractograph of Specimen 1102 Showing the Areas Investigated

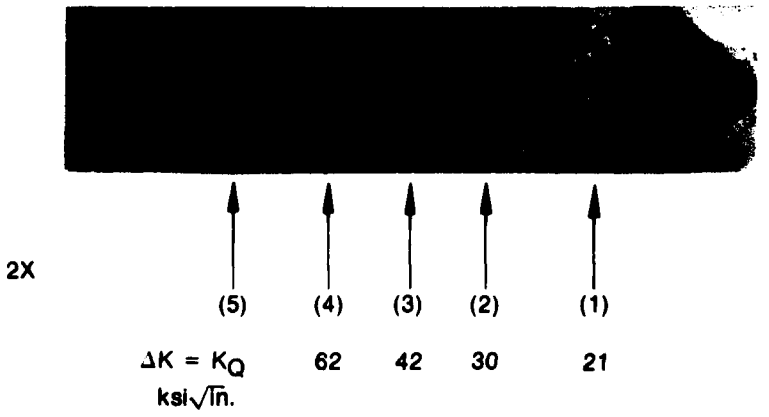

Figure 25. Macrofractograph of Specimen 1101 Showing the Areas Investigated

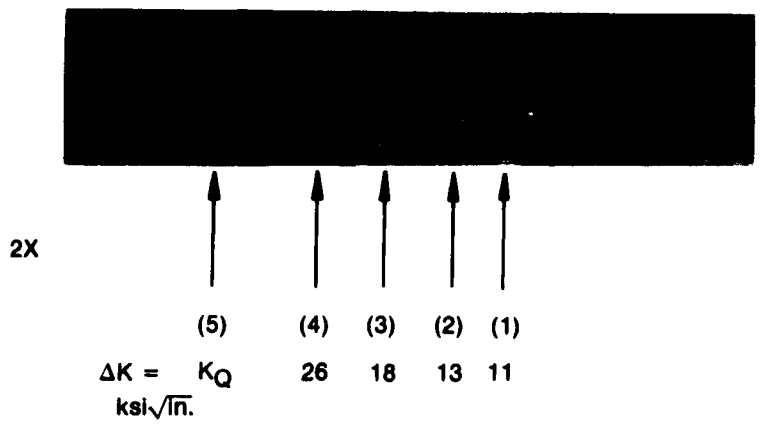

FD 158118

Figure 26. Macrofractograph of Specimen 1106 Showing the Areas Investigated

Typical

Mag: 3500X

Mag: 6500X

FD 158119

Figure 27. Compact Specimen No. 1101 Area 1

Area 1

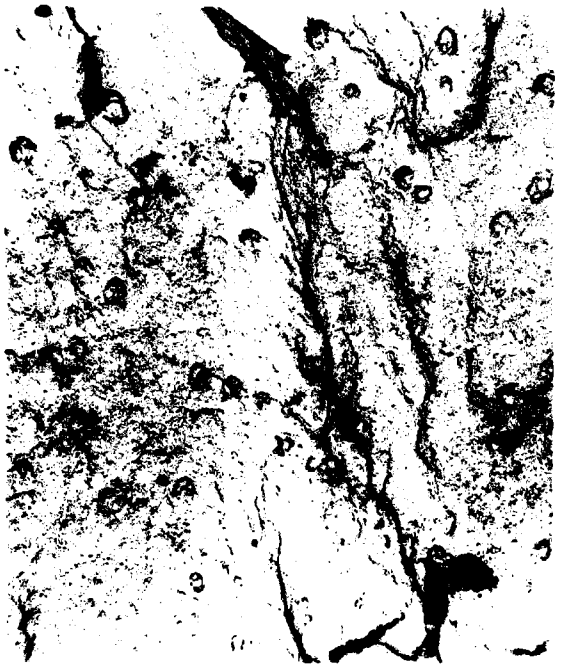

Mag: 3500X

Area 2

Mag: 3500X

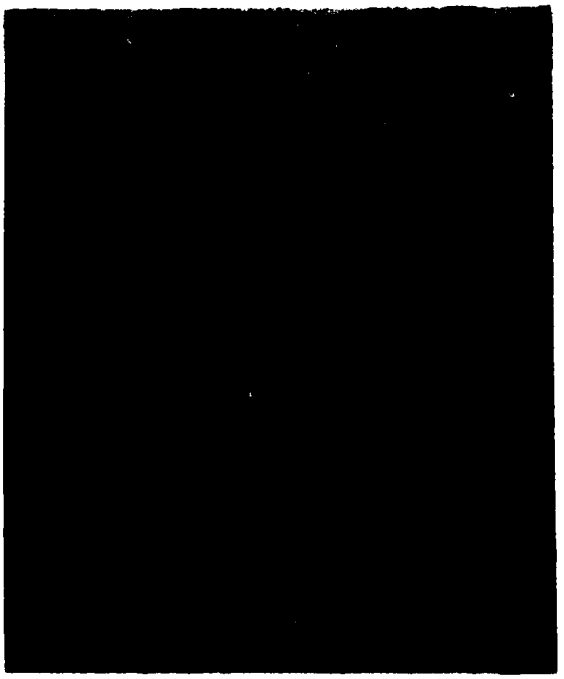

Mag: 6500X

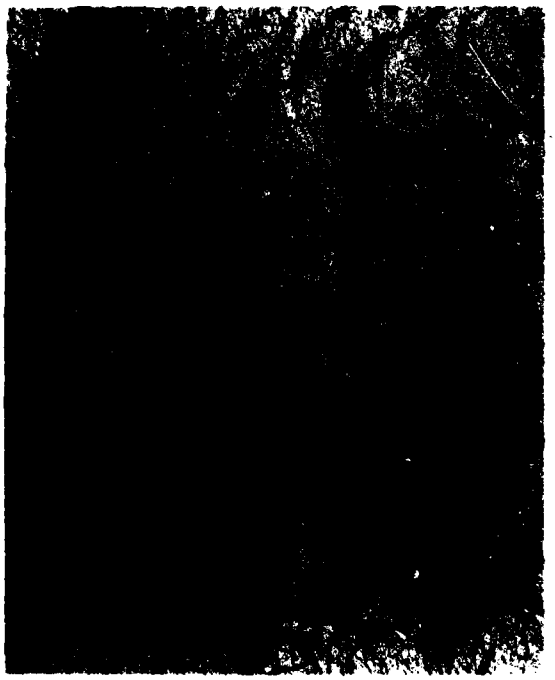

Mag: 6500X

FD 158120

Figure 28. Compact Specimen No. 1106

AREA 3

Mag: 3500X

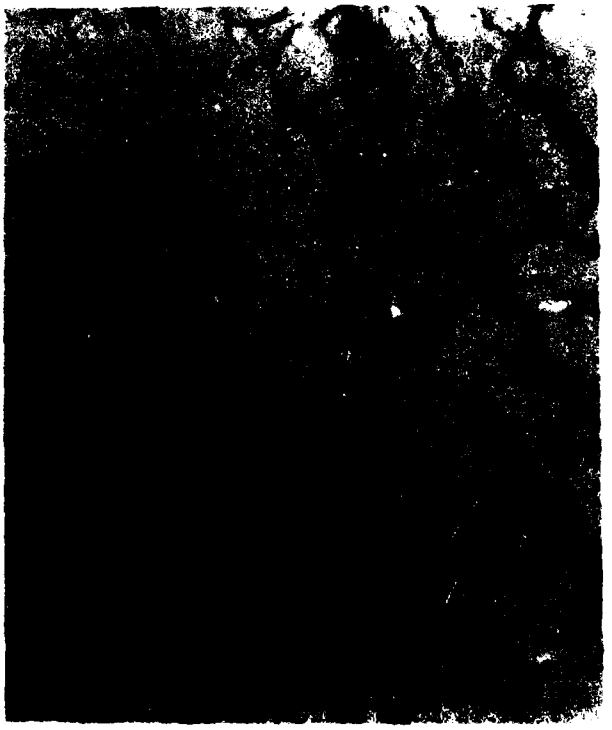

Mag: 6500X

FD 158121

Figure 29. Compact Specimen No. 1106 Area 3

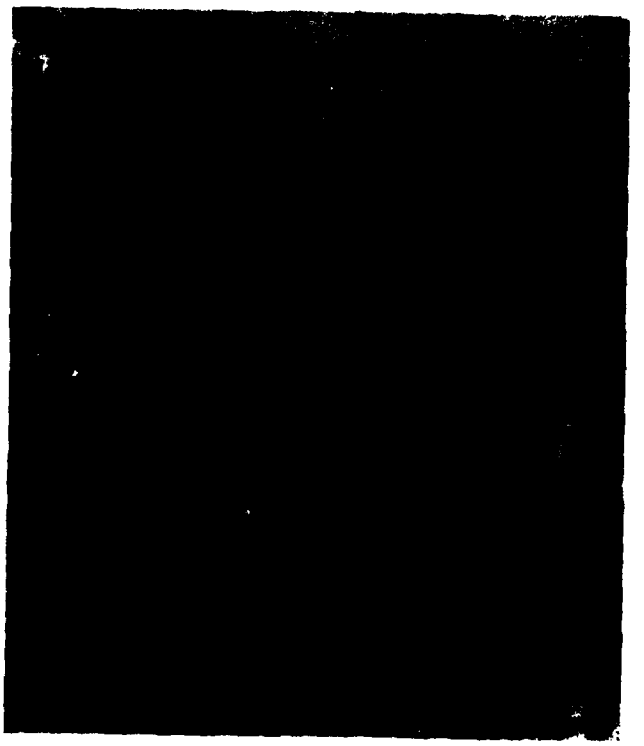

Mag: 6500X

Mag: 10,000X

FD 15812.

Figure 30. Compact Specimen No. 1102 Area 3

Mag: 10,000X

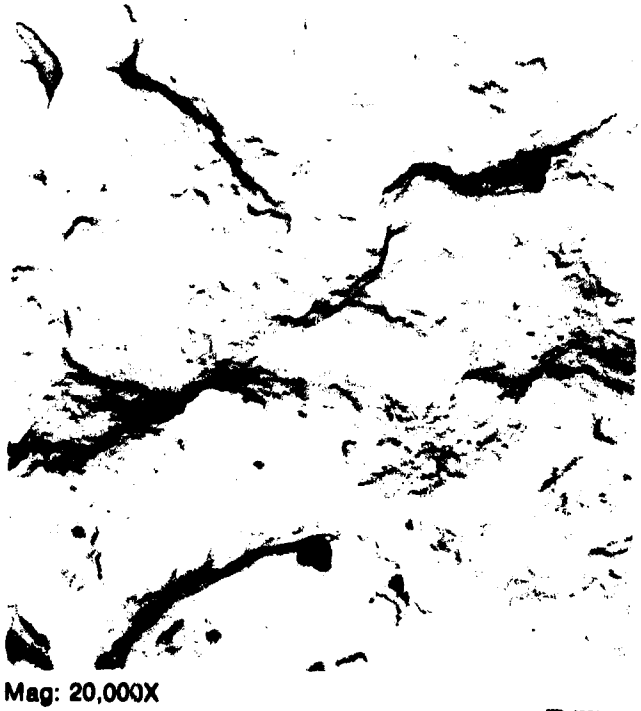

Mag: 20,000X

FD 158123

Figure 31. Compact Specimen No. 1102 Area 1

Area 2

Mag: 10,000X

Mag: 10,000X

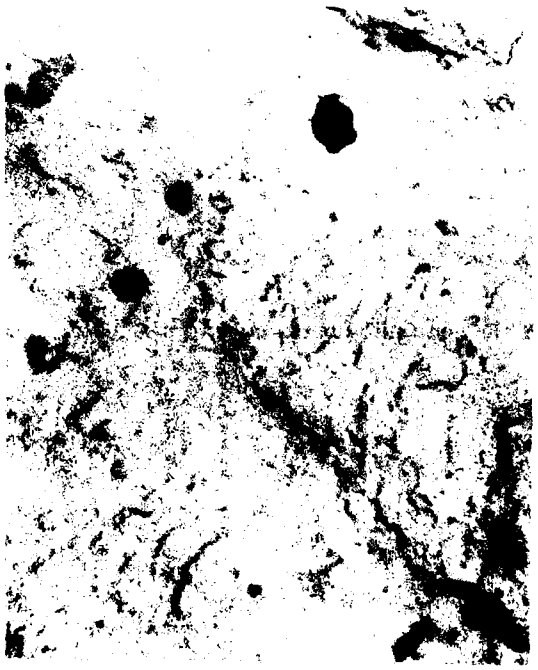

Mag: 20,000X

Mag: 20,000X

FD 158124

Figure 32. Compact Specimen No. 1102 Area 2

Phase II: Development of An Interpolative Model

Introduction

The objective of Phase II was to develop an interpolative model to permit accurate predictions of crack propagation rates for an advanced powder metallurgy (P/M) superalloy (AF2-1DA) under different stress-temperature-time conditions. This generalized interpolative model, based on the hyperbolic sine equation

$$\log (da/dN) = C_1 \sinh (C_2 (\log (\Delta K) + C_3)) + C_4, \tag{1}$$

completely describes the effects of stress ratio (R), cyclic frequency (ν), and temperature (T) on the crack growth rate in this material.

Interpolative capacity forms the fundamental strength of the hyperbolic sine model. The procedure known as the interpolation algorithm for calculating the SINH coefficients, describing fatigue crack propagation (FCP) for any frequency, stress ratio, and temperature, is illustrated in the following paragraphs (reprinted from Reference 7).

Determination of SINH Coefficients

The coefficients (e.g., C_2, C_3, and C_4) at any intermediate value of an element life-controlling parameter, can be determined from equation 9:

$$C_j = C_{j_{base}} + \Delta C_j; \qquad j = 2,3,4 \tag{9}$$

where:

$$C_j = \begin{bmatrix} C_2 \\ C_3 \\ C_4 \end{bmatrix} = \text{interpolated values of coefficients}$$

and:

$$\Delta C_j = \begin{bmatrix} \Delta C_2 \\ \Delta C_3 \\ \Delta C_4 \end{bmatrix} = \text{differences from baseline values}$$

Since the SINH coefficients are linear functions of the controlling parameters, * it is evident that:

$$\begin{bmatrix} \Delta C_2 \\ \Delta C_3 \\ \Delta C_4 \end{bmatrix} = \begin{bmatrix} \partial C_2/\partial \nu, & \partial C_2/\partial R, & \partial C_2/\partial T \\ \partial C_3/\partial \nu, & \partial C_3/\partial R, & \partial C_3/\partial T \\ \partial C_4/\partial \nu, & \partial C_4/\partial R, & \partial C_4/\partial T \end{bmatrix} \times \begin{bmatrix} \Delta \nu \\ \Delta R \\ \Delta T \end{bmatrix} \tag{10}$$

$N \times 1 \qquad\qquad N \times N \qquad\qquad N \times 1$

where:

$$\begin{bmatrix} \Delta \nu \\ \Delta R \\ \Delta T \end{bmatrix} = \text{Differences from baseline values}$$

*Strictly speaking, the coefficents are nonlinear functions of ν, R, and T; however, they are linear functions of other functions. This simplification was used here for presentation clarity.

and the N × N partial derivative matrix is easily determined from the slopes of the lines relating each coefficient with each rate controlling parameter. The computation of the intermediate coefficients, using equation 9, is then straightforward.

Advanced Regression Considerations

The output of the interpolation algorithm is the set of SINH coefficients describing Fatigue Crack Propagation (FCP) under the conditions input. A parallel consideration, necessary in the modeling phase, is some multiple regression capability which will allow simultaneous consideration of several different collections of data, each differing from the others by only one FCP controlling parameter. The data for one test condition are usually regressed separately: data at one condition are not allowed to influence the model at another condition. However, if the final model is to be truly interpolative, behavior at one condition will be used to describe FCP at another condition. Therefore, the data must be permitted to exhibit their mutual influence during the modeling process.

Pratt & Whitney Aircraft has developed a mathematical technique to accomplish this. Individual sets of data are treated independently relative to some of the SINH coefficients, while the entire collection is treated as an entity with respect to the interpolative coefficents (functions of ν, R or T). This improved model has been programmed (MOD-1) and is in use. The P&WA modeling philosophy, the basic model formulation including characteristics of the sinh (math function) and SINH (model), as well as the SINH descriptions of basic FCP, have been discussed previously. The actual computational procedure required to perform the desired data modeling, referred to as the Method of Least Squares, is described in detail here.

The goal of this procedure is to determine model coefficients so that the resulting curve through the data will have the least (minimum) summed squared error between calculated and observed values for the dependent variable (Figure 33). In this instance, the independent and dependent variables, x and y, are log (ΔK) and log (da/dN), respectively.

Define the sum of the squared errors as

$$E^2 = \sum_{i=1}^{n} E_i^2 = \sum (y_{cal_i} - y_i)^2 \tag{11}$$

Since $y_{cal_i} = f(C_2, C_3, C_4, x_i)$, E is also a function of C_2, C_3, C_4.

Now, E^2 will be a minimum when each of its partial derivatives is zero simultaneously. That is

$$\frac{\partial E^2}{\partial C_2} = \frac{2E\partial E}{\partial C_2} = 0 \tag{12}$$

$$\frac{\partial E^2}{\partial C_3} = \frac{2E\partial E}{\partial C_3} = 0 \tag{13}$$

$$\frac{\partial E^2}{\partial C_4} = \frac{2E\partial E}{\partial C_4} = 0 \tag{14}$$

when f is the SINH model,

$$E_i = C_1 \sinh (C_2 (x_i + C_3)) + C_4 - y_i \tag{15}$$

and

$$\frac{\partial E}{\partial C_2} = C_1 \cosh (C_2 (x_i + C_3)) (x_i + C_3) \tag{16}$$

$$\frac{\partial E}{\partial C_3} = C_1 \cosh (C_2 (x_i + C_3)) (C_2) \tag{17}$$

$$\frac{\partial E}{\partial C_4} = 1 \tag{18}$$

Now, substituting equations 15, 16, 17 and 18 into equations 12, 13 and 14, and solving* the resulting three simultaneous equations provides the values for C_2, C_3 and C_4 for which equation 11 will be a minimum.

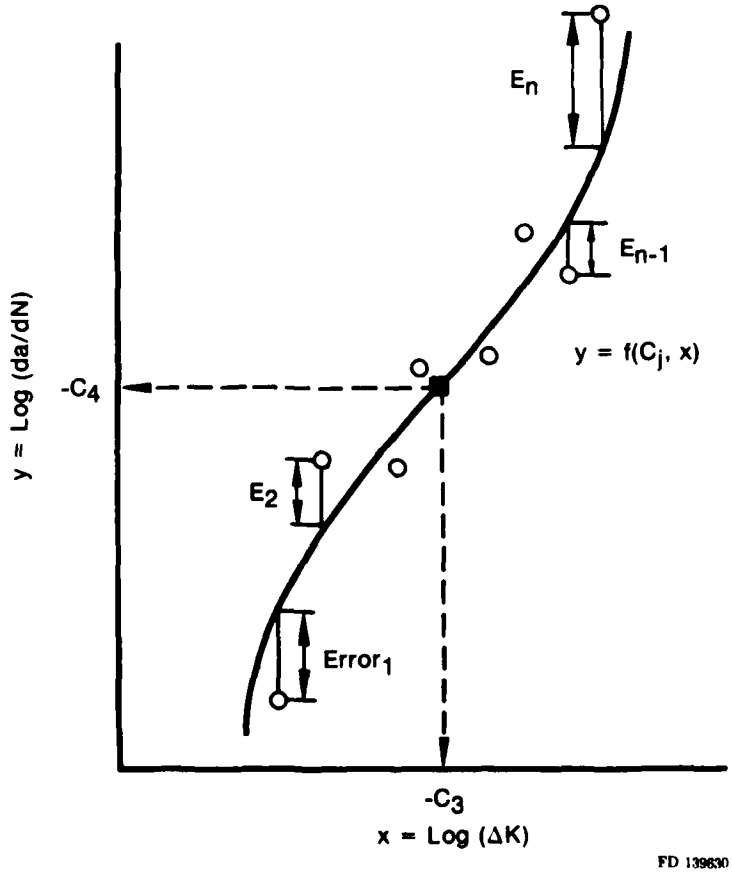

Figure 33. Method of Least Squares

* In this instance, the resulting simultaneous equations are nonlinear in C_2, C_3, and C_4. The solution therefore requires some iterative procedure such as an N-dimensional Newton-Raphson method.

The foregoing discussion explains the procedure for determining the coefficients for one SINH curve. Suppose further that each SINH representation of FCP is related to each other, the relationship depending on differences in frequency, stress ratio, or temperature. Consider frequency as an example, and assume that the points of inflection are linearly related, viz:

$$C_3,j = C_{33} + C_{34}\ (C_4,j) \tag{19}$$

for j different SINH curves.

Assume also that C_2 and C_4 are related to test frequency by equations 20 and 21:

$$C_4,j = C_{35} + C_{36}\ \log\ (\nu) \tag{20}$$

$$C_2,j = C_{37} + C_{38}\ \log\ (\nu) \tag{21}$$

Coefficients C_{33} through C_{38} can then be determined by substituting equations 19, 20 and 21 into equation 15 and differentiating with respect to C_{33} through C_{38} in a manner analogous to that used in determining C_2, C_3, and C_4 in the foregoing discussion.

Effect of Cyclic Frequency

Previous experience with P/M alloys indicates that changing test frequency, while holding stress ratio and temperature constant, produces crack growth curves similar in shape but shifted along a nearly vertical line passing through the points of inflection. The location of these inflection points is related to test frequency; reduced frequency (increased cycle duration) are observed to accelerate crack growth rate.

The AF2-1DA crack growth rates for cyclic frequencies 0.0083 Hz, 0.17 Hz, and 20 Hz (649°C, R = 0.5) are shown individually in Figures 34, 35 and 36, respectively. The comparison of these crack growth rates is shown in Figure 37; note that points of inflection are represented by a piecewise linear function, with each segment having the form: $C_3 = C_{33} + C_{34} \times C_4$. Figure 38 illustrates the relationships between C_2, C_3, C_4, and frequency.

The coefficients are linearly related and equations for all interpolative SINH frequency model coefficients are shown in Figure 38, except C_1 which was held constant at 0.5. This model completely describes the effect of frequency on FCP in AF2-1DA at this temperature and stress ratio.

Effect of Stress Ratio

As with frequency, stress ratio effects are easily described using the SINH model. The individual data sets used in the 649°C, 20 Hz stress ratio model (R = 0.1, R = 0.5, R = 0.8) are shown in Figures 39, 40 and 41. The comparison of these crack growth rates is shown in Figure 42. As indicated by Figure 42, it was necessary to use a piece-wise linear function to describe the relationship between C_3 and C_4. Each segment of this function is of the form:

$$C_3 = C_{33} + C_{34} \times C_4.$$

The SINH crack growth rate curve can be calculated for any positive stress ratio by using the relationships between C_2, C_3, and C_4, and stress ratio given in Figure 43. Again, C_1 was held constant at 0.5 completing the model. This model completely describes the effects of stress ratio at this temperature and frequency.

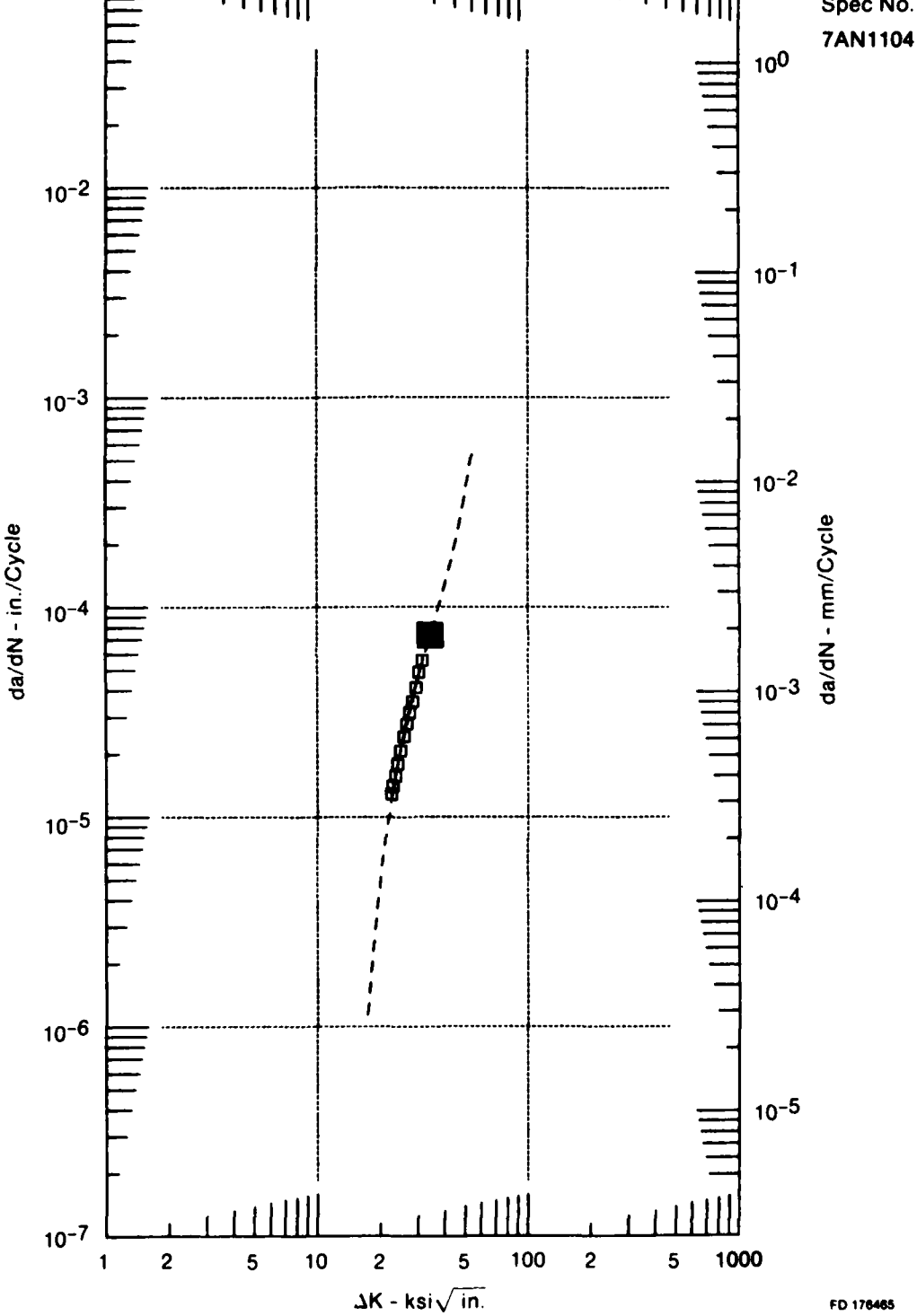

Figure 34. AF2-1DA Crack Growth Data at 649°C, 0.0083 Hz, R = 0.1

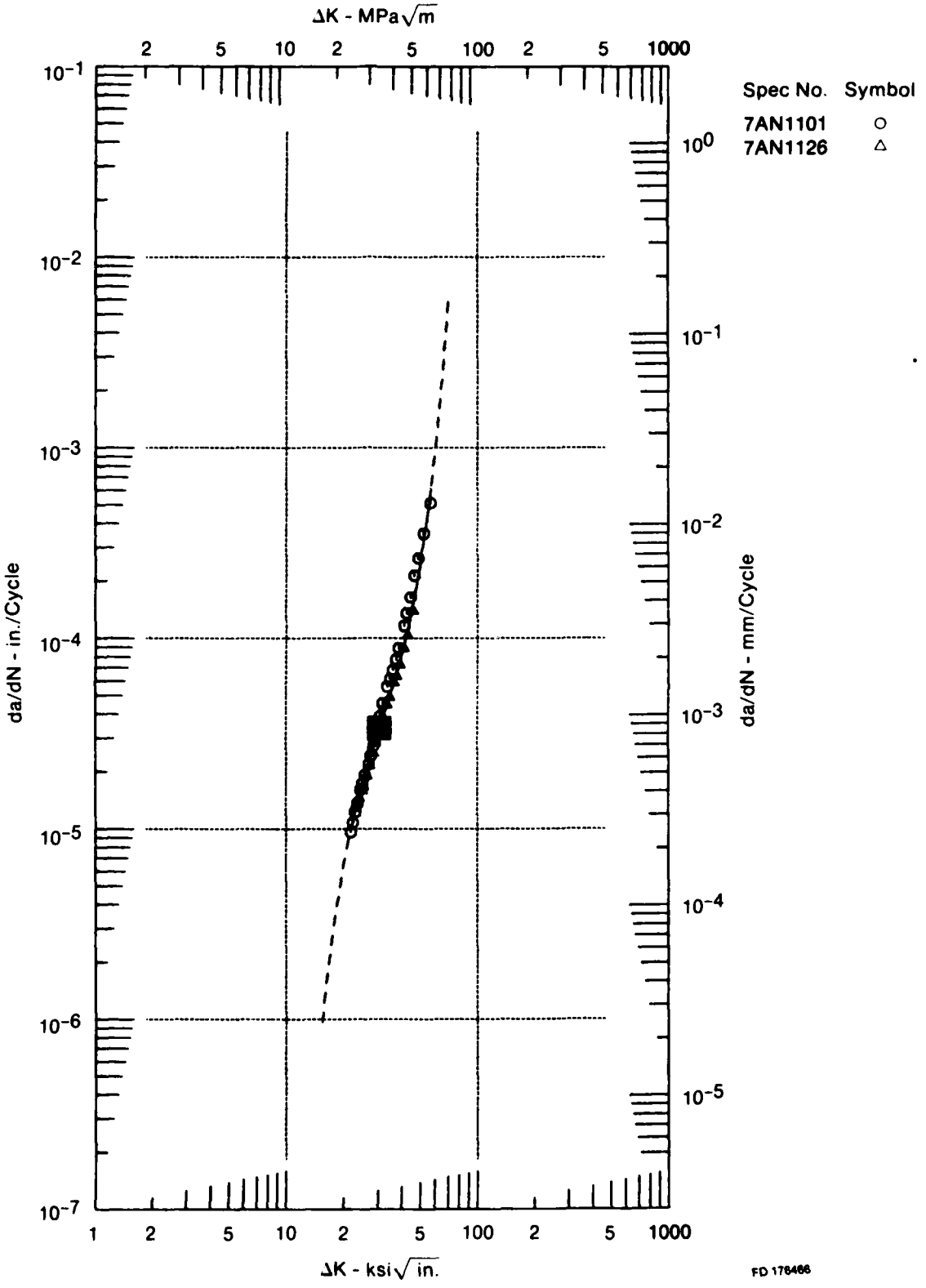

Figure 35. AF2-1DA Crack Growth Data at 649°C, 0.17 Hz, R = 0.1

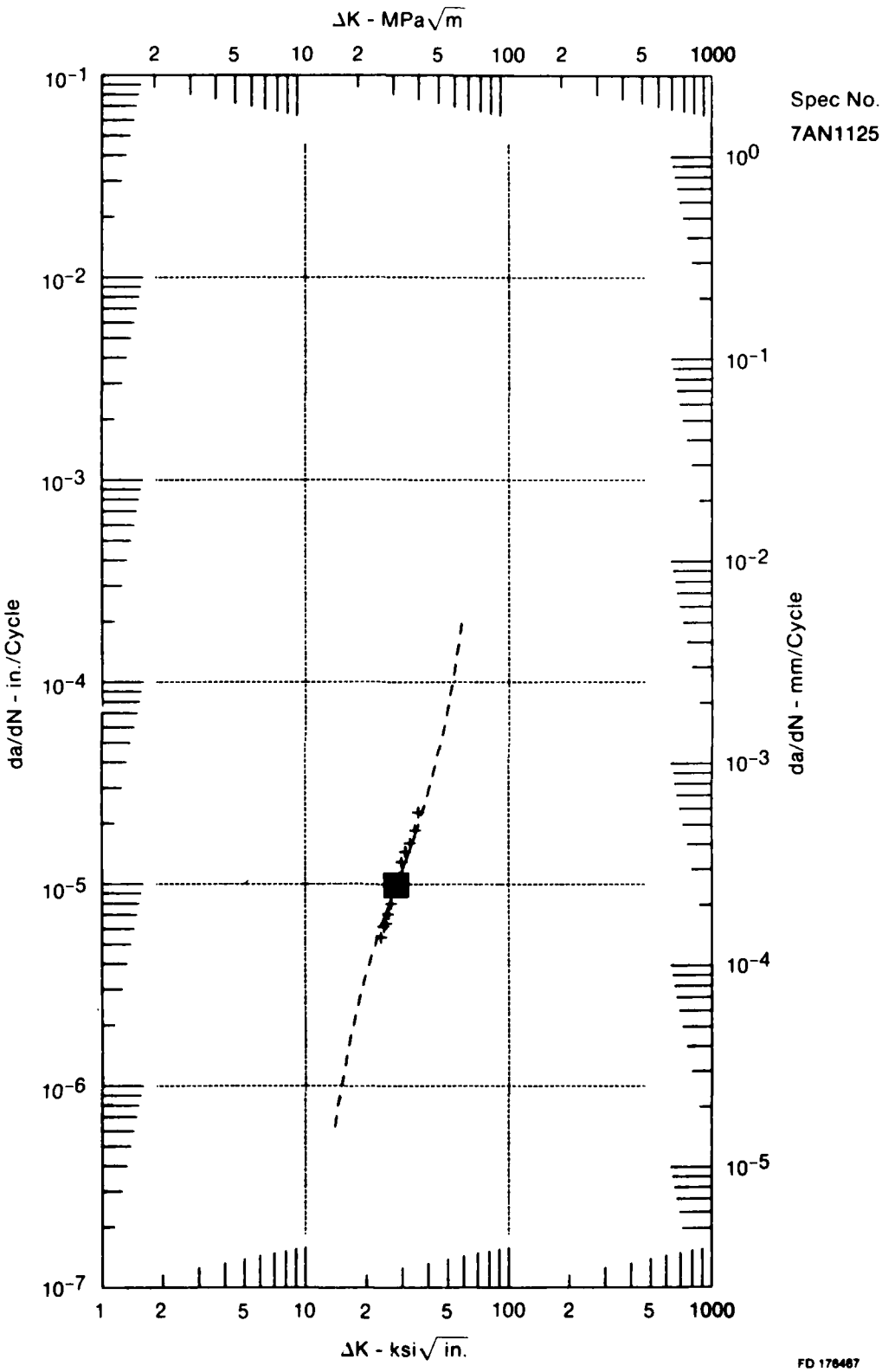

Figure 36. AF2-1DA Crack Growth Data at 649°C, 20 Hz, R = 0.1

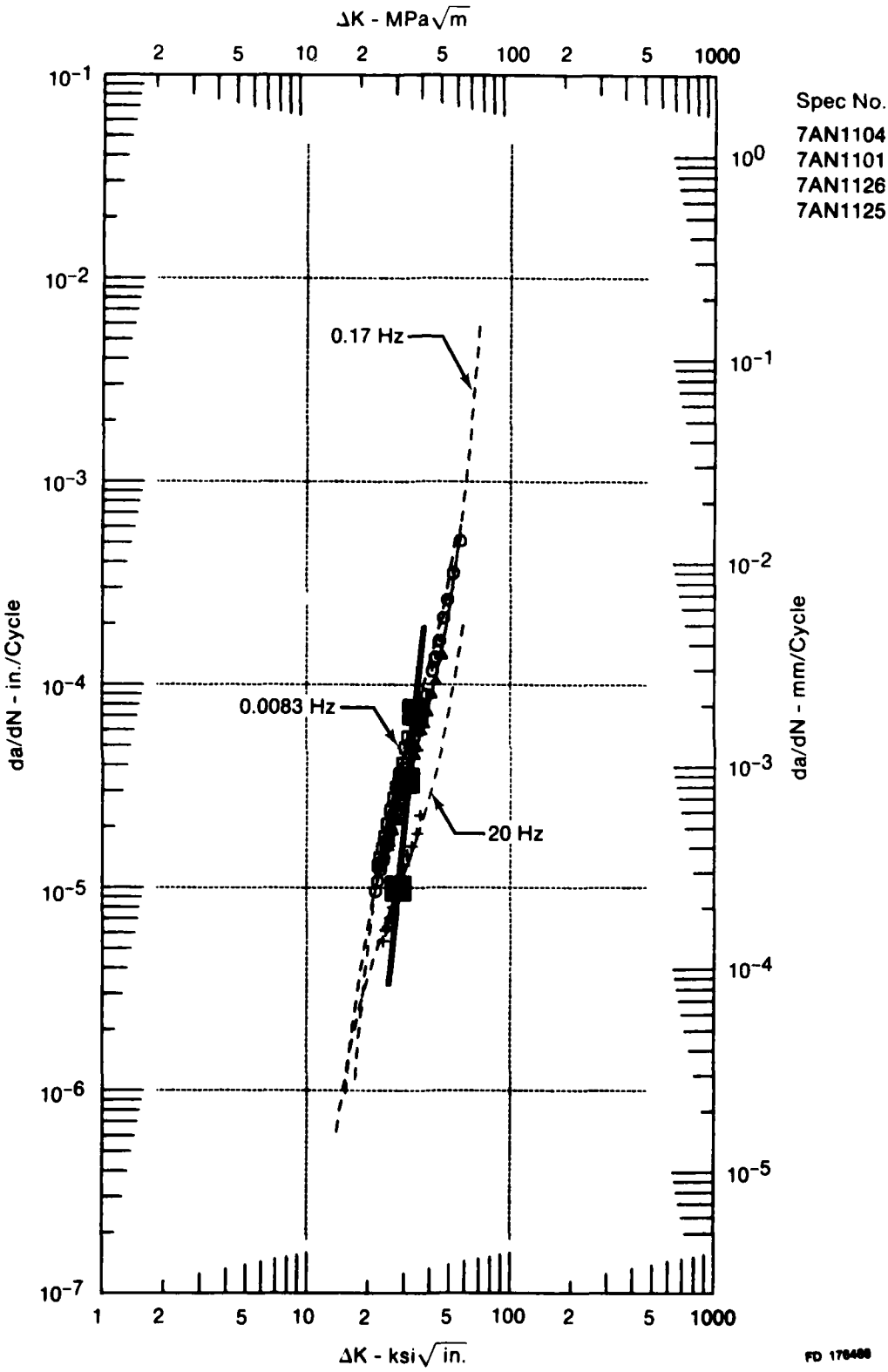

Figure 37. Effect of Frequency on Crack Growth Rates at 649°C, R = 0.1

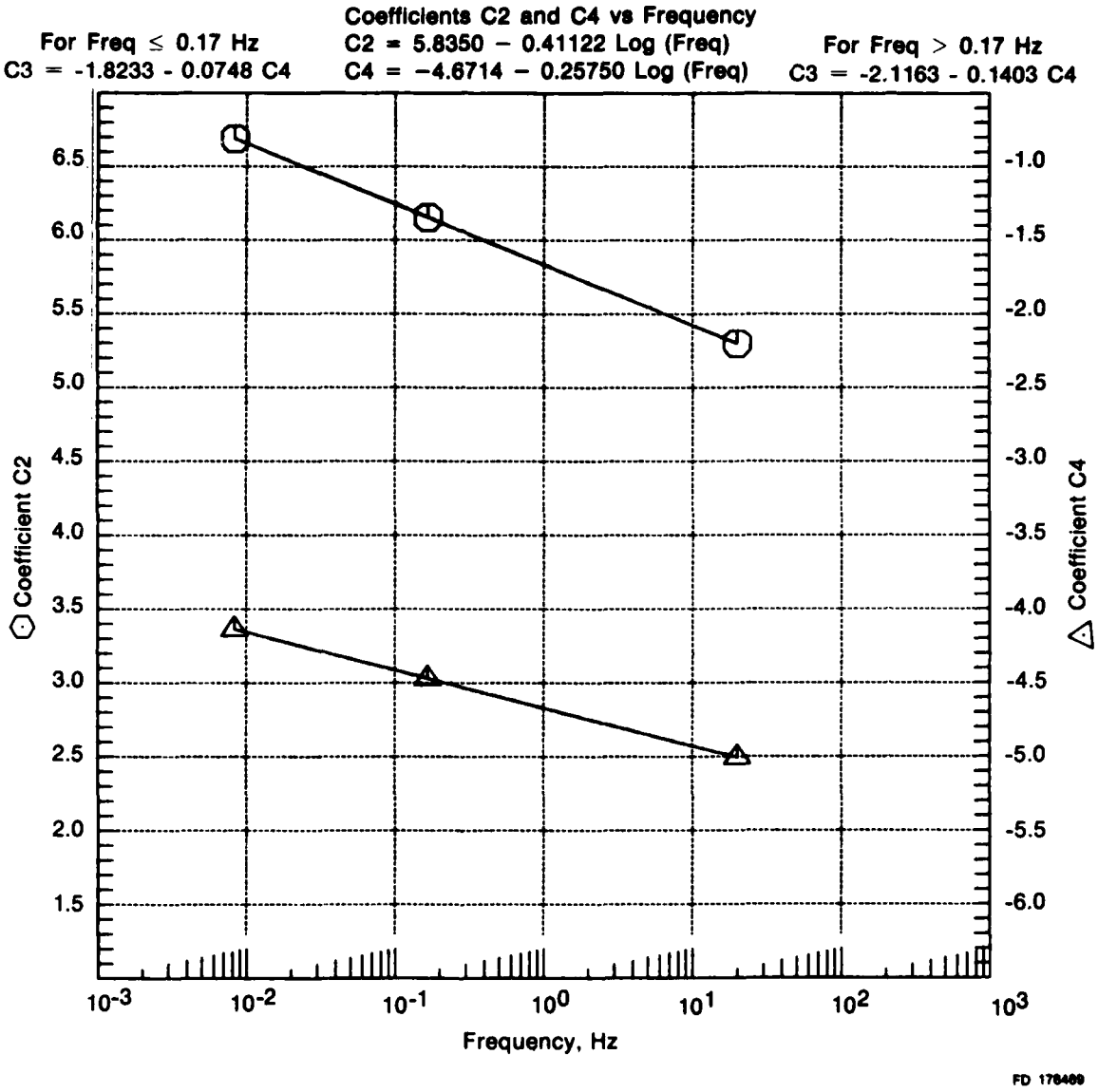

Figure 38. Effect of Frequency on SINH Coefficients, 649°C, R = 0.1

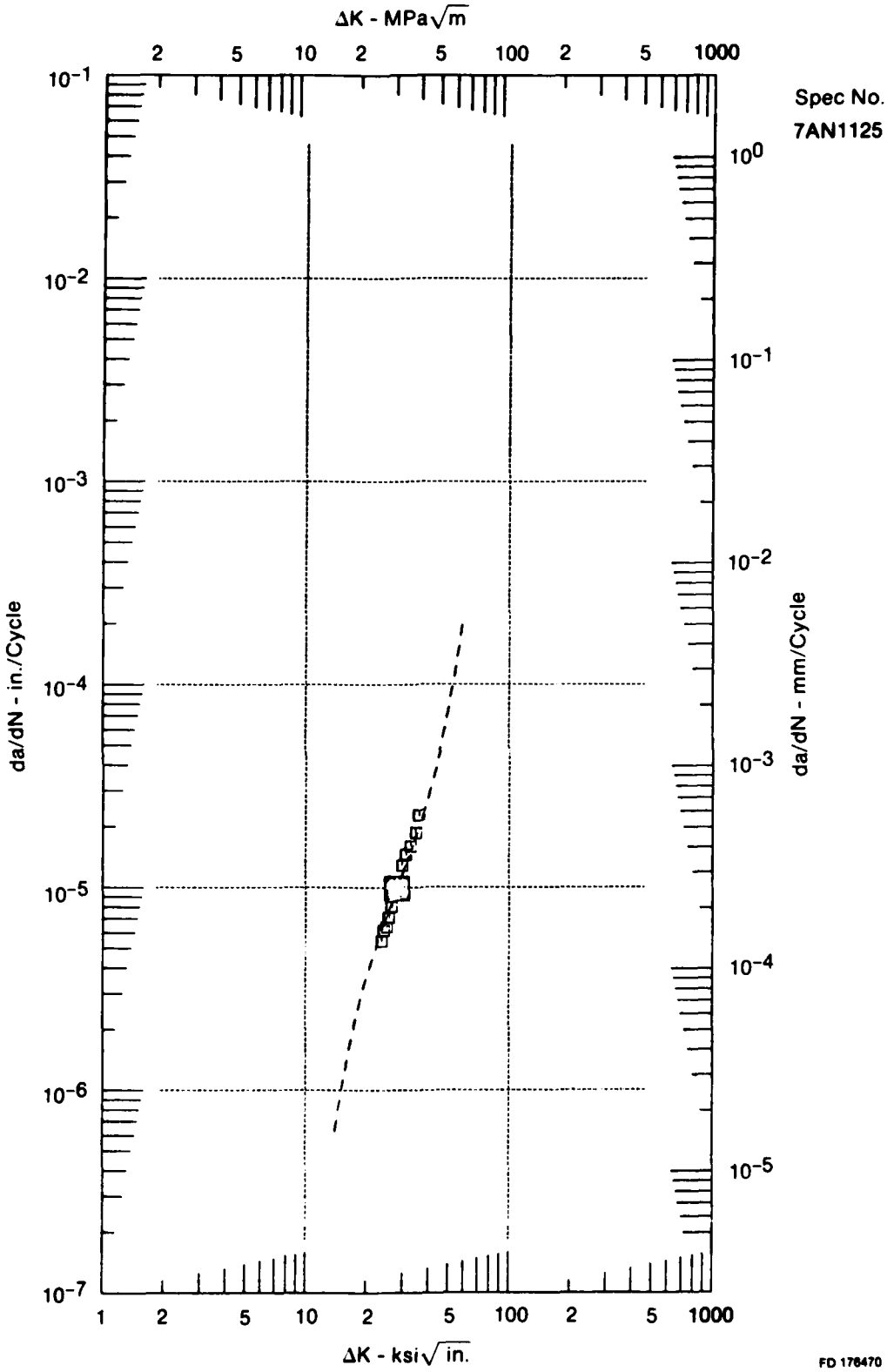

Figure 39. AF2-1DA Crack Growth Data at 649°C, 20 Hz, R = 0.1

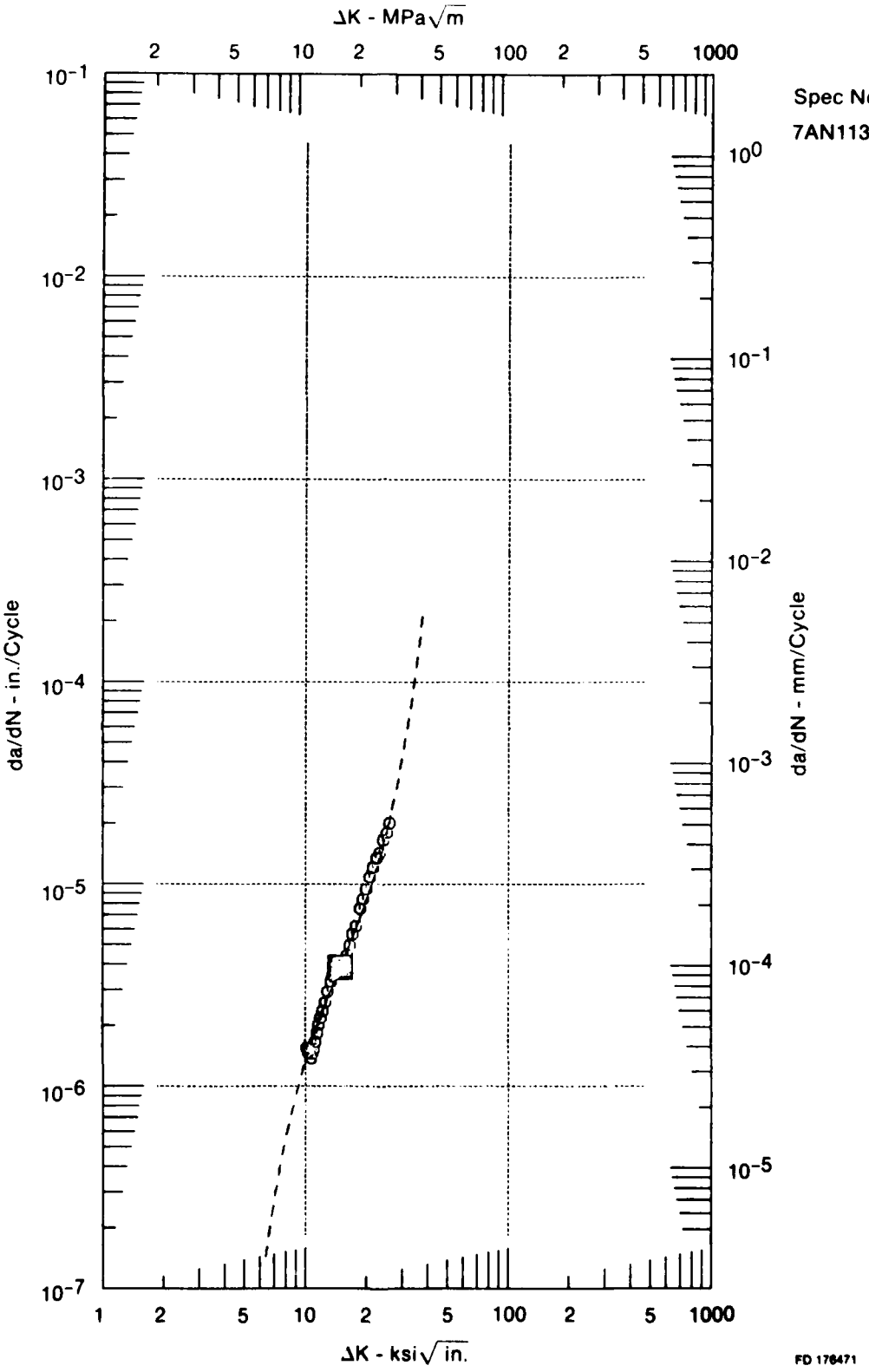

Figure 40. AF2-1DA Crack Growth Data at 649°C, 20 Hz, R = 0.5

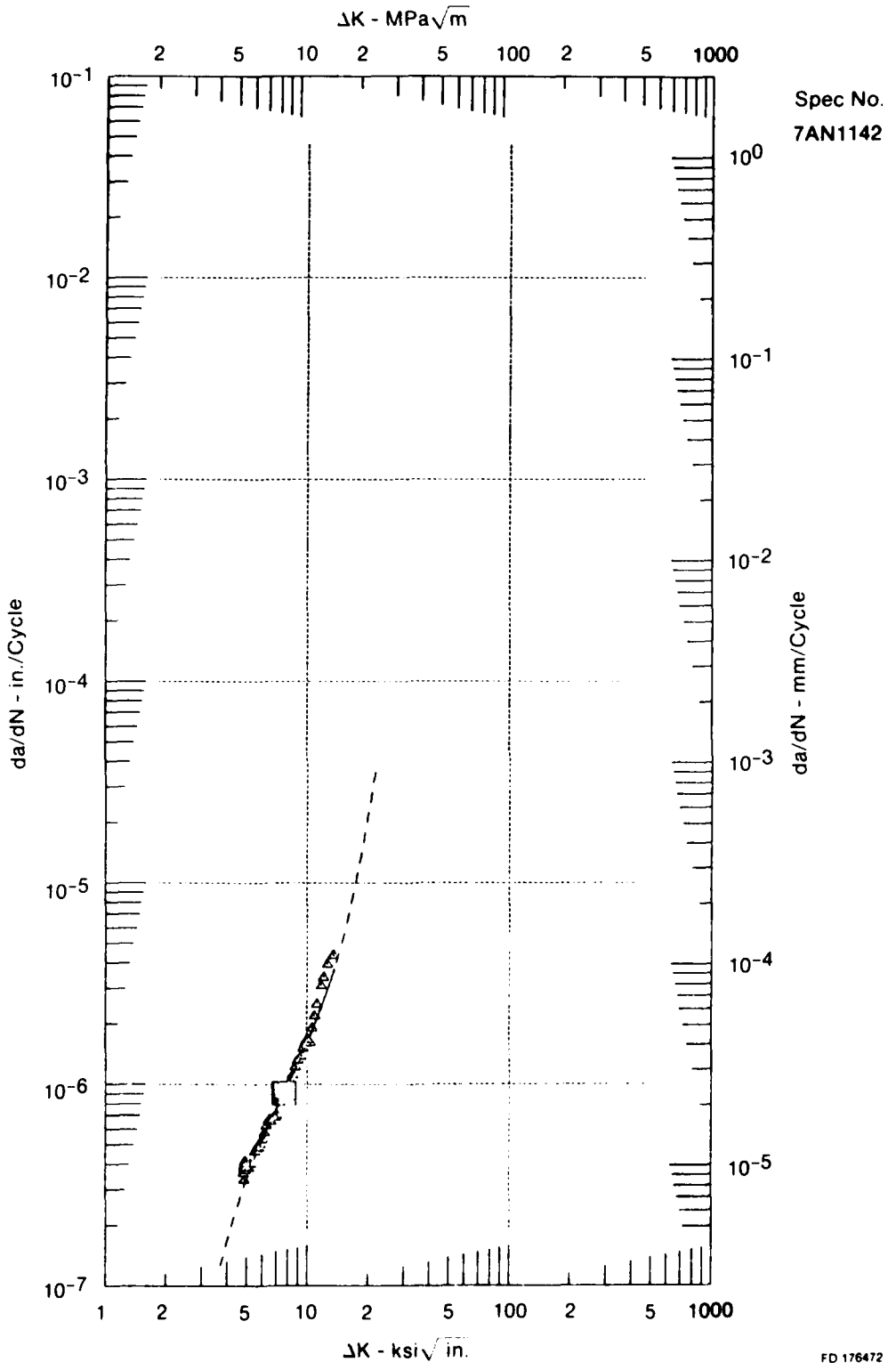

Figure 41. AF2-1DA Crack Growth Data at 649°C, 20 Hz, R = 0.8

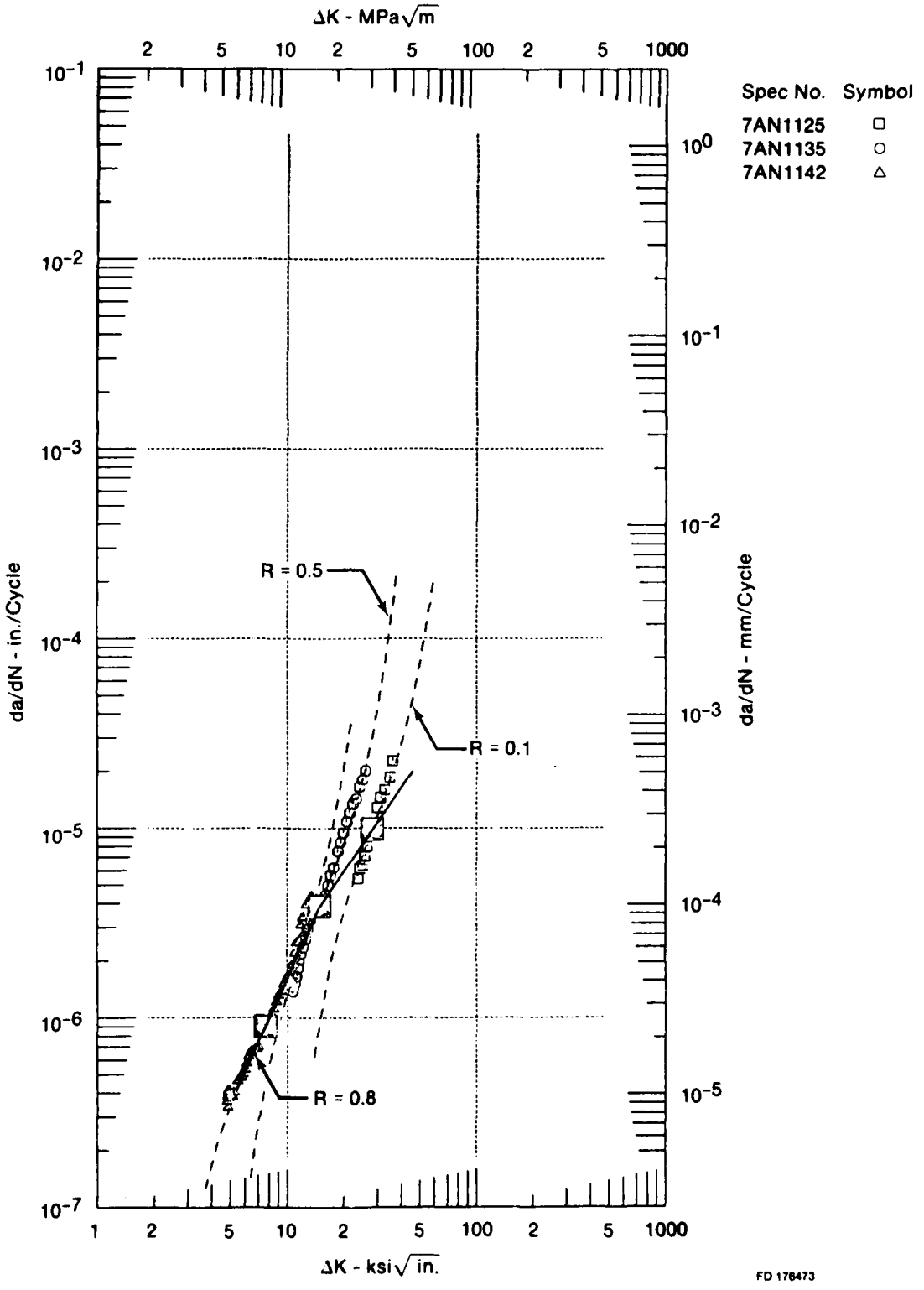

Figure 42. Effect of Stress Ratio on Crack Growth Rates at 649°C, 20 Hz

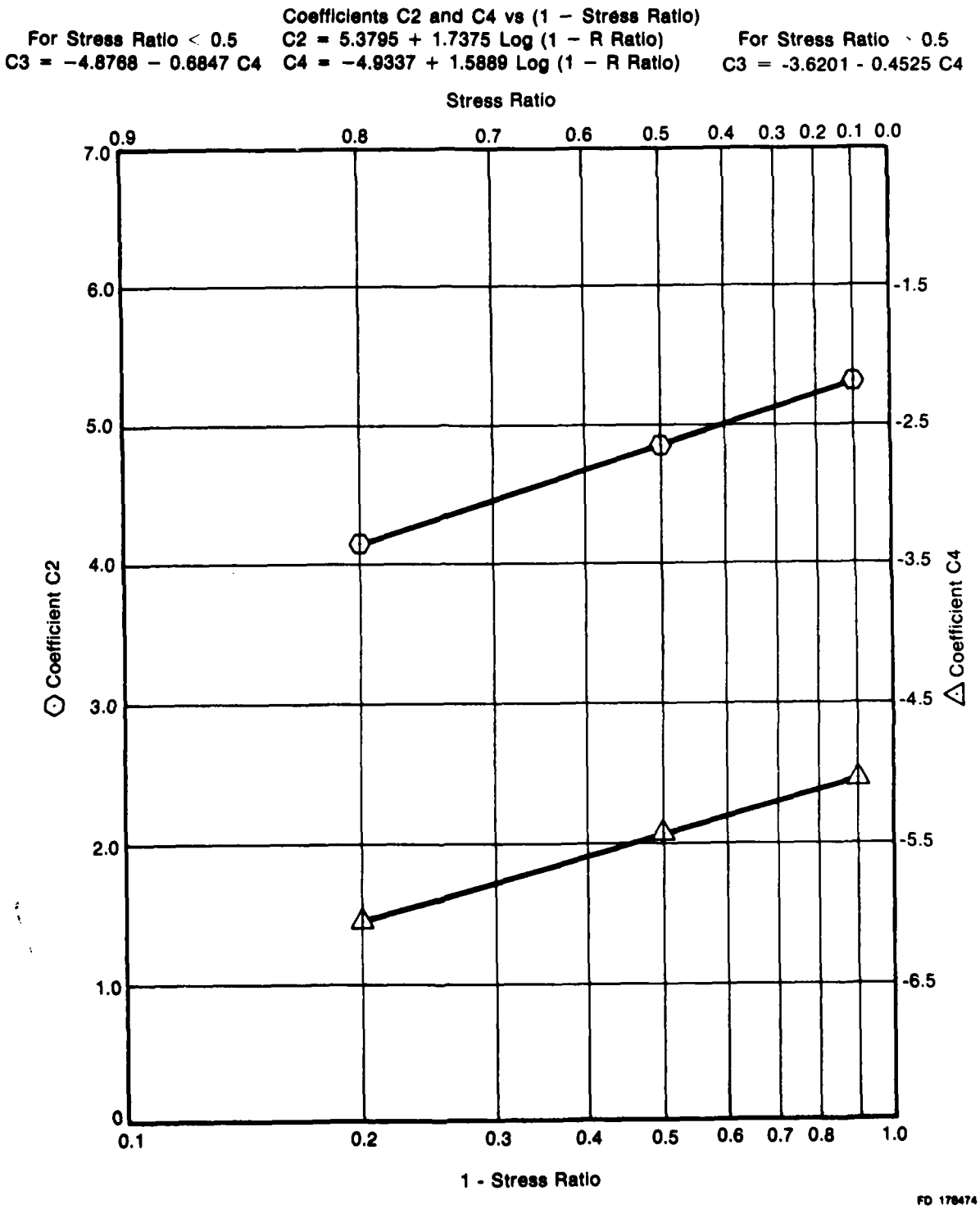

Figure 43. Effect of Stress Ratio on SINH Coefficients, 649°C, 20 Hz

The individual data sets used in the 649°C, 0.17 Hz stress ratio model (R = 0.1, R = 0.5) appear in Figures 44 and 45. The points of inflection describe a straight line in Figure 46 such that C_3 (horizontal inflection location) is a linear function of C_4 (vertical location); $C_3 = C_{33} + C_{34} \times C_4$. The SINH crack growth rate curve can be calculated for any positive stress ratio (keeping temperature and frequency constant) by using the relationship between stress ratio and C_2, C_3, and C_4 given in Figure 47.

The individual data sets used in the 649°C, 0.0083 Hz stress ratio model (R = 0.1, R = 0.5, R = 0.8) appear in figures 48, 49, and 50. Again, comparison of these crack growth rates in Figure 51 indicates that the points of inflection describe a straight line. The SINH crack growth rate curve can be calculated for any positive stress ratio by using the relationship between stress ratio and C_2, C_3, and C_4 given in Figure 52.

Since the effect of stress ratio on crack growth rates can vary significantly with frequency (Reference 1), a stress ratio model is needed near the extremes of the frequencies of interest. In this case, the 20 Hz model and the 0.0083 Hz model, which were discussed in the preceding paragraphs, are used in conjunction with the 0.17 Hz model to describe the effects of stress ratio over the active frequency range.

Effect of Temperature

Similar to frequency and stress ratio, the effects of temperature can be described using the SINH model. Figures 53, 54 and 55 show the individual data sets (427, 649 and 760°C) used in the temperature model. The composite plot of these data sets (Figure 56) shows that once again the inflection points describe the straight line $C_3 = C_{33} + C_{34} \times C_4$. The relationship between C_2, C_4, and temperature is shown in Figure 57 with the equations for all the SINH model coefficients except C_1 ($C_1 = 0.5$). This model completely describes the effects of temperature on AF2-1DA crack growth rates even where data are unavailable.

Effect of Hold Time

The length of time a crack tip is subjected to maximum tensile load each cycle will obviously affect the crack growth rate. The differences in propagation rates due to varying hold times can be characterized by the SINH model. Figures 58 through 61 illustrate the 649°C, R = 0.1, individual data sets at 30 sec, 120 sec, 300 sec, and 600 sec hold times, respectively. The effect of these hold times on crack growth rate can easily be seen in Figure 62, as can the linear relationship ($C_3 = C_{33} + C_{34} \times C_4$) between the inflection points. The relationship between C_2, C_4 and hold time is shown in Figure 63. This SINH model describes the effects of maximum tensile hold time on AF2-1DA crack growth rates between 30 sec and 600 sec hold times (649°C, R = 0.1), even where data are unavailable.

As temperature increases, the amount of oxidation and creep at the crack tip also increases, therefore, larger differences in crack growth rates due to changes in hold times are expected. The individual data sets for the 760°C dwell model are shown in Figures 64 and 65 (zero and 120 sec dwells). Only a two-point model is used (Figure 66) for reasons explained in the Model Verification Section. The SINH crack growth rate curve can be calculated for any hold time between zero and 120 seconds (760°C, R = 0.1) by using the relationships, given in Figure 67, between C_2, C_3, C_4 and maximum tensile hold time.

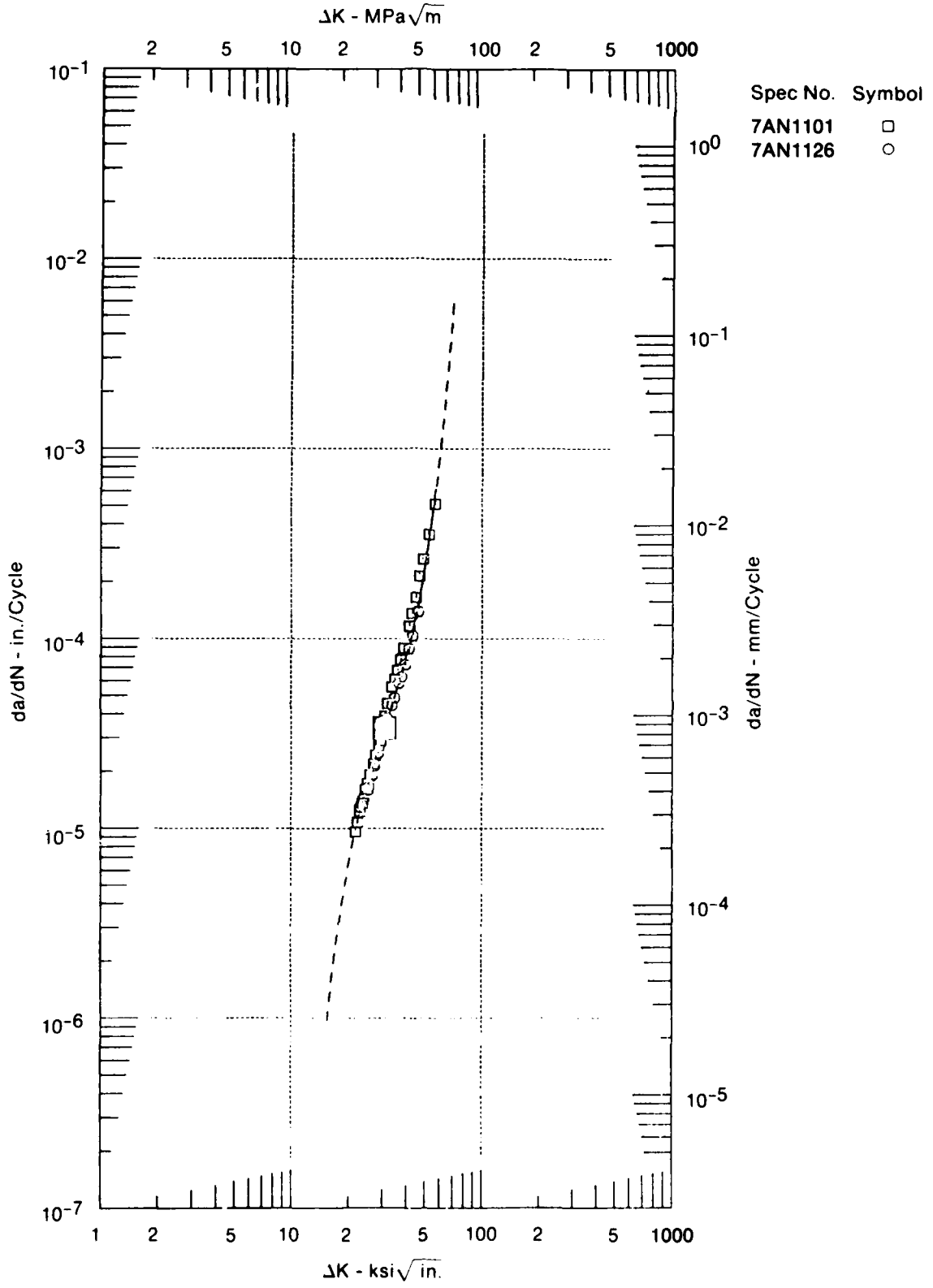

Figure 44. AF2-1DA Crack Growth Data at 649°C, 0.17 Hz, R = 0.1

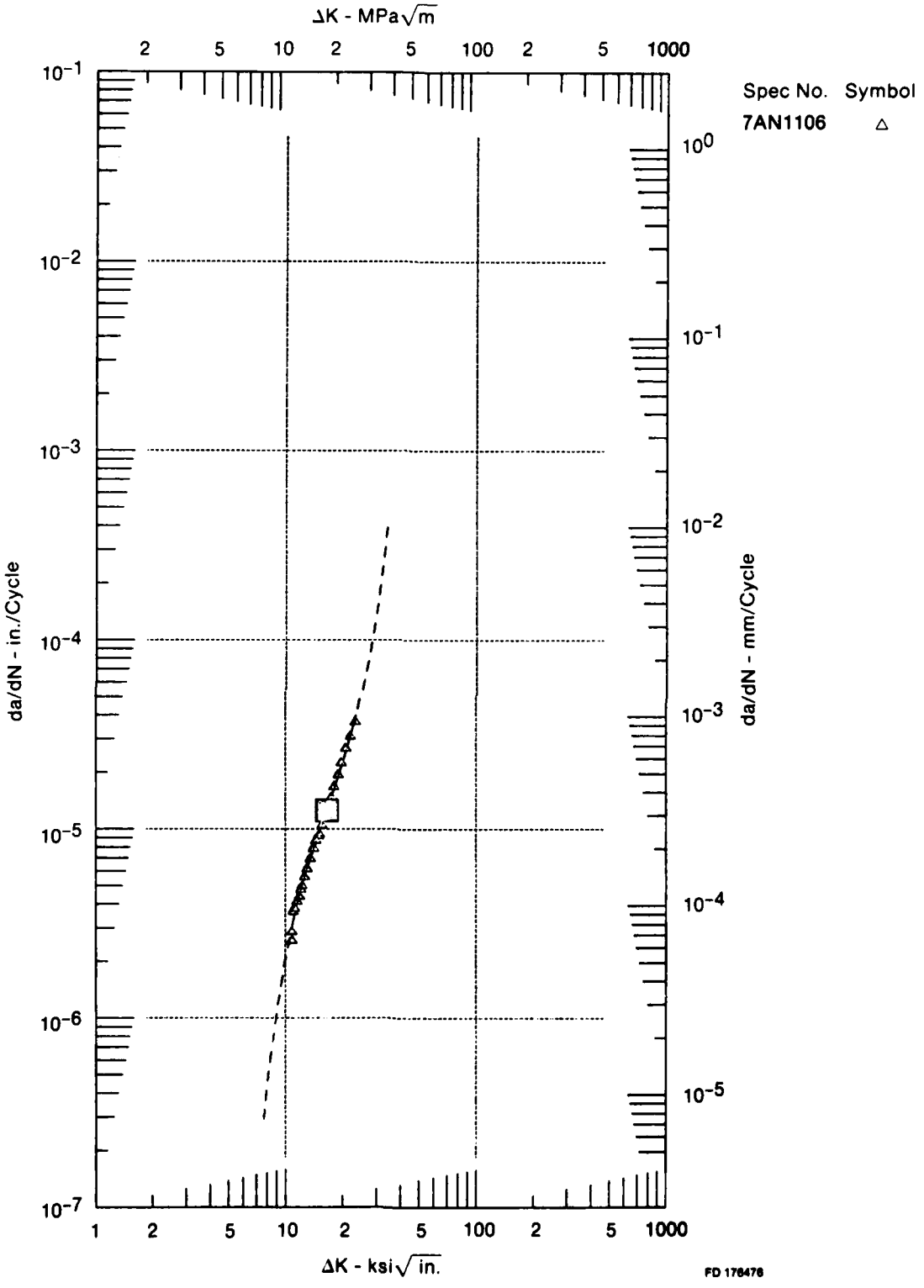

Figure 45. AF2-1DA Crack Growth Data at 649°C, 0.17 Hz, R = 0.5

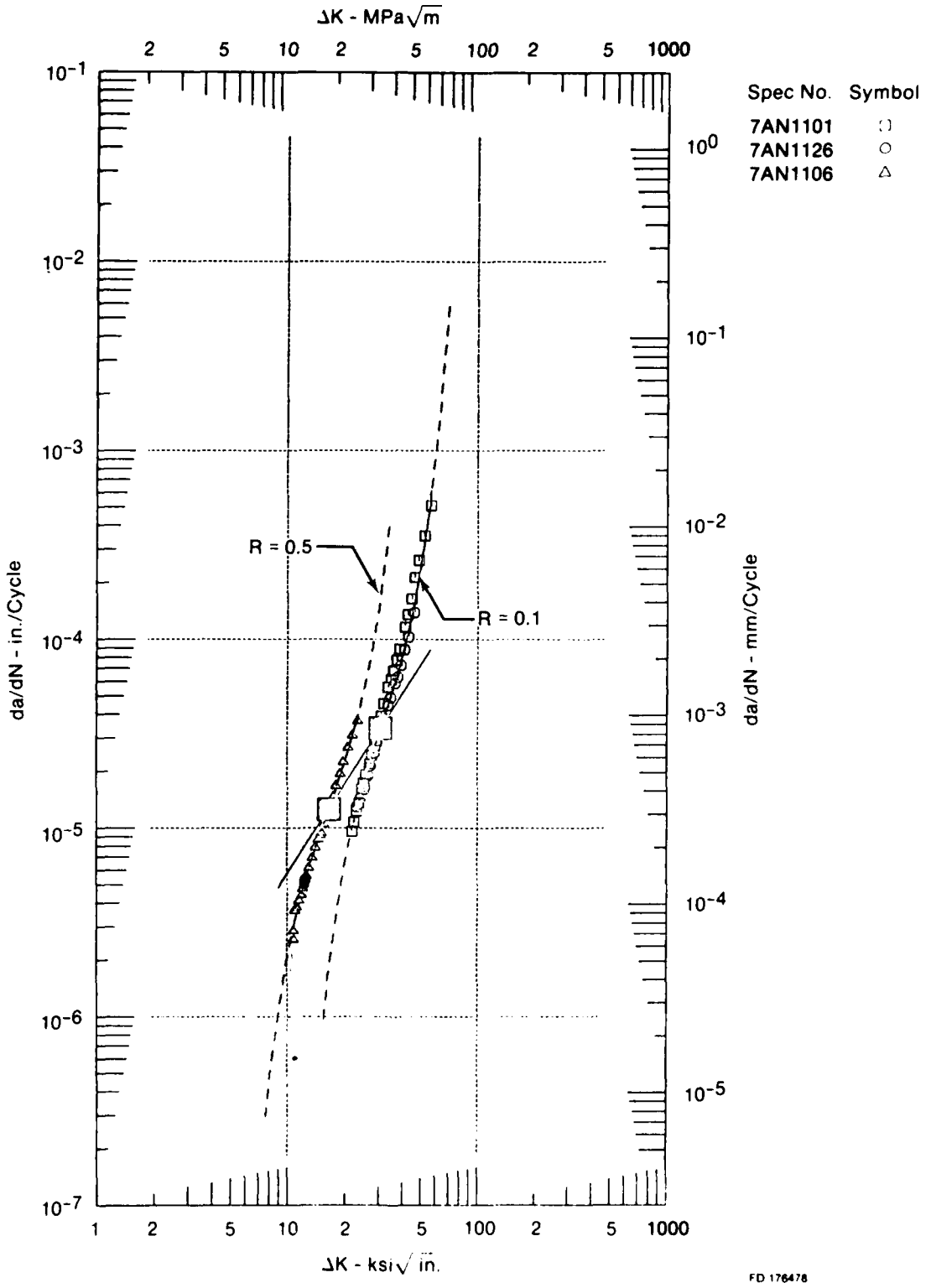

Figure 46. Effect of Stress Ratio on Crack Growth Rate at 649 C, 0.17 Hz

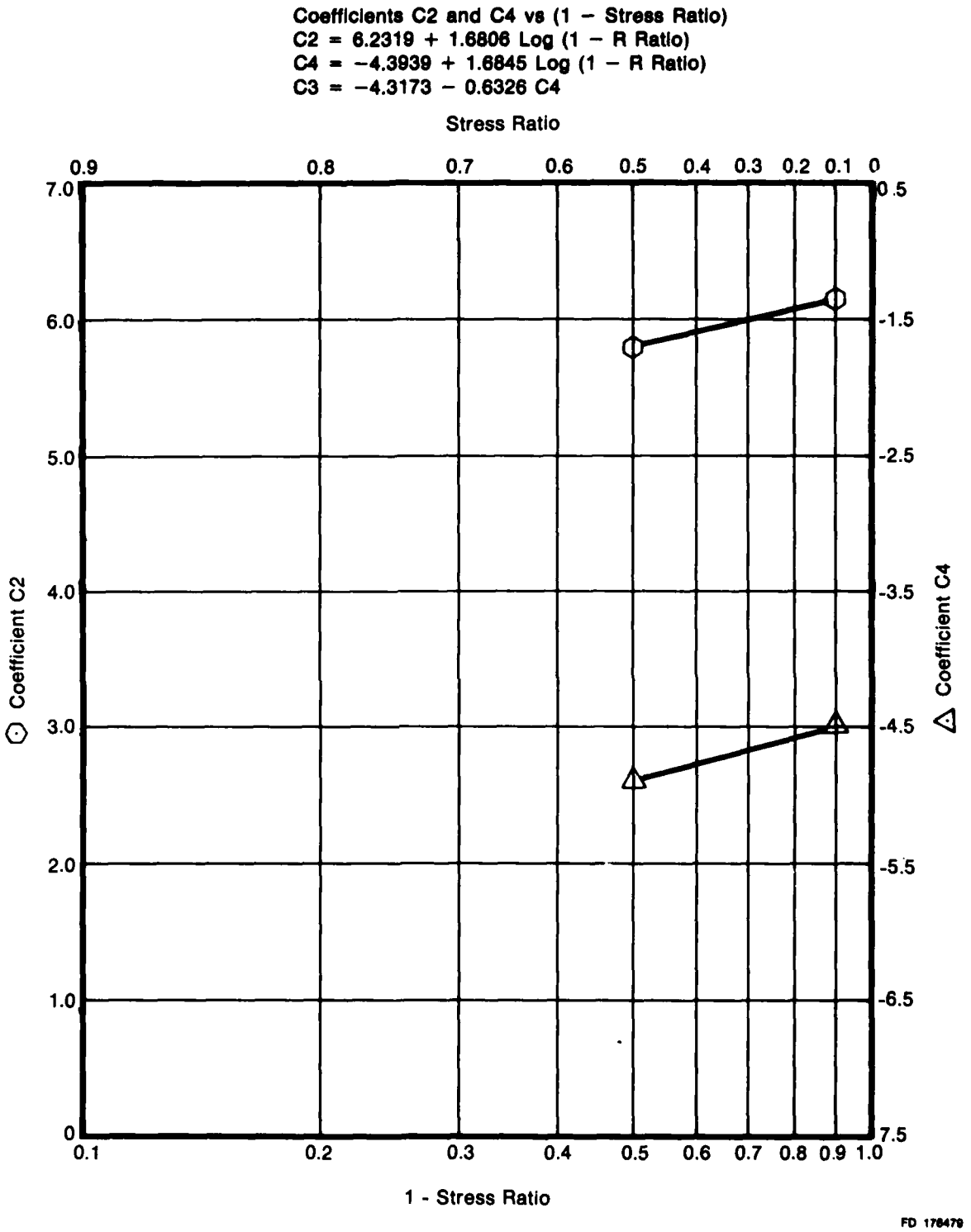

Figure 47. Effect of Stress Ratio on SINH Coefficients, 649°C, 0.17 Hz

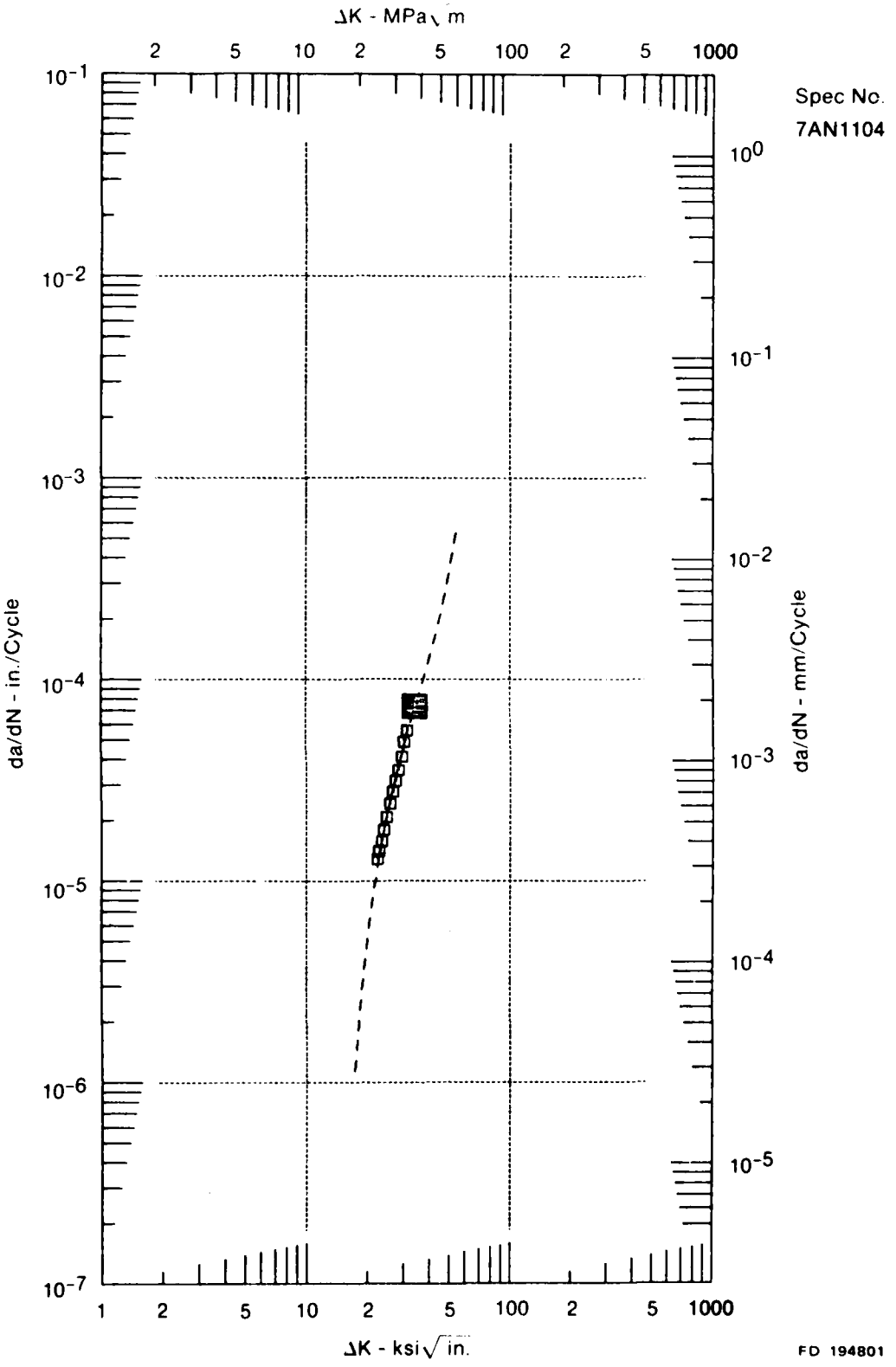

Figure 48. AF2-1DA Crack Growth Data at 649°C, 0.0083 Hz, R= 0.1

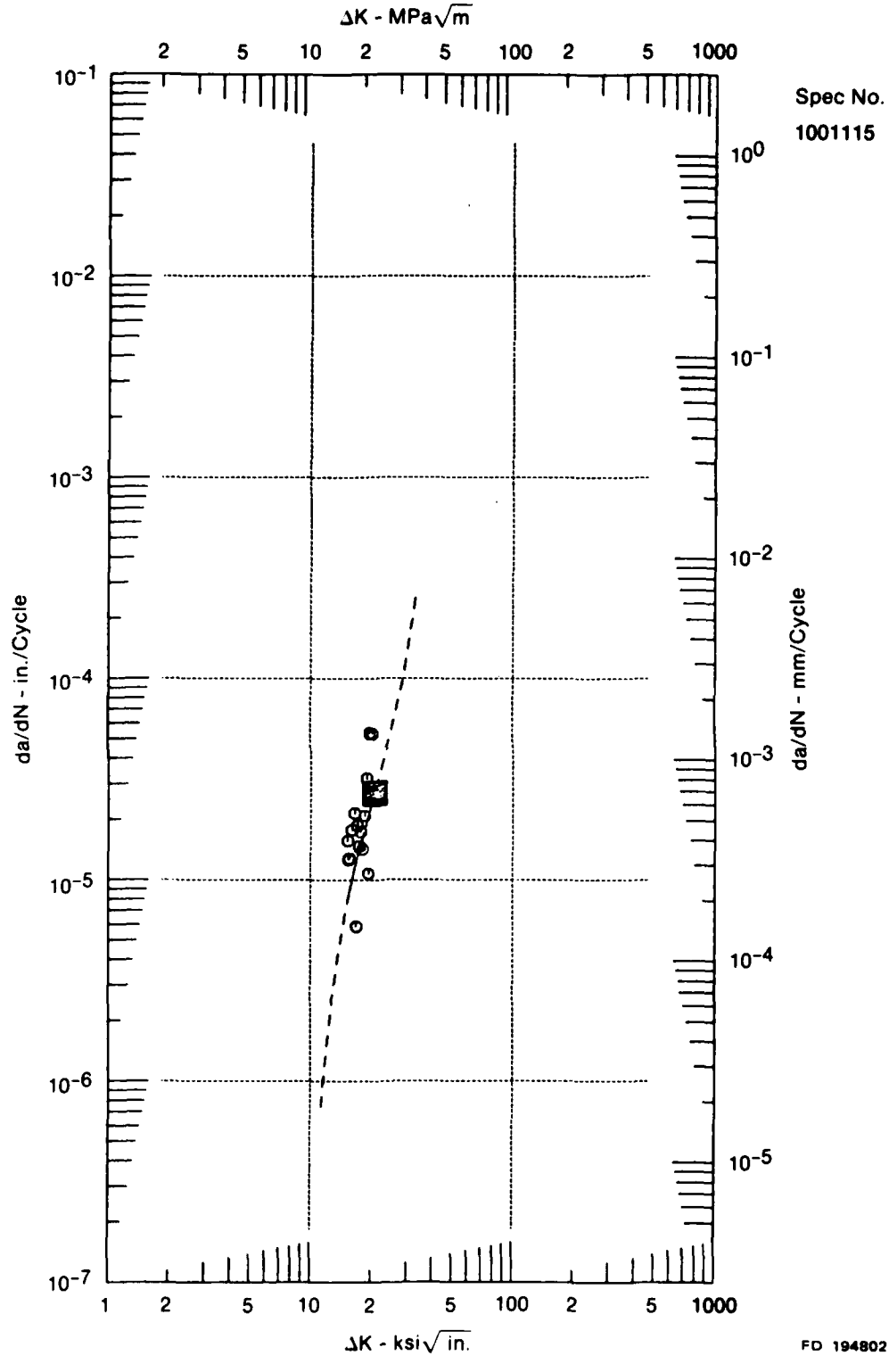

Figure 49. AF2-1DA Crack Growth Data at 649°C, 0.0083 Hz, R= 0.5

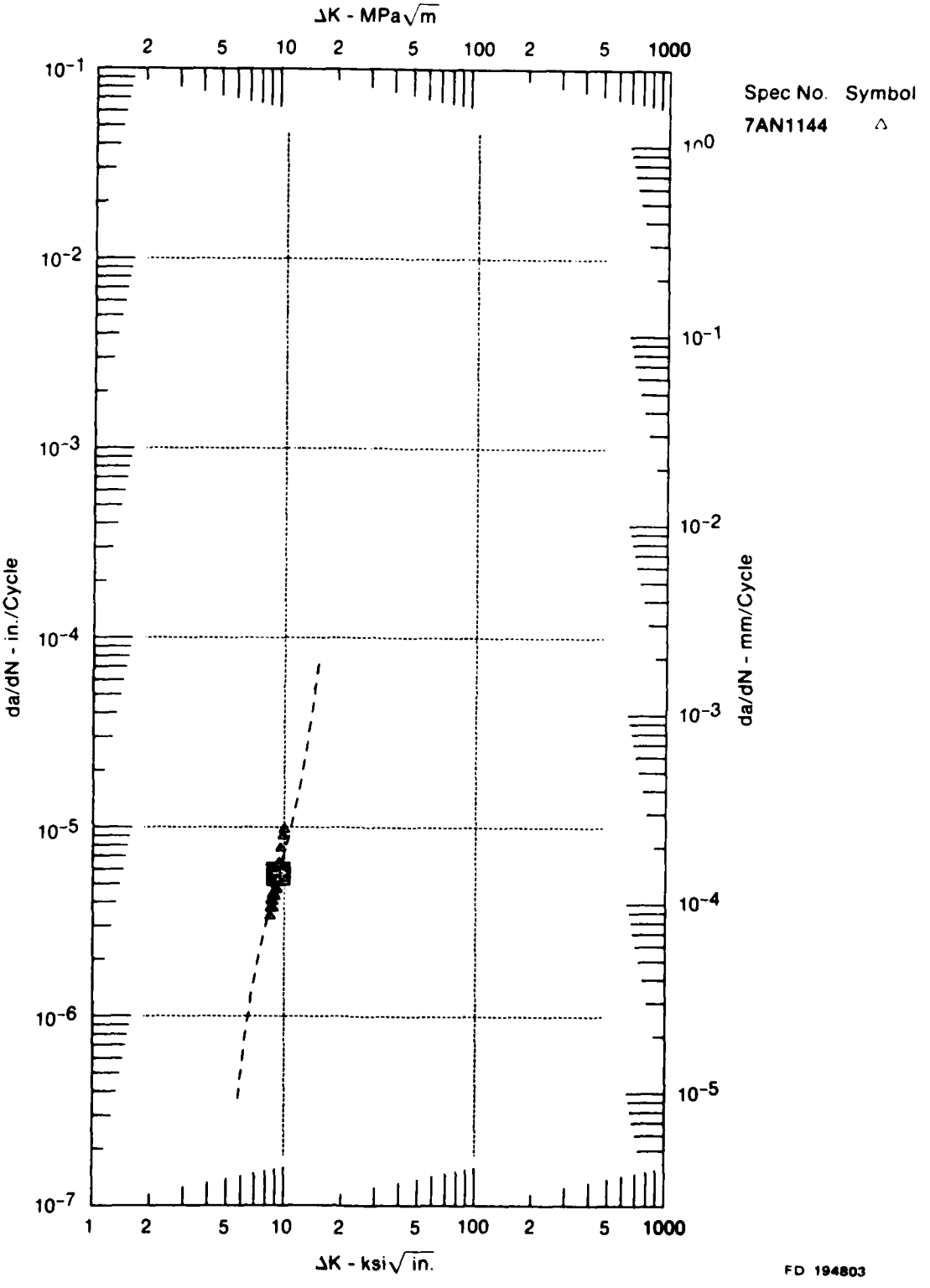

Figure 50. AF2-1DA Crack Growth Data at 649°C, 0.0083 Hz, R= 0.8

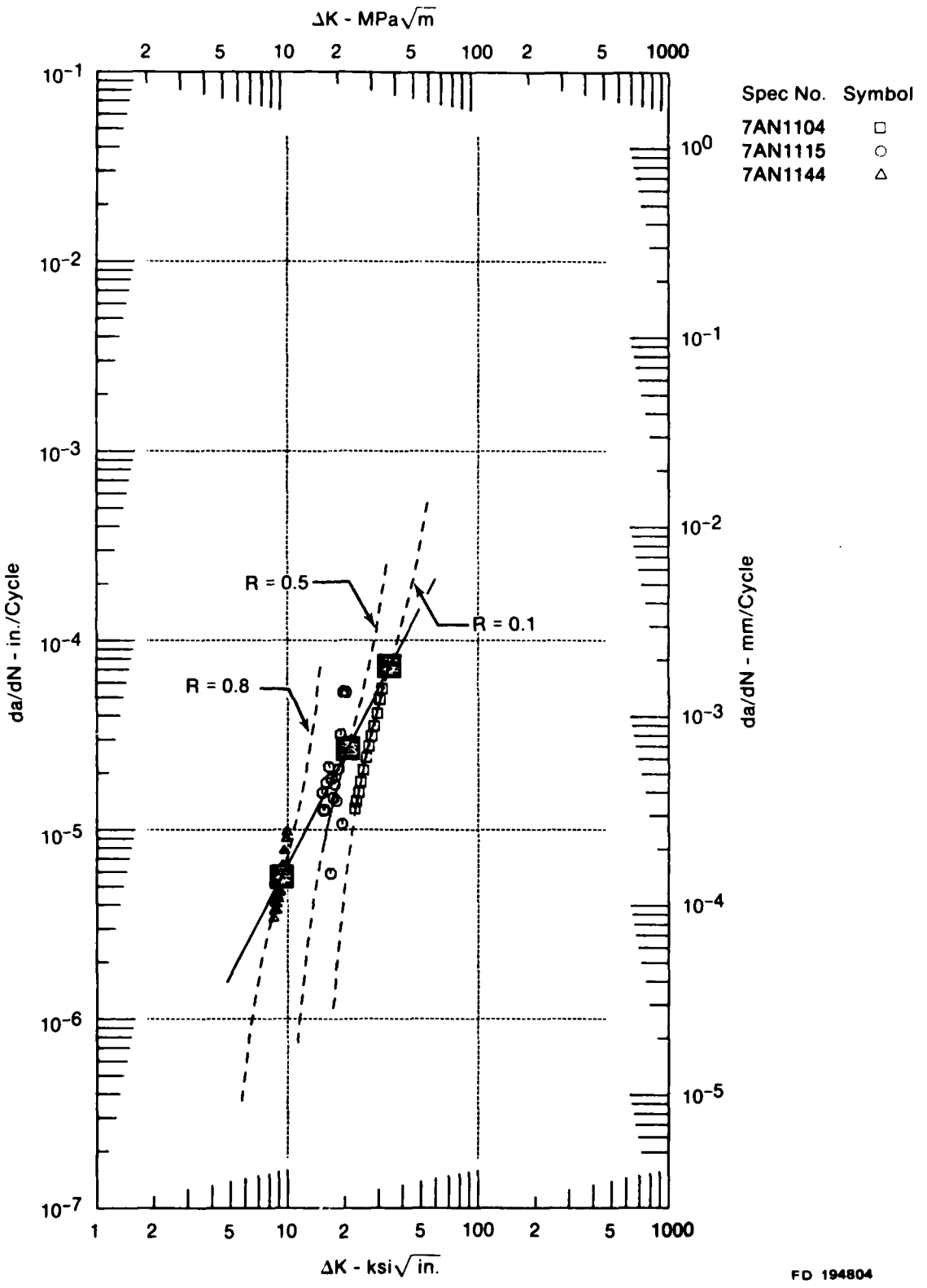

Figure 51. Effect of Stress Ratio on Crack Growth Rates at 649°C, 0.0083 Hz

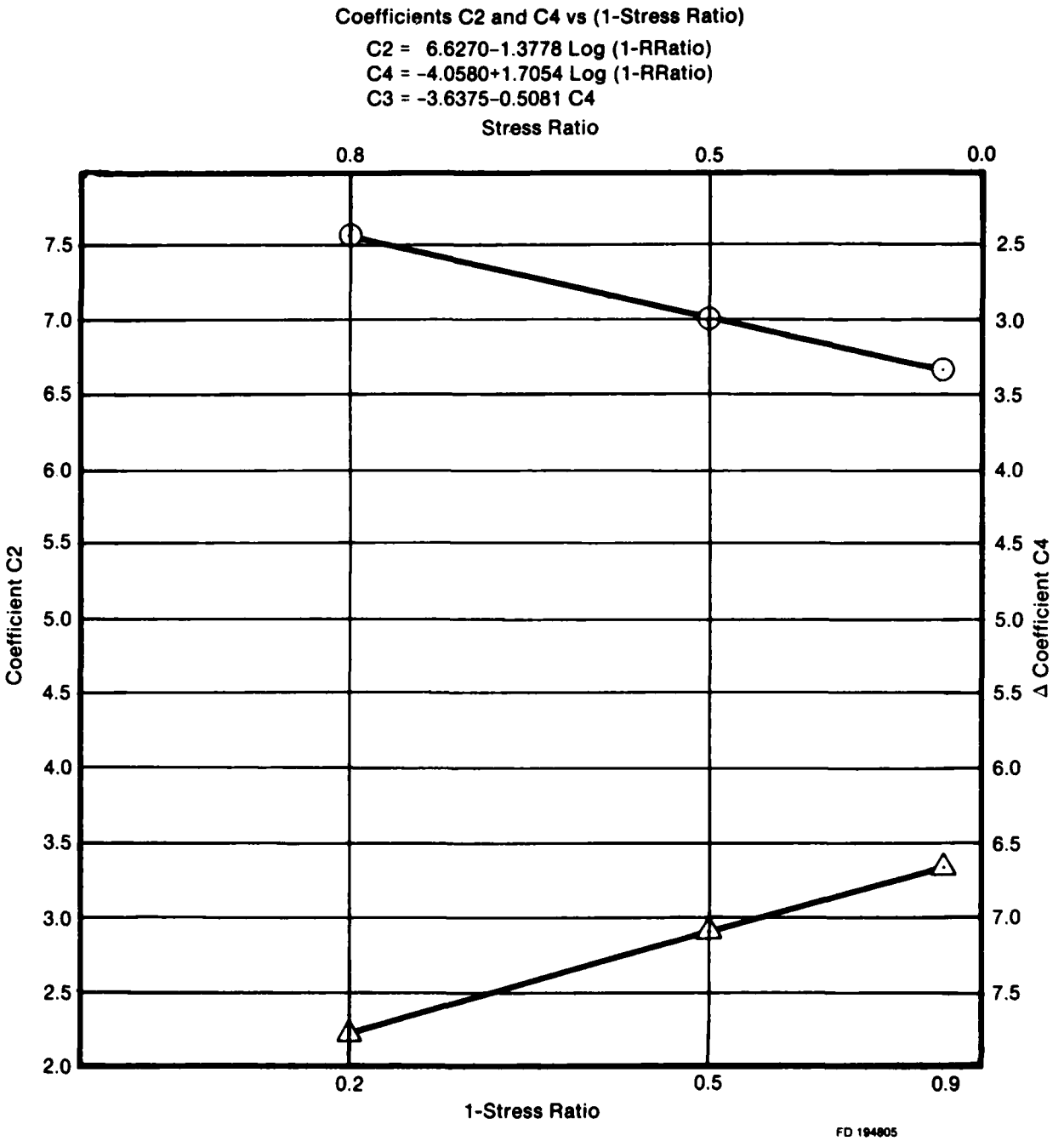

Figure 52. Effect of Stress Ratio on SINH Coefficients, 649°C, 0.0083 Hz

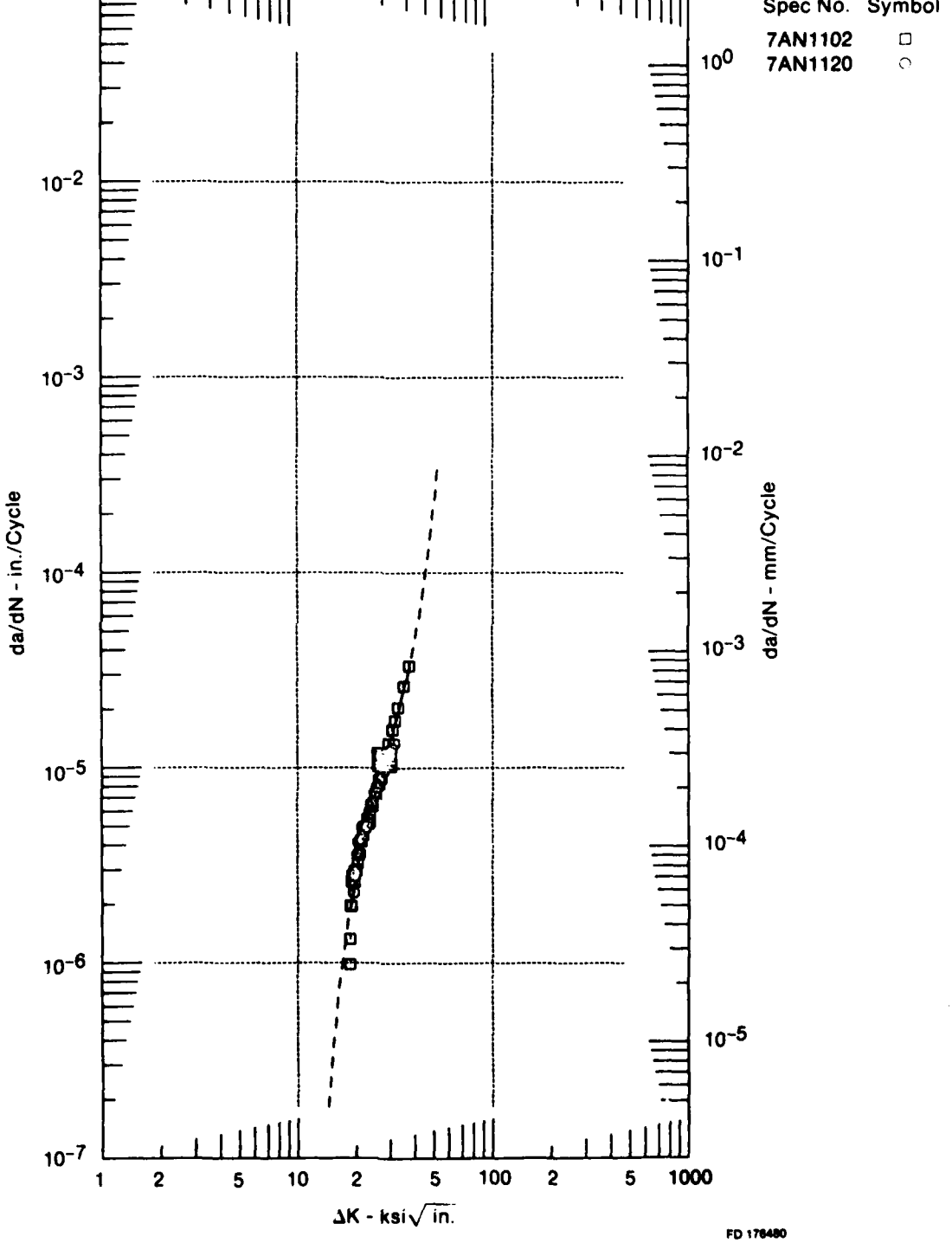

Figure 53. AF2-1DA Crack Growth Data at 427°C, 0.17 Hz, R = 0.1

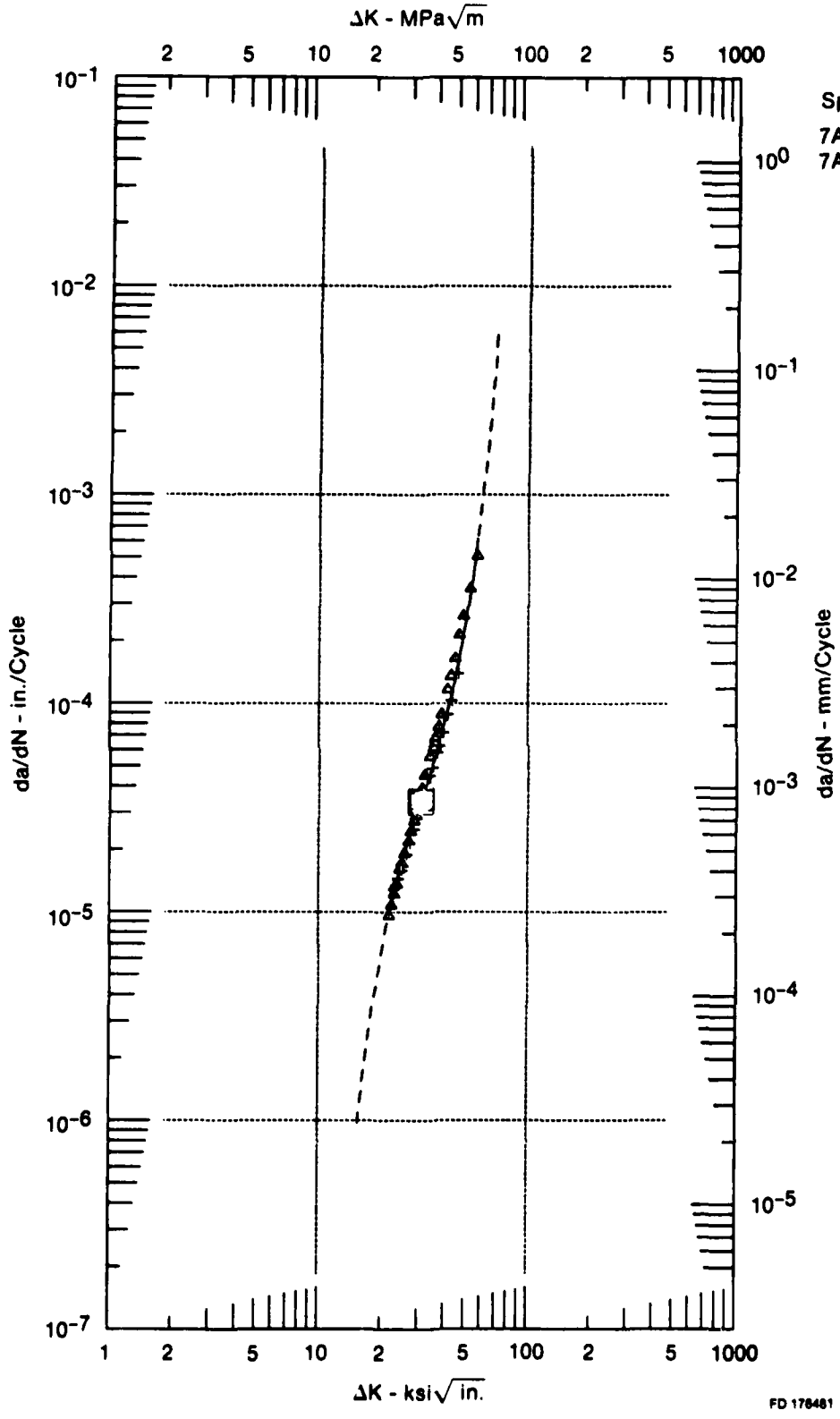

Figure 54. AF2-1DA Crack Growth Data at 649°C, 0.17 Hz, R = 0.1

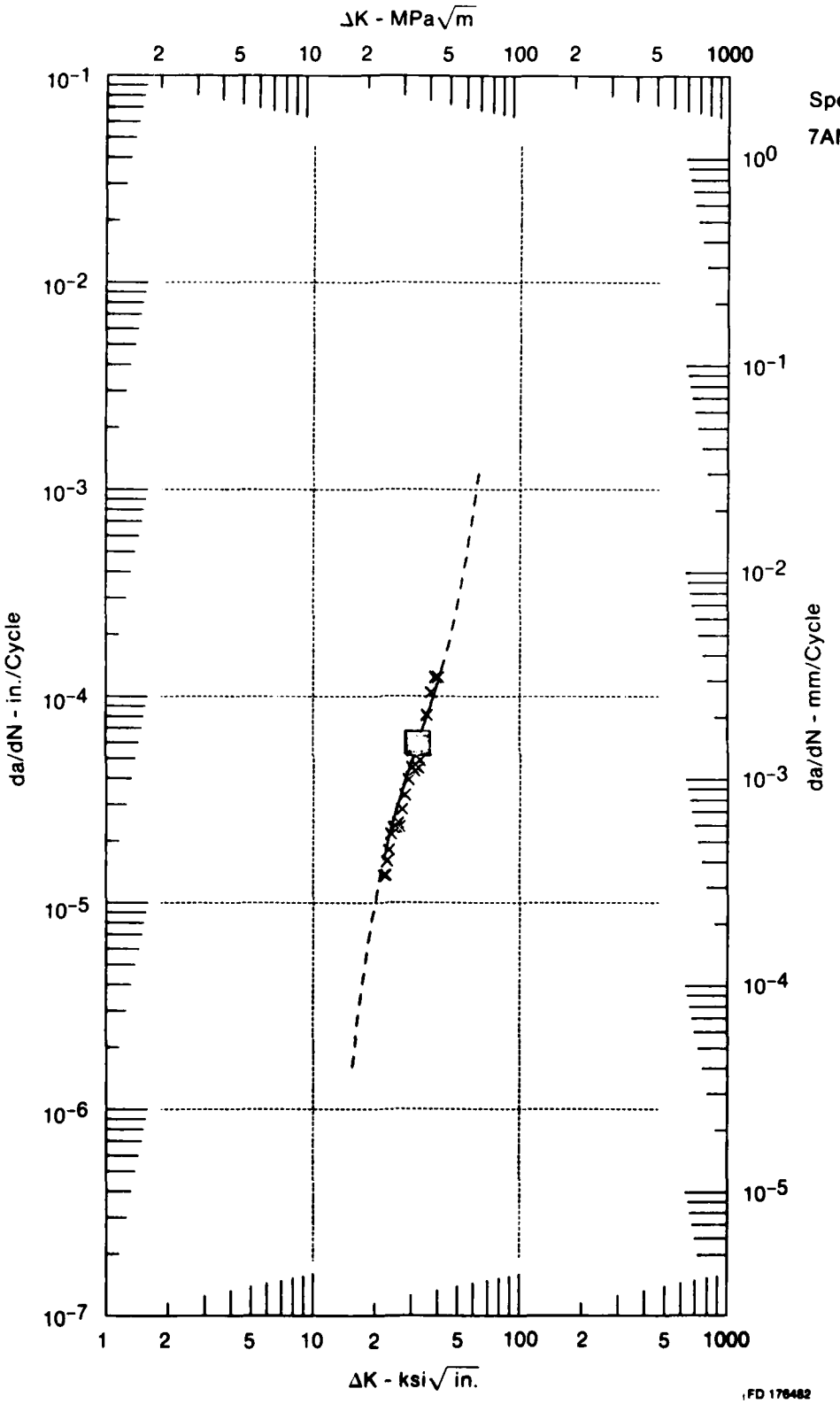

Figure 55. AF2-1DA Crack Growth Data at 760°C, 0.17 Hz, R = 0.1

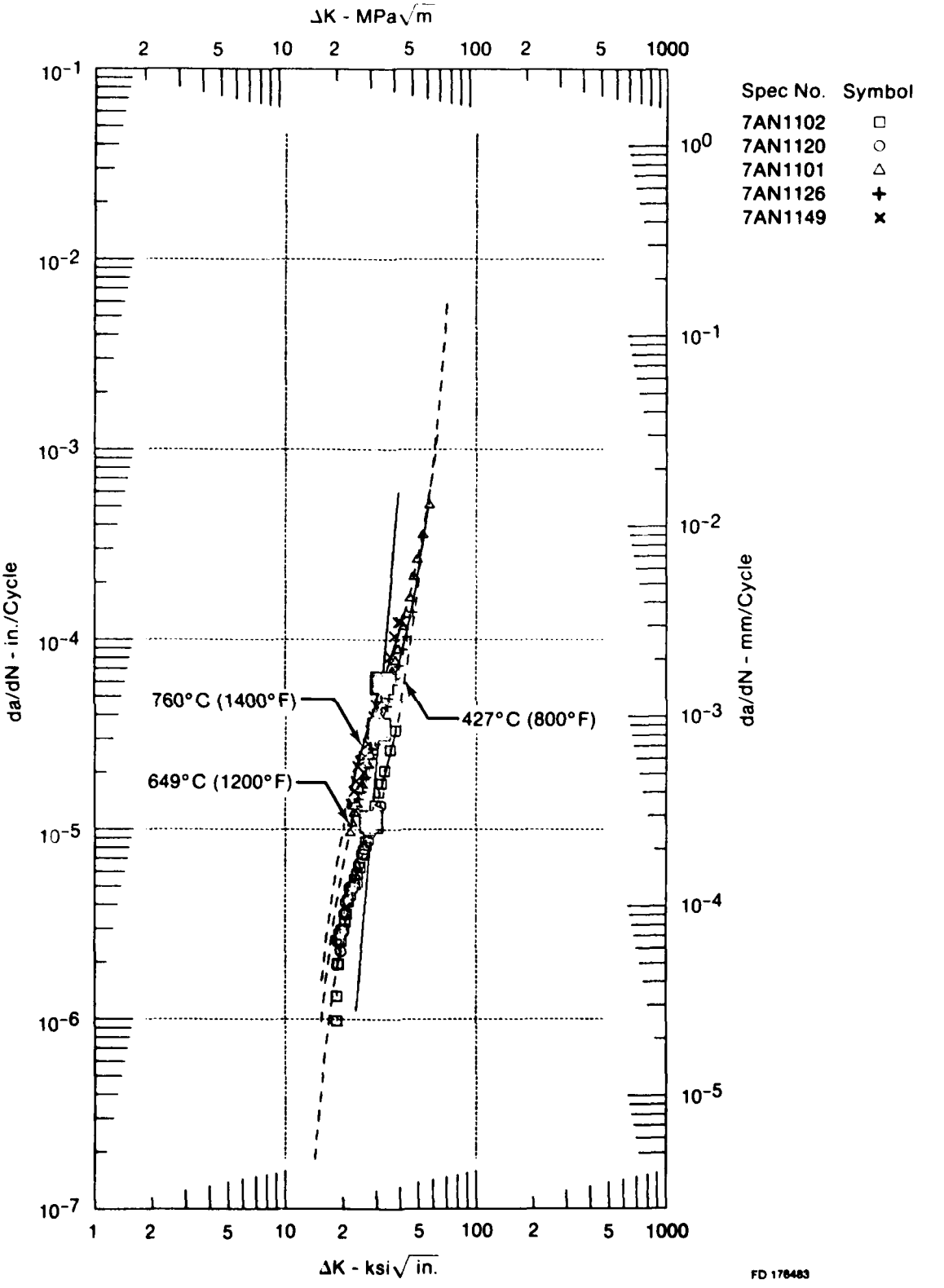

Figure 56. Effect of Temperature on Crack Growth Rates at 0.17 Hz, R = 0.1

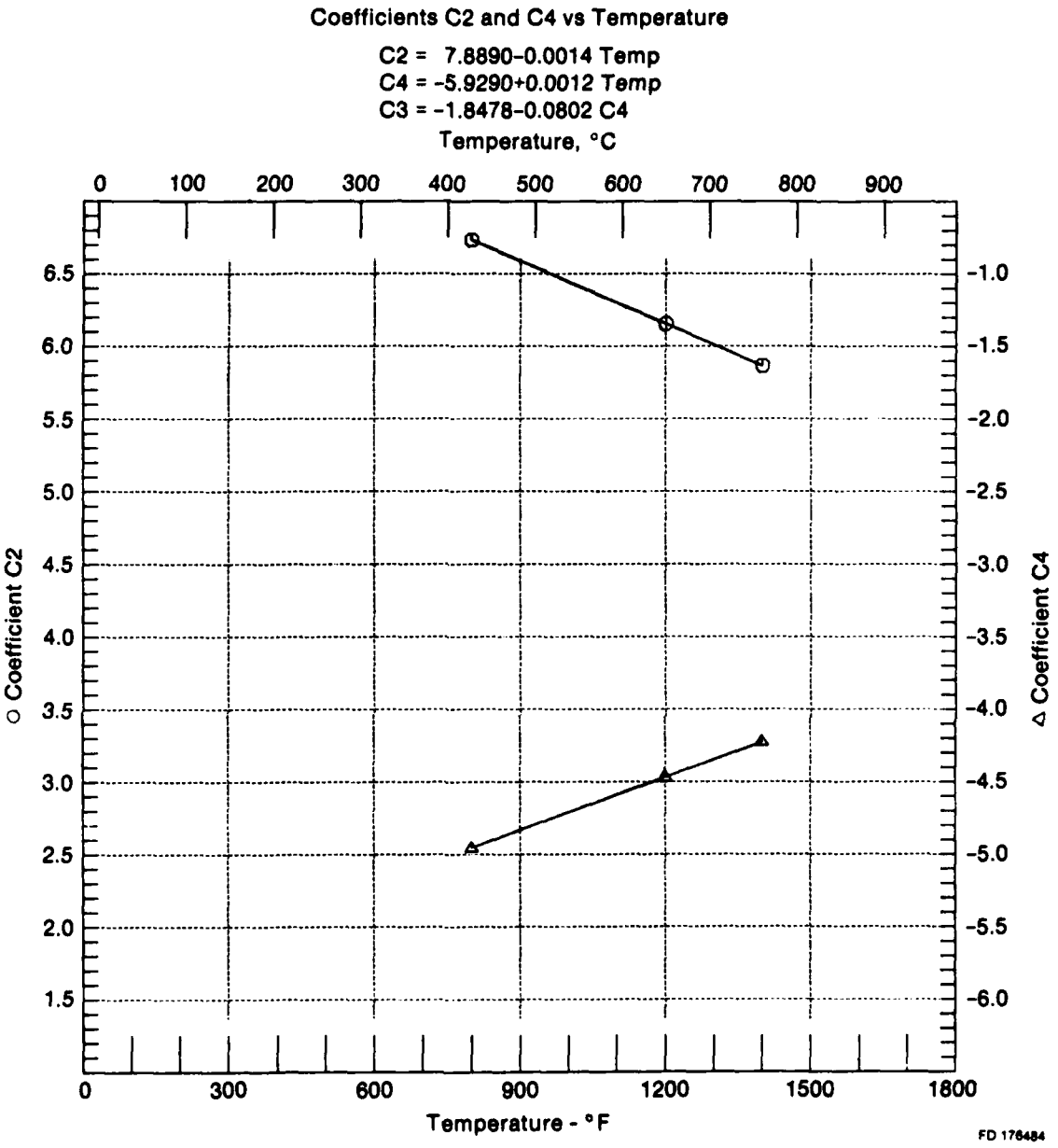

Figure 57. Effect of Temperature on SINH Coefficients at 0.17 Hz, R = 0.1

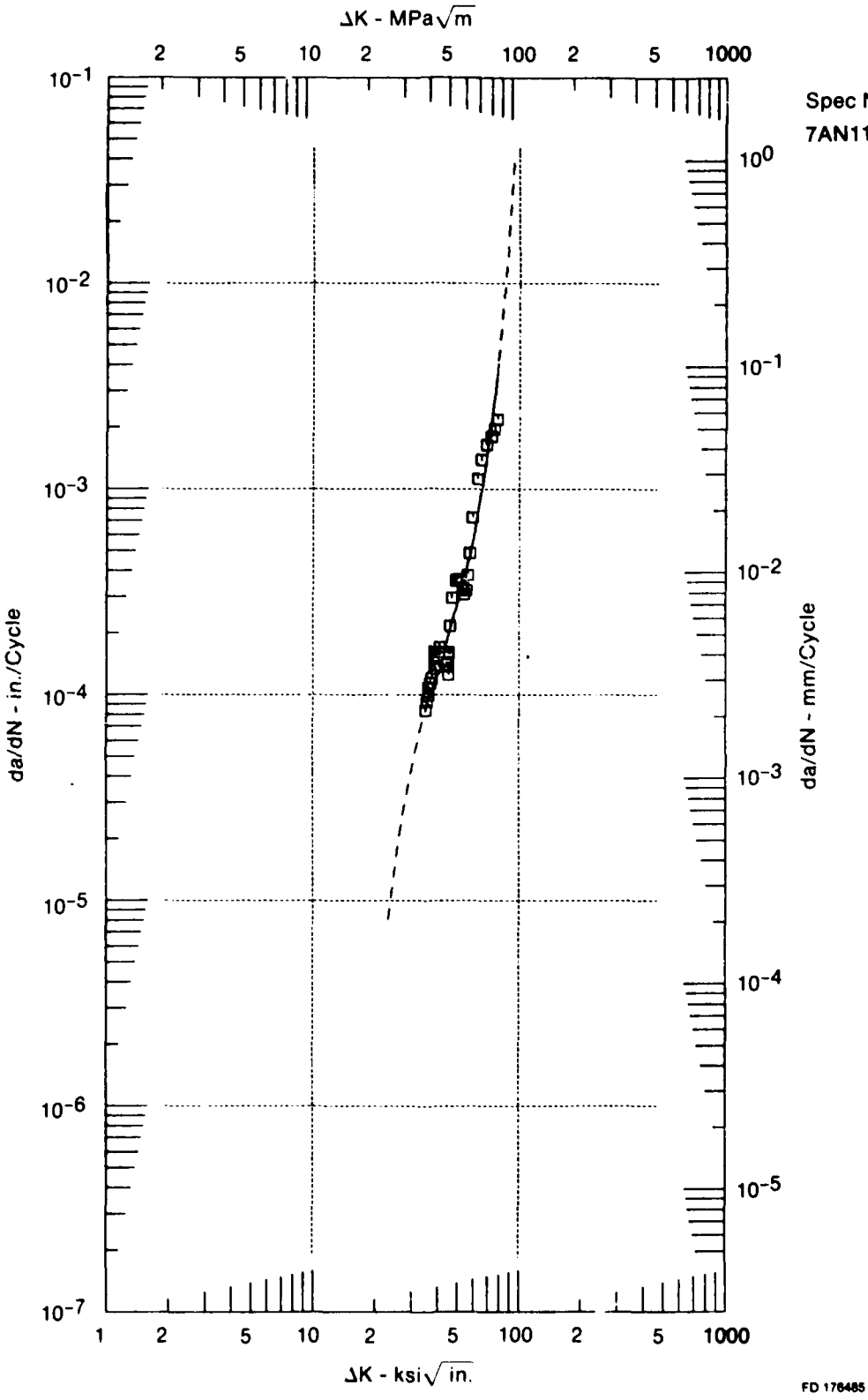

Figure 58. AF2-1DA Crack Growth Data at 649°C, 30 Sec Dwell, R = 0.1

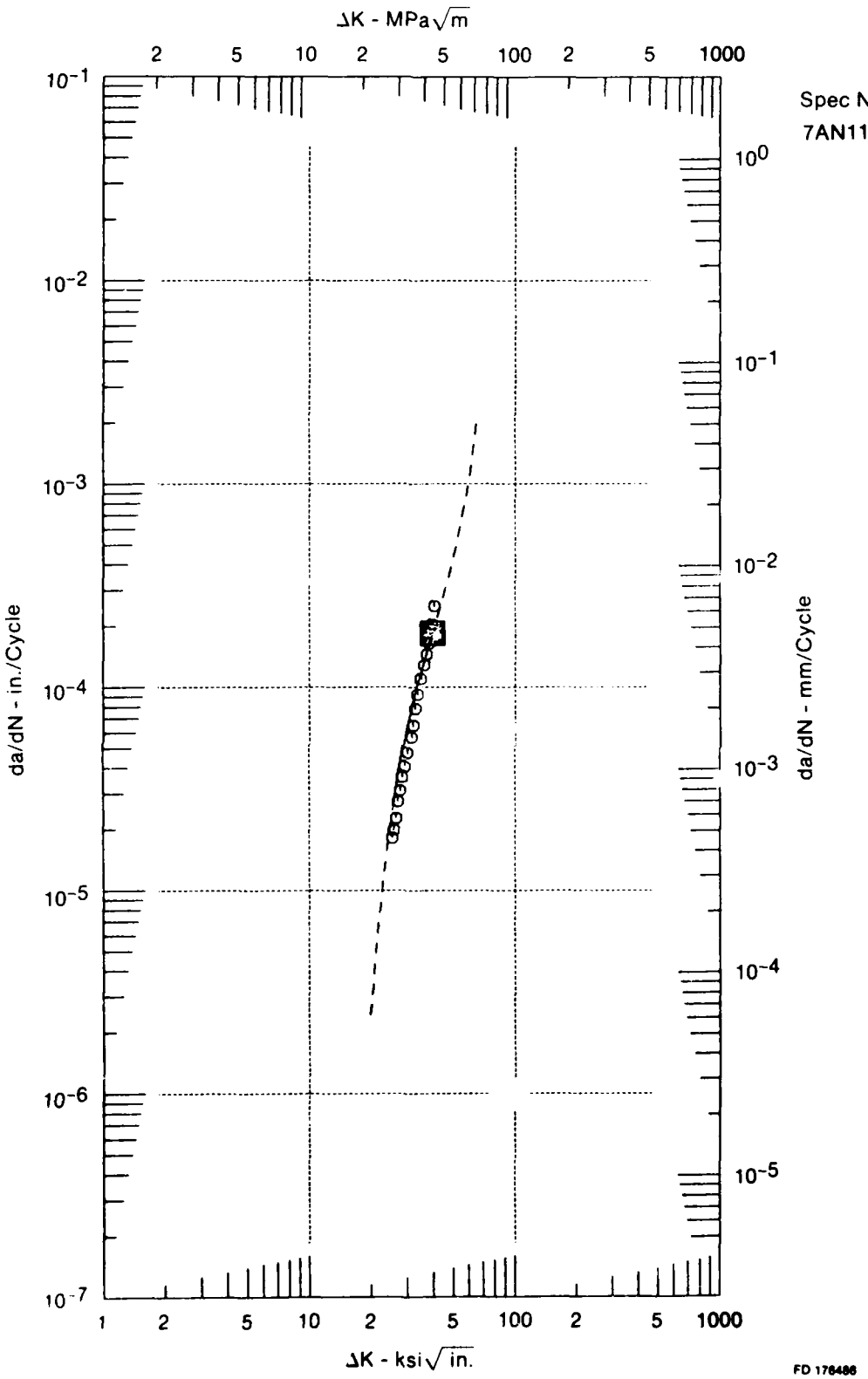

Figure 59 AF2-1DA Crack Growth Data at 649°C, 120 Sec Dwell, R = 0.1

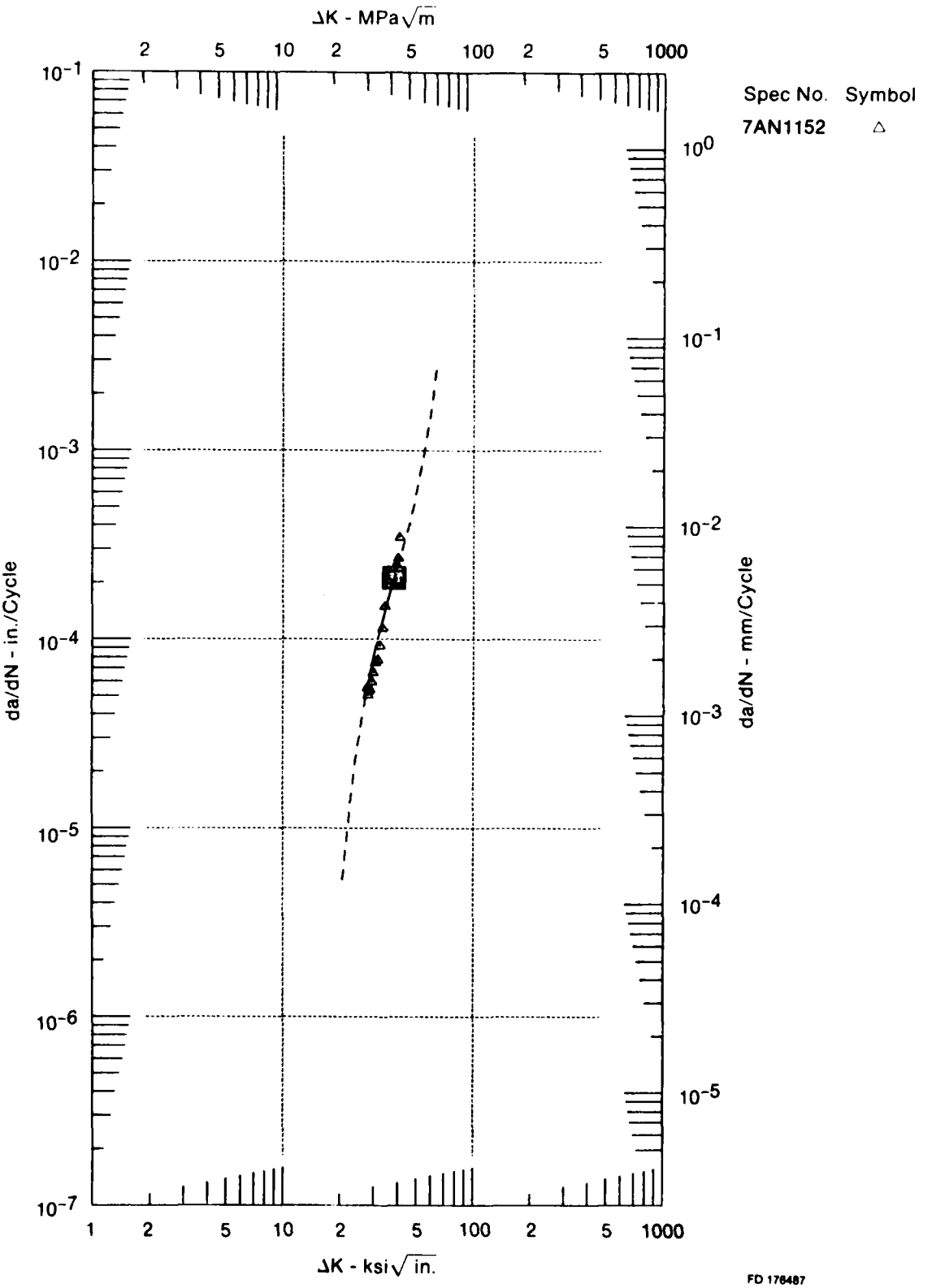

Figure 60. AF2-1DA Crack Growth Data at 649°C, 300 Sec Dwell, R = 0.1

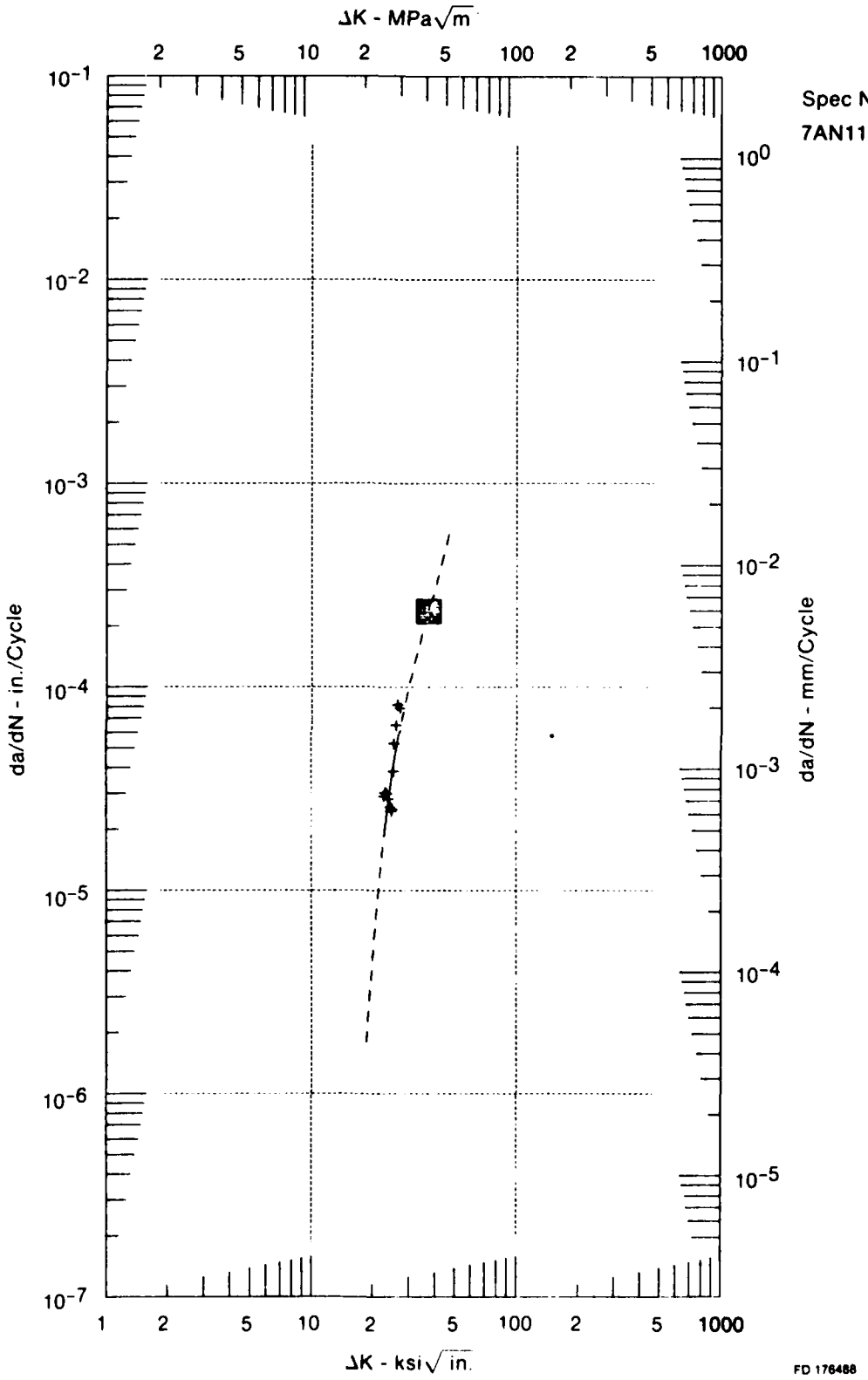

Figure 61. AF2-1DA Crack Growth Data at 649°C, 600 Sec Dwell, R = 0.1

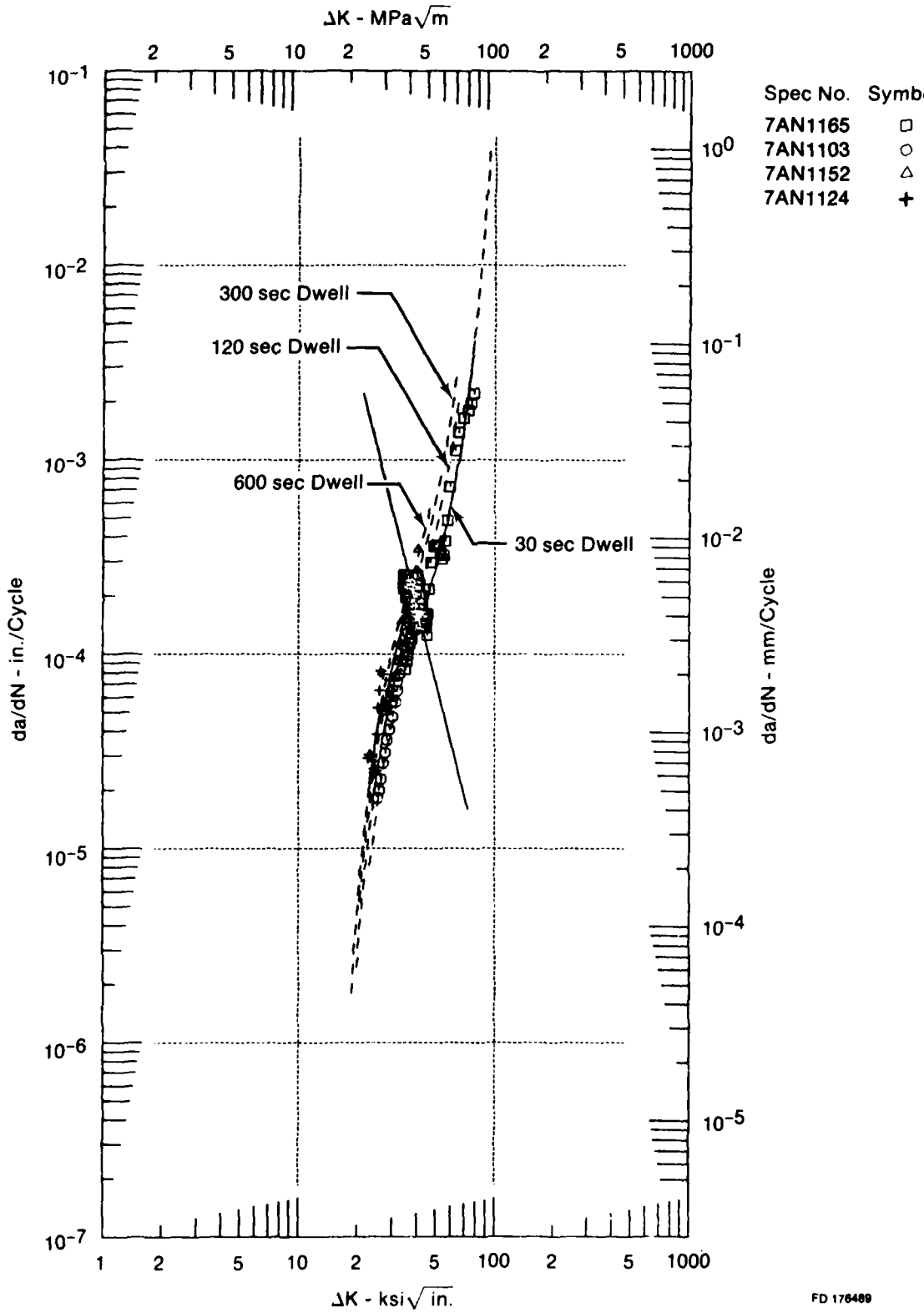

Figure 62. Effect of Maximum Tensile Hold Time on AF2-1DA Crack Growth Rate at 649°C, R = 0.1

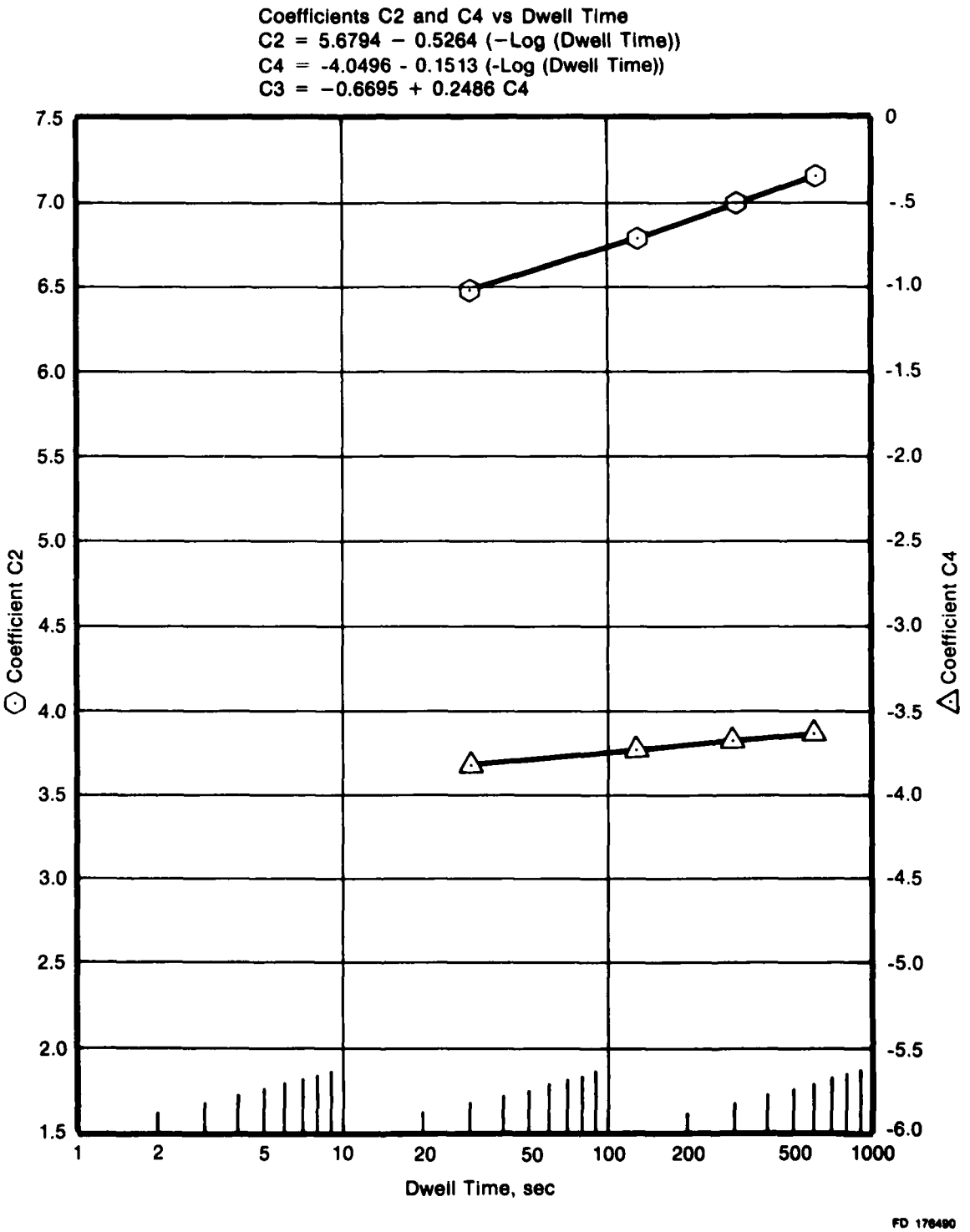

Figure 63. Effect of Dwell Time on SINH Coefficients at 649°C, R = 0.1

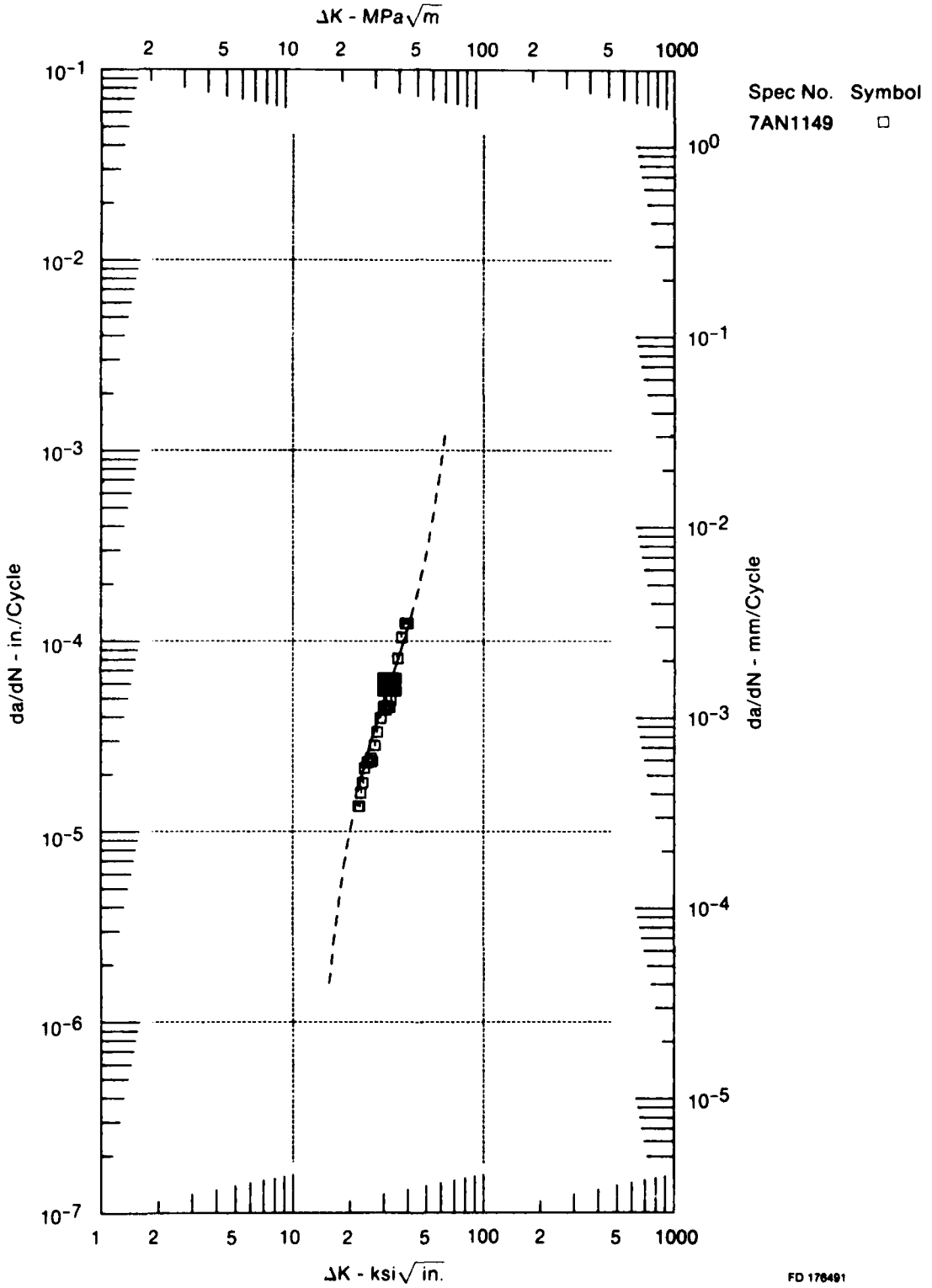

Figure 64. AF2-1DA Crack Growth Data at 760°C, 0.17 Hz (Zero Dwell), R = 0.1

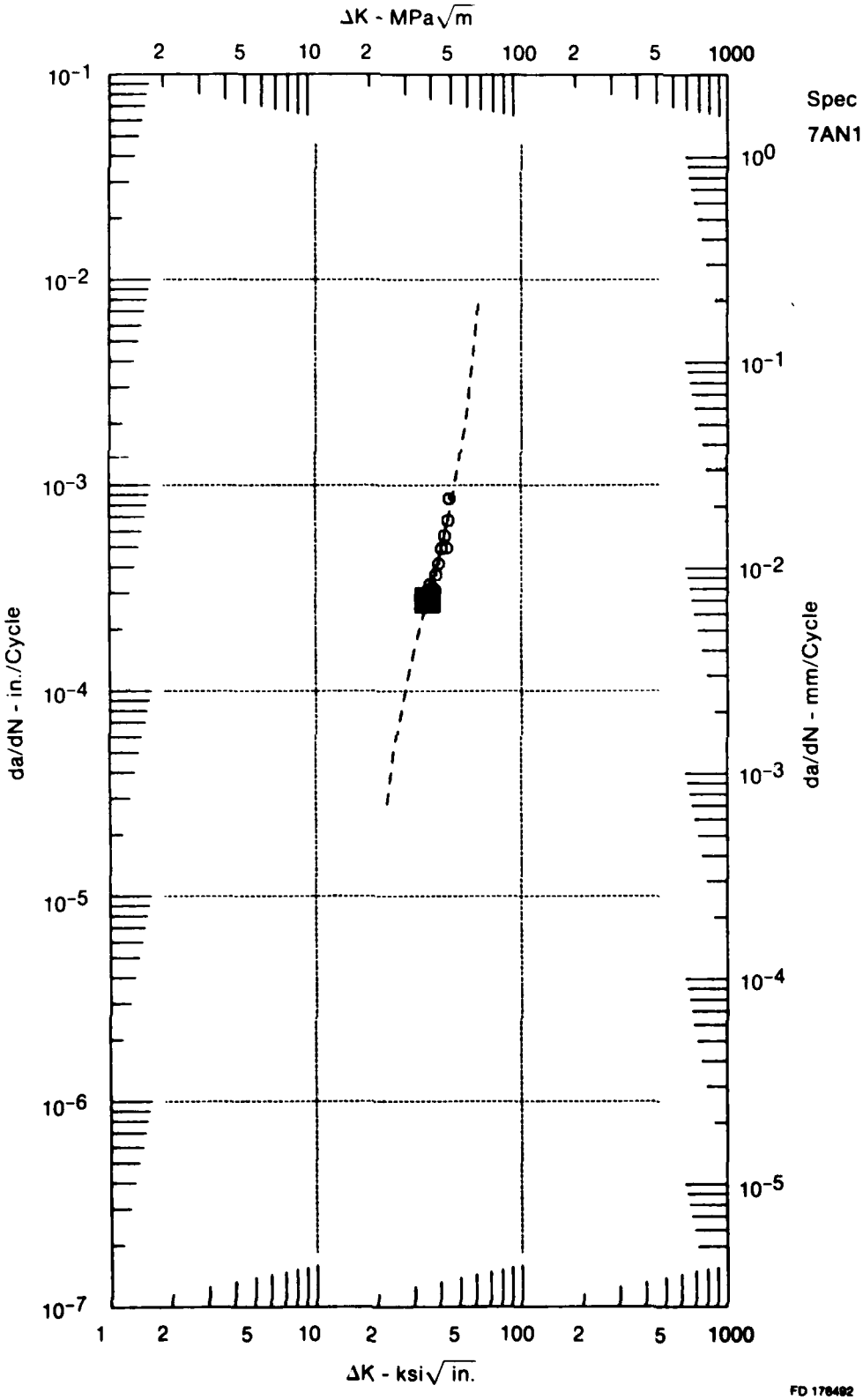

Figure 65. AF2-1DA Crack Growth Data at 760°C, 120 Sec Dwell, R = 0.1

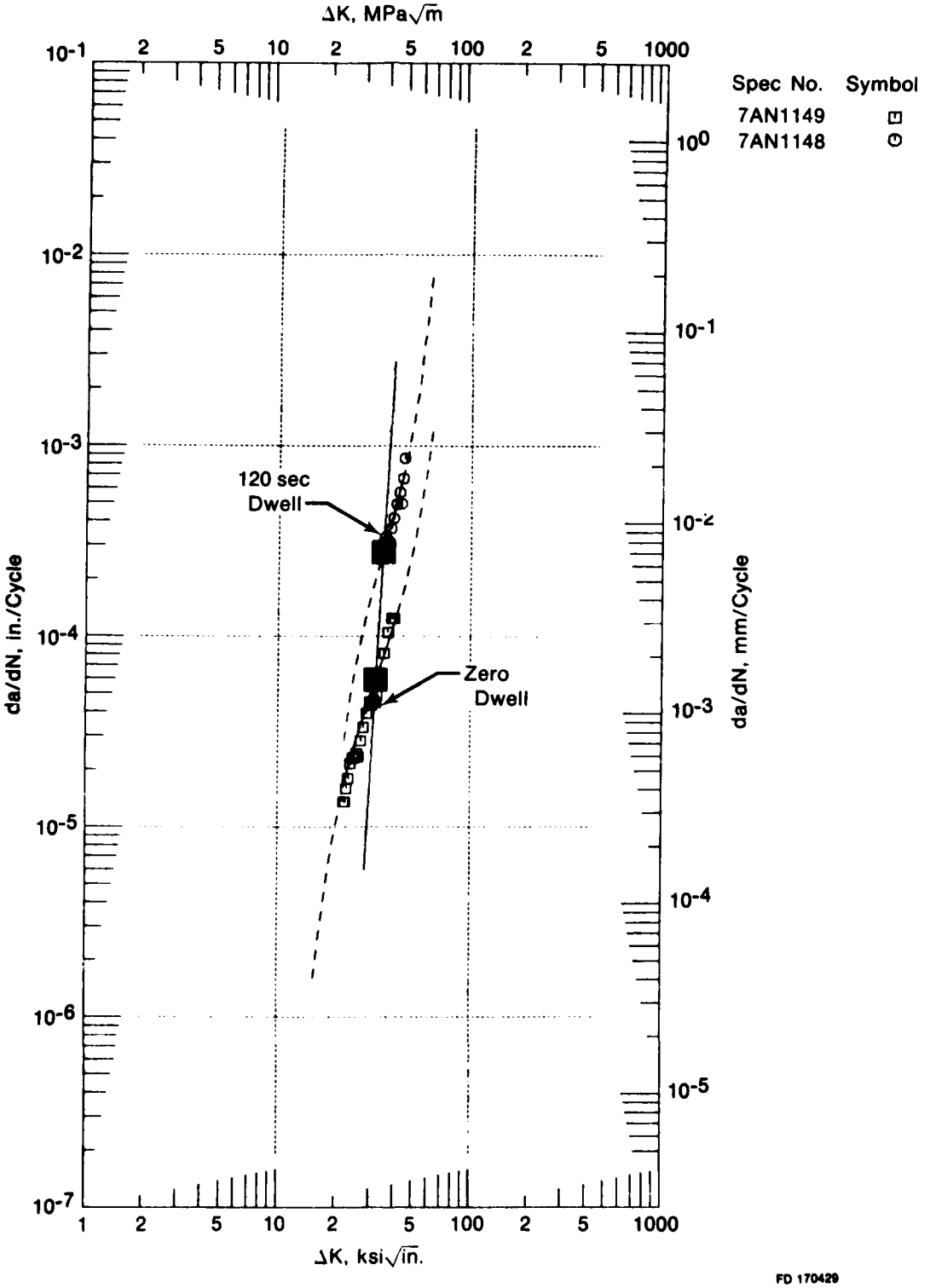

Figure 66. Effect of Dwell Time on AF2-1DA Crack Growth Rate at 760°C, R = 0.1

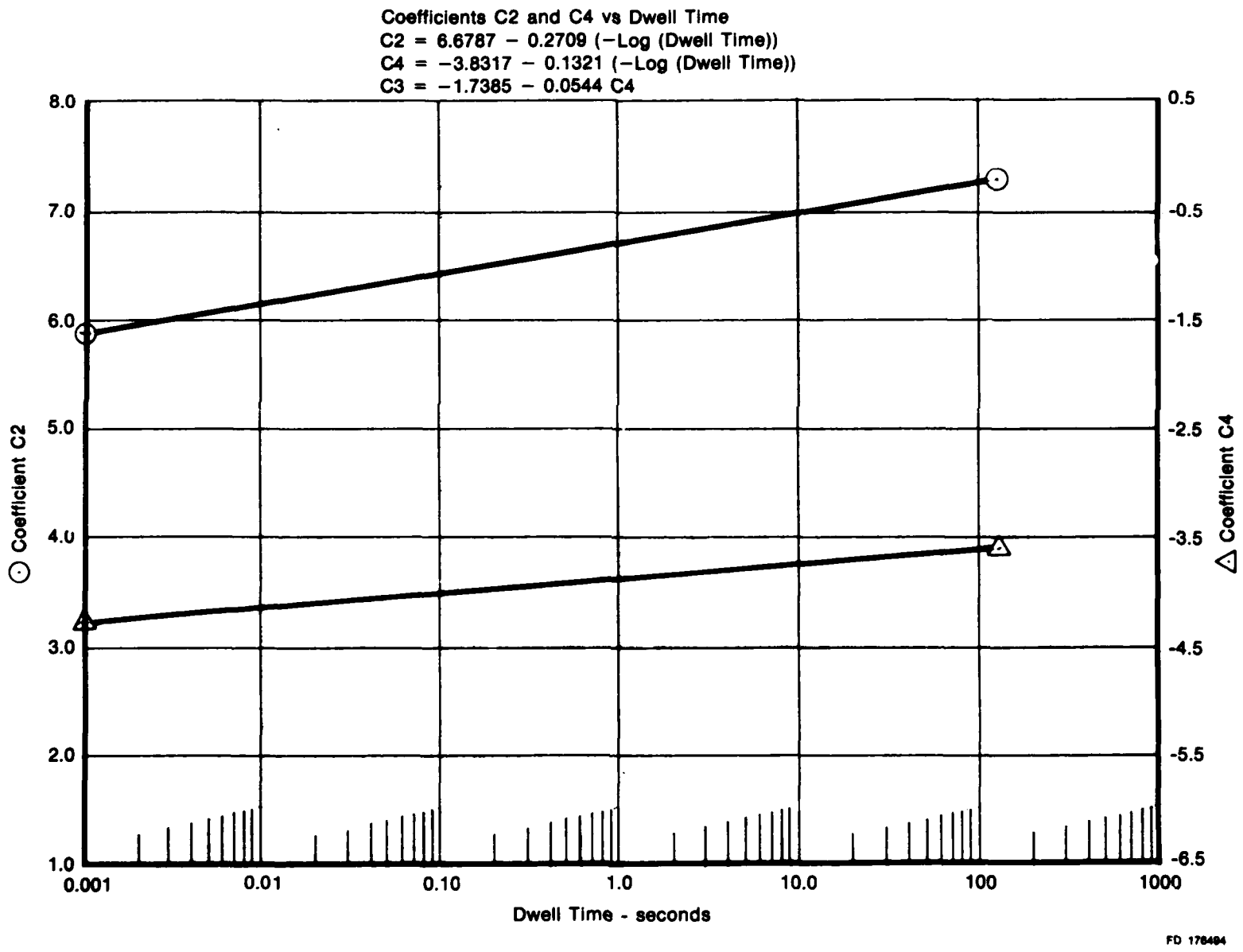

Figure 67. Effect of Dwell Time on SINH Coefficients at 760°C, R = 0.1

Phase III: Model Demonstration

Statistical Confidence of the Model

A mathematical model describing crack propagation has utilitarian value only insofar as it can be used in life prediction; the overall accuracy of a model can be measured by the accuracy of the resulting prediction. To provide a basis for comparing the accuracy of various life predictions, a simple correlative parameter is used, N_{pred}/N_{act}, the quotient of predicted and actual cyclic lives. Ideally, this quotient is 1.0 and decimal deviations from the ideal can be quickly interpreted as percent error of the prediction.

One of the objectives of model development is to quantify the intrinsic error of the model. The fundamental test of model validity is its ability to "predict" the lives of the specimens which were actually used in its development. Therefore, the ex post facto lives of all specimens contributing to current model development have been calculated and statistics of model success collected. The resulting distribution of N_{pred}/N_{act} provides a quantitative assessment of the prediction error to be expected during the model demonstration.

The procedure used for characterization of the statistical reliability of the crack propagation models is summarized as follows:

- Generate an interpolative crack propagation model from a series of related (da/dN, ΔK) data sets using multiple regression capability (MOD-1).
- Using the generated model, predict the (da/dN, ΔK) curves for the test conditions of the specimens used to generate the model.
- Produce specimen life calculations by integrating the crack propagation curves.
- Calculate a value of N_{pred}/N_{act} for each of the test specimens employed in the model.
- After completing the above four steps for each separate model (e.g., cyclic frequency, stress ratio, temperature), the entire population of values of N_{pred}/N_{act} for all models is analyzed statistically.
- The results of the statistical analysis are used to characterize model reliability and suggest possible model improvements.

This process has been applied to all models presented in this report, and the resulting statistics have been a significant aid to model evaluation. Such an assessment fully describes the error in the model, since linear relationships between similar SINH coefficients are imposed. By requiring that the linear model functions *precisely* locate the modeling curves, a rigid interpolation model is obtained, and all error in the model is forced to appear in the SINH "fits" of the individual data sets. Therefore, an analysis of the collection of values of N_{pred}/N_{act} associated with a particular model is a critical test of the inherent error of the model.

The results of the statistical analysis of each of the crack propagation models presented in this report are found in Table 4. The statistical parameters derived from each model represent calculations based on an assumed log-normal probability distribution for all such data. The collection of values of N_{pred}/N_{act} for all specimens used to generate the models is presented in a log-normal probability plot in Figure 68. The mean value of this sample population is 0.975 and the log standard deviation is 0.0514. This implies that the error in life prediction may be expected to be less than 25% for 95% of the future life predictions using the models.

Experimental Verification

Two compact specimens were tested at each of two previously untried conditions to verify the interpolative, predictive ability of the SINH crack growth model. The two test conditions (538°C, R = 0.65, 0.017 Hz and 718°C, R = 0.1, 15-sec dwell at maximum tensile load) were provided by the Air Force Project Engineer. The predicted crack growth rate curves were given to him prior to testing with an explanation for revising the dwell model to predict the 15-sec dwell test.

Revision of the dwell model was required since prediction of the verification test crack growth rate required extrapolation into a region where crack extension is not a linear function of dwell time. Figure 69 depicts the effects of dwell time on crack growth rates at 760°C. The original interpolative dwell model employed a minimum dwell time of 120 sec. However, one of the verification tests included a 15 sec dwell. As indicated by Figure 69, a linear extrapolation from 120 sec dwell to 15 sec dwell (dotted lines) would result in a significant deviation from the data. Therefore, the dwell model was revised to take 0 to 120 sec dwell times into account. The revision allows the model to be interpolated between 0 and 120 sec dwell times, rather than extrapolating from the 120 sec dwell, resulting in a more accurate representation of actual conditions. All dwell predictions were made using the revised model.

Figure 70 presents a comparison of the da/dN vs ΔK curve and the actual data for the 538°C, R = 0.65, 0.017 Hz verification testing. The curves correlate well with the data, N_{pred}/N_{act} = 0.789 for Specimen 1167 and N_{pred}/N_{act} = 1.008 for Specimen 1168. Therefore, the specimen life predictions detailed in Figures 71 and 72 fall well within the expected limits of the model (i.e., less than 25% error).

Figure 73 illustrates the comparison of the predicted da/dN vs ΔK curve and the actual data for the 718°C, R = 0.1, 15 sec dwell testing. Here again, the curves describe the data well, N_{pred}/N_{act} = 0.843 for Specimen 1153 and N_{pred}/N_{act} = 1.022 for Specimen 1154. Thus, specimen life predictions shown in Figures 74 and 75 fall within the expected limits of the model previously described.

Conclusions

- The interpolative hyperbolic sine (SINH) model accurately predicts crack propagation life of AF2-1DA at elevated temperatures.
- At elevated temperatures (427°C $\leq$ T $\leq$ 760°C), the thickness-independent data require specimens for cyclic tests to be a minimum of 6.35 mm thick and for cyclic/dwell tests to be a minimum of 12.70 mm thick.
- Additional studies are needed at various temperatures to determine the effect of dwell length on crack growth rates.

TABLE 4.
STATISTICAL EVALUATION OF THE CRACK PROPAGATION MODELS

20 Hz, 1200°F Stress Ratio Model

Spec No.	R	N_p/N_A
1125	0.1	0.930
1135	0.5	0.982
1142	0.8	1.036

Mean $N_p/N_A = 0.982$ Log $(\sigma) = 0.224 \times 10^{-1}$

0.0083 Hz, 1200°F Stress Ratio Model

Spec No.	R	N_p/N_A
1104	0.1	1.031
1115	0.5	1.067
1144	0.8	1.436

Mean $N_p/N_A = 1.164$ Log $(\sigma) = 0.7914 \times 10^{-1}$

Frequency Model

Spec No.	R	N_p/N_A
1104	0.1	0.923
1101	0.1	0.930
1126	0.1	1.002
1125	0.1	1.031

Mean $N_p/N_A = 0.970$ Log $(\sigma) = 0.2397 \times 10^{-1}$

1400°F Dwell Model

Spec No.	R	N_p/N_A
1149	0.1	0.825
1148	0.1	1.027

Mean $N_p/N_A = 0.920$ Log $(\sigma) = 0.6736 \times 10^{-1}$

10 cpm, R = 0.1 Temperature Model

Spec No.	R	N_p/N_A
1102	0.1	0.999
1120	0.1	0.915
1101	0.1	1.002
1126	0.1	0.923
1149	0.1	0.825

Mean $N_p/N_A = 0.930$ Log $(\sigma) = 0.3466 \times 10^{-1}$

1200°F Dwell Model

Spec No.	R	N_p/N_A
1165	0.05	0.761
1103	0.1	0.922
1152	0.1	1.037
1124	0.1	1.042

Mean $N_p/N_A = 0.930$ Log $(\sigma) = 0.6417 \times 10^{-1}$

10 cpm, 1200°F Stress Ratio Model

Spec No.	R	N_p/N_A
1101	0.1	1.002
1126	0.1	0.923
1106	0.5	1.014

Mean $N_p/N_A = 0.979$ Log $(\sigma) = 0.224 \times 10^{-1}$

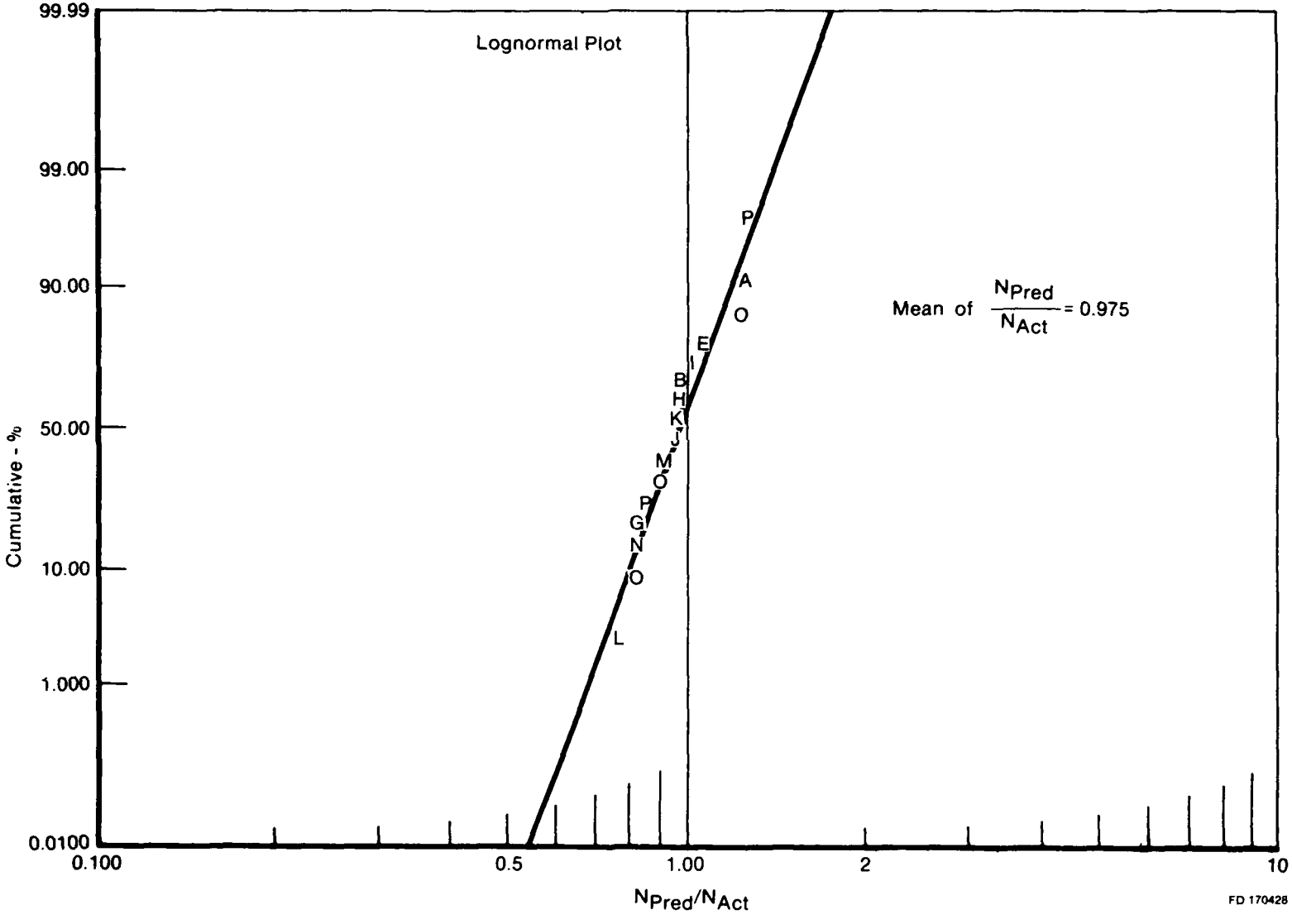

Figure 68. Probability Plot for Collection of Values of N_{Pred}/N_{Act} for Crack Propagation Specimens Used in Model Development

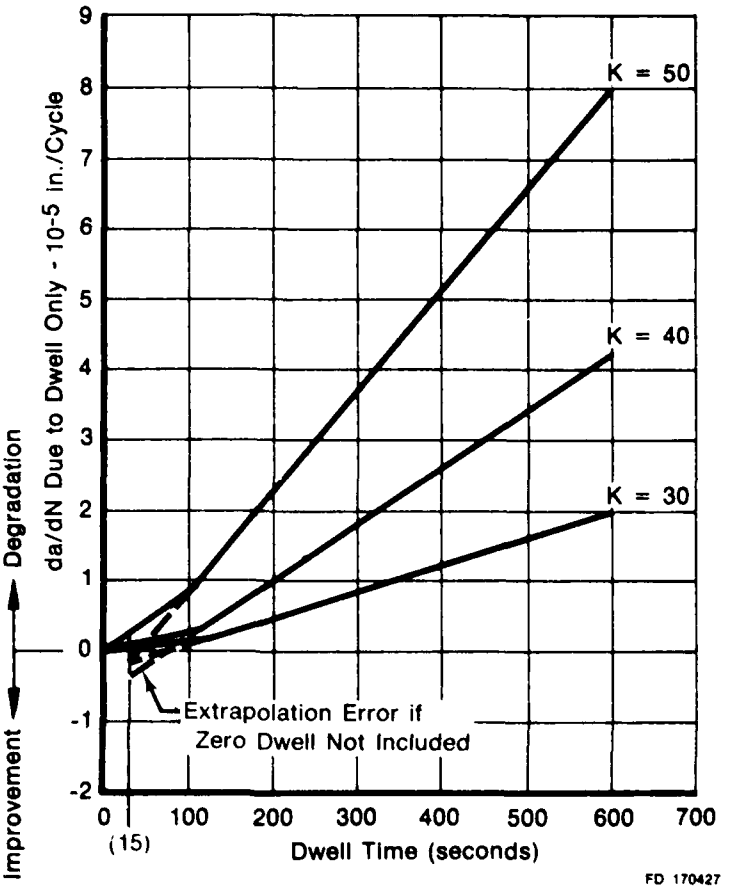

Figure 69. Effect of Dwell Length on Crack Growth Rates at 760°C

AD-A089 296 PRATT AND WHITNEY AIRCRAFT GROUP WEST PALM BEACH FL G--ETC F/G 11/6
EVALUATION OF CRACK GROWTH IN ADVANCED P/M ALLOYS.(U)
MAR 80 D L SIMS, F K HAAKE F33615-77-C-5093
UNCLASSIFIED PWA-FR-12126 AFML-TR-79-4160 NL

END
DATE FILMED
10 80
DTIC

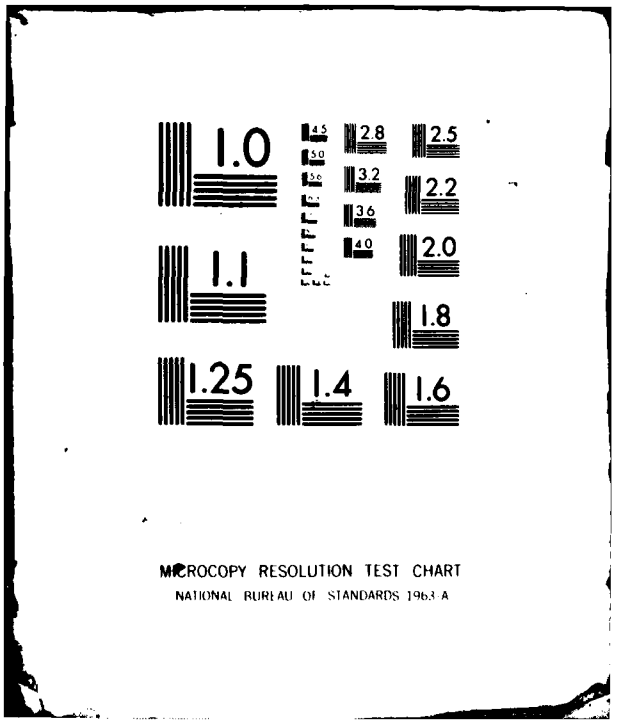
1.0
1.1
1.25
1.4
1.6
1.8
2.0
2.2
2.5
2.8
3.2
3.6
4.0
4.5
5.0
5.6
MICROCOPY RESOLUTION TEST CHART
NATIONAL BUREAU OF STANDARDS 1963-A

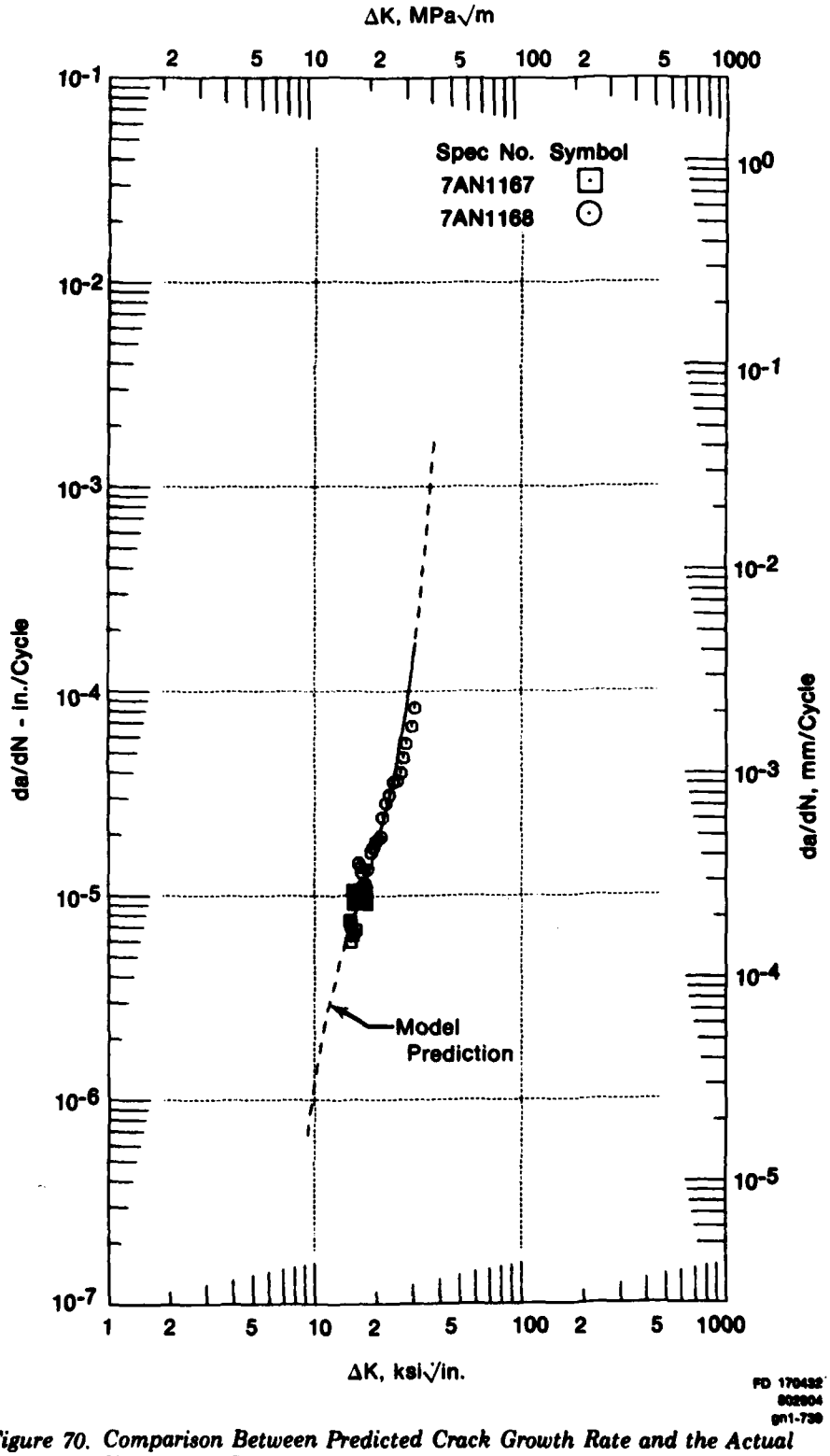

Figure 70. Comparison Between Predicted Crack Growth Rate and the Actual Verification Data at 538°C, R = 0.65, 0.017 Hz

AF2-1DA
Modified Compact Tension Specimen Crack Growth Prediction
Interpolative Hyperbolic Sine Model

Specimen No. 1167 MCT Specimen
Initial Crack 0.808 in.
Max Load 2.504 kips
Temperature 1000 Degrees F

N_{Act} = 46950 Cycles
N_{Pred} = 37023 Cycles
N_{Pred}/N_{Act} = 0.789

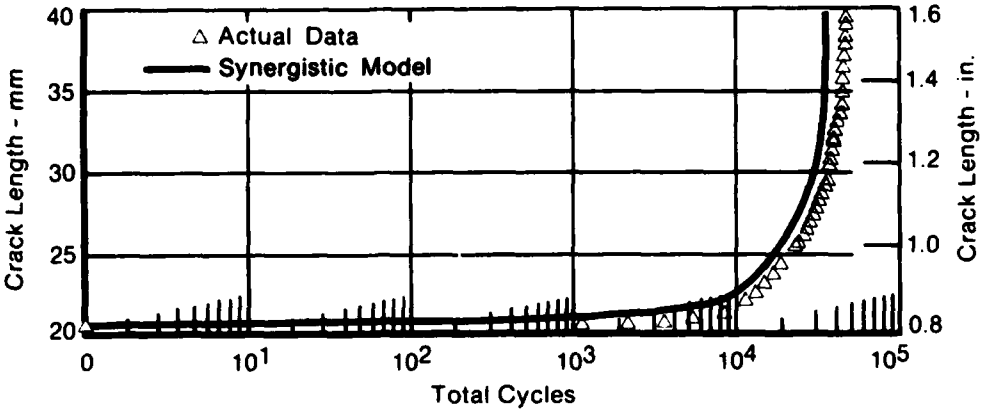

FD 170433

Figure 71. Life Prediction for Verification Specimen 1167 Tested at 538°C. R = 0.65, 0.017 Hz

AF2-1DA
Modified Compact Tension Specimen Crack Growth Prediction
Interpolative Hyperbolic Sine Model

Specimen No. 1168 MCT Specimen
Initial Crack 1.040 in.
Max Load 2.381 kips
Temperature 1000 Degrees F

N_{Act} = 23200 Cycles
N_{Pred} = 23377 Cycles
N_{Pred}/N_{Act} = 1.008

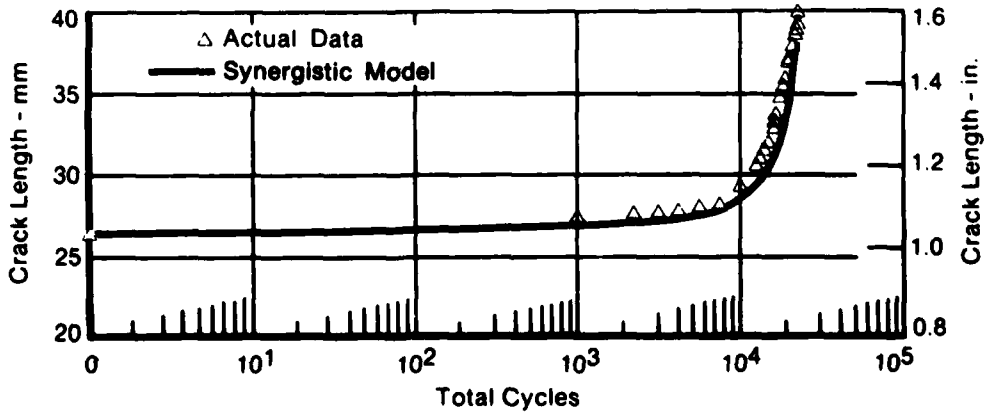

FD 170430

Figure 72. Life Prediction for Verification Specimen 1168 Tested at 538°C, R = 0.65, 0.017 Hz

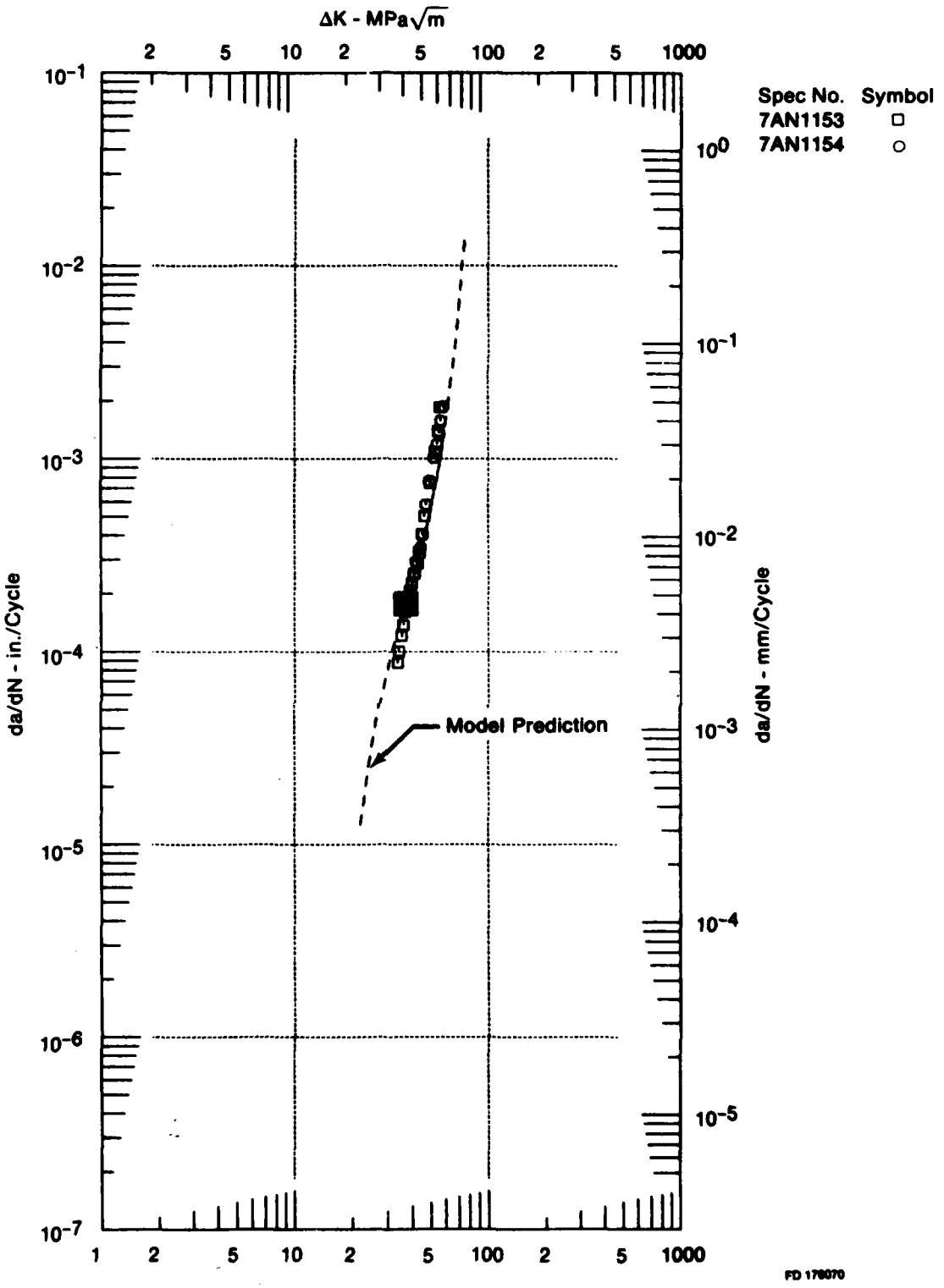

Figure 73. Comparison of Model Prediction and the Actual Crack Growth Data at 718°C, R = 0.1, 15 sec Dwell

AF2-1DA
Modified Compact Tension Specimen Crack Growth Prediction
Interpolative Hyperbolic Sine Model

Specimen No.	1153 MCT Specimen	N_{Act} = 2545 Cycles
Initial Crack	0.997 in.	N_{Pred} = 2145 Cycles
Max Load	3.556 kips	N_{Pred}/N_{Act} = 0.843
Temperature	1325 Degrees F	

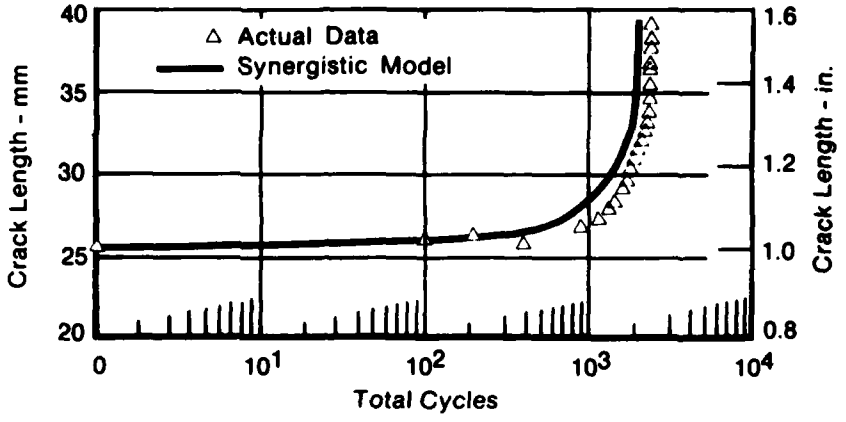

FD 194806

Figure 74. Life Prediction for Verification Specimen 1153 Tested at 718°C, R = 0.1, 15 sec Dwell

AF2-1DA
Modified Compact Tension Specimen Crack Growth Prediction
Interpolative Hyperbolic Sine Model

Specimen No.	1154 MCT Specimen	N_{Act} = 1165 Cycles
Initial Crack	0.939 in.	N_{Pred} = 1191 Cycles
Max Load	4.440 kips	N_{Pred}/N_{Act} = 1.022
Temperature	1325 Degrees F	

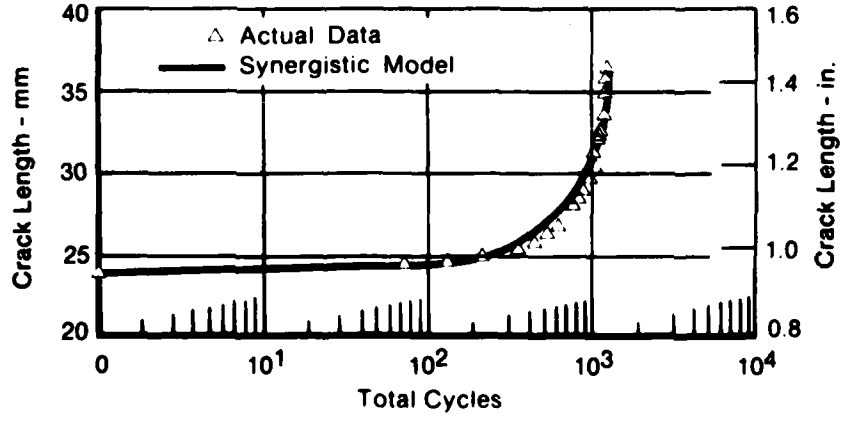

FD 194806

Figure 75. Life Prediction for Verification Specimen 1154 Tested at 718°C, R = 0.1, 15 sec Dwell

APPENDIX
AF2-1DA
CRACK PROPAGATION
DATA

7AN1101 AF2-1DA 1200F AIR 10 CPM
R= 0.10 THICKNESS=12.700 MM
PMAX= 11.458 KN WIDTH=61.450 MM
COMPACT SPECIMEN

NO.	CYCLES	A(MM)	DEL K (MPA*√M)	DA/DN (MM/CYCLE)
1	14500.	22.87		
2	17010.	23.44		
3	19500.	23.94		
4	22000.	24.56	23.94	2.441E-04
5	24500.	25.06	24.53	2.737E-04
6	27000.	25.85	25.26	3.102E-04
7	29030.	26.44	25.96	3.449E-04
8	31420.	27.40	26.97	4.065E-04
9	32700.	27.86	27.59	4.379E-04
10	34040.	28.44	28.34	4.843E-04
11	36060.	29.54	29.69	5.536E-04
12	37000.	30.02	30.45	6.167E-04
13	38050.	30.73	31.45	6.928E-04
14	38720.	31.09	32.15	7.351E-04
15	39500.	31.81	33.11	8.564E-04
16	40200.	32.39	34.13	9.915E-04
17	40800.	32.86	35.27	1.153E-03
18	41600.	33.93	37.17	1.417E-03
19	42000.	34.55	38.44	1.550E-03
20	42380.	35.17	39.89	1.726E-03
21	42740.	35.78	41.41	1.958E-03
22	43000.	36.23	42.66	2.249E-03
23	43420.	37.19	45.54	2.958E-03
24	43600.	37.79	47.16	3.430E-03
25	43780.	38.47	49.34	4.160E-03
26	43930.	39.06	51.53	5.408E-03
27	44050.	39.59	53.97	6.647E-03
28	44180.	40.47	57.72	8.997E-03
29	44280.	41.61	62.28	1.294E-02
30	44330.	42.06		
31	44380.	42.86		
32	44430.	44.08		

7AN1102 AF2-1DA 800F AIR 10 CPM
R= 0.10 THICKNESS=12.776 MM
PMAX= 11.120 KN WIDTH=61.316 MM
COMPACT SPECIMEN

NO.	CYCLES	A(MM)	DEL K (MPA*√M)	DA/DN (MM/CYCLE)
1	16700.	22.33		
2	19700.	22.67		
3	23210.	22.93		
4	27606.	23.20	21.96	7.445E-05
5	33000.	23.50	22.29	7.577E-05
6	38030.	24.01	22.64	8.325E-05
7	43090.	24.41	23.06	9.107E-05
8	48000.	24.86	23.48	1.065E-04
9	53100.	25.42	24.03	1.151E-04
10	57901.	25.90	24.65	1.256E-04
11	62700.	26.82	25.32	1.375E-04
12	67[illegible].	27.25	26.04	1.481E-04
13	72170.	27.99	26.93	1.608E-04
14	77155.	28.87	27.87	1.882E-04
15	80120.	29.40	28.63	2.179E-04
16	83000.	29.97	29.48	2.507E-04
17	86000.	30.79	30.59	2.851E-04
18	89215.	31.80	32.14	3.400E-04
19	91470.	32.65	33.52	3.964E-04
20	93100.	33.15	34.70	4.435E-04
21	94700.	33.94	36.02	5.166E-04
22	96750.	35.06	38.36	6.678E-04
23	98250.	35.95	40.94	8.425E-04
24	99750.	37.30	44.70	1.093E-03
25	100512.	38.28	47.38	1.452E-03
26	101000.	38.96	49.79	2.008E-03
27	101500.	39.66		
28	102000.	41.01		
29	102513.	43.22		

7AN1103 AF2-1DA 1200F AIR 2 HOWL
R= 0.10 THICKNESS=12.751 MM
PMAX= 14.469 KN WIDTH=61.166 MM
COMPACT SPECIMEN

NO.	CYCLES	A(MM)	DEL K (MPA*√M)	DA/DN (MM/CYCLE)
1	0.	21.74		
2	336.	21.99		
3	1036.	22.26		
4	1936.	22.66	28.13	4.614E-04
5	2836.	23.08	28.55	5.032E-04
6	3836.	23.49	29.16	5.774E-04
7	4836.	24.12	29.86	6.979E-04
8	5636.	24.83	30.59	7.873E-04
9	6300.	25.23	31.30	9.165E-04
10	7000.	26.01	32.18	1.039E-03
11	7650.	26.55	33.12	1.210E-03
12	8300.	27.52	34.38	1.441E-03
13	8600.	27.88	35.02	1.646E-03
14	8900.	28.40	35.84	1.993E-03
15	9200.	28.96	36.75	2.337E-03
16	9500.	29.65	38.08	2.786E-03
17	9750.	30.57	39.45	3.267E-03
18	9900.	31.02	40.47	3.678E-03
19	10050.	31.47	41.65	4.162E-03
20	10200.	32.15	42.92	5.181E-03
21	10300.	32.70	44.12	6.348E-03
22	10400.	33.25	45.75	7.651E-03
23	10500.	34.13	47.81	9.621E-03
24	10570.	34.88	49.61	1.368E-02
25	10640.	35.59		
26	10710.	36.67		
27	10760.	38.68		

7AN1104 AF2-1DA 1200F AIR .5 CPM
R= 0.10 THICKNESS=12.700 MM
PMAX= 10.844 KN WIDTH=61.224 MM
COMPACT SPECIMEN

NO.	CYCLES	A(MM)	DEL K (MPA*√M)	DA/DN (MM/CYCLE)
1	0.	23.36		
2	521.	23.56		
3	1504.	23.85		
4	2749.	24.20	22.51	2.920E-04
5	2984.	24.29	22.56	2.909E-04
6	3700.	24.56	22.76	2.869E-04
7	4700.	24.75	23.01	2.764E-04
8	6000.	25.14	23.35	2.737E-04
9	7400.	25.48	23.72	2.775E-04
10	8900.	25.95	24.14	3.022E-04
11	10400.	26.37	24.60	3.264E-04
12	11900.	26.84	25.15	3.561E-04
13	13467.	27.49	25.78	3.966E-04
14	14967.	28.10	26.50	4.539E-04
15	16467.	28.72	27.35	5.255E-04
16	17992.	29.57	28.42	6.102E-04
17	19037.	30.28	29.32	7.001E-04
18	19851.	30.89	30.18	7.952E-04
19	20600.	31.39	31.09	9.009E-04
20	21355.	32.13	32.20	1.050E-03
21	22000.	32.85	33.40	1.241E-03
22	22525.	33.50	34.69	1.407E-03
23	23035.	34.25		
24	23558.	35.18		
25	23908.	35.78		

7AN1106 AF2-1DA 1200F AIR 10 CPM
R= 0.50 THICKNESS=11.874 MM
PMAX= 7.957 KN WIDTH=60.963 MM
COMPACT SPECIMEN

NO.	CYCLES	A(MM)	DEL K (MPA*√M)	DA/DN (MM/CYCLE)
1	3650.	28.51		
2	7100.	28.87		
3	10600.	29.17		
4	17040.	29.87	12.63	1.048E-04
5	21910.	30.34	12.95	1.117E-04
6	24850.	30.72	13.16	1.209E-04
7	28000.	31.14	13.41	1.273E-04
8	32000.	31.58	13.77	1.416E-04
9	36000.	32.22	14.20	1.566E-04
10	40000.	32.83	14.71	1.769E-04
11	44000.	33.57	15.32	2.004E-04
12	46700.	34.10	15.80	2.203E-04
13	48700.	34.59	16.23	2.325E-04
14	49600.	34.83	16.44	2.383E-04
15	51600.	35.29	16.90	2.647E-04
16	53600.	35.80	17.48	2.867E-04
17	55600.	36.33	18.16	3.254E-04
18	57630.	37.23	19.02	3.707E-04
19	59000.	37.56	19.70	4.249E-04
20	60600.	38.30	20.70	4.906E-04
21	61800.	38.85	21.54	5.674E-04
22	63000.	39.67	22.76	6.756E-04
23	64000.	40.27	23.98	7.847E-04
24	64970.	41.10	25.54	9.322E-04
25	65860.	41.94	27.25	1.245E-03
26	66660.	42.85	29.74	1.757E-03
27	67260.	43.71	32.64	2.555E-03
28	67900.	45.43		
29	68100.	46.50		
30	68200.	47.49		

7AN1112 AF2-1DA 800F AIR 10 CPM
R= 0.50 THICKNESS= 6.350 MM
PMAX= 5.862 KN WIDTH=61.239 MM
COMPACT SPECIMEN

NO.	CYCLES	A(MM)	DEL K (MPA*√M)	DA/DN (MM/CYCLE)
1	2500.	23.54		
2	5380.	23.69		
3	10300.	23.84		
4	20000.	24.22	13.50	4.026E-05
5	35090.	24.88	13.88	4.641E-05
6	45000.	25.30	14.16	4.926E-05
7	55000.	25.97	14.47	5.299E-05
8	63000.	26.29	14.74	5.469E-05
9	71310.	26.74	15.03	5.953E-05
10	79300.	27.28	15.33	6.097E-05
11	87920.	27.73	15.70	6.966E-05
12	96600.	28.48	16.16	7.267E-05
13	102600.	28.77	16.48	7.882E-05
14	109600.	29.55	16.93	8.433E-05
15	114200.	29.69	17.23	8.909E-05
16	118800.	30.29	17.60	9.358E-05
17	122000.	30.54	17.83	9.533E-05
18	126000.	30.94	18.21	1.048E-04
19	130000.	31.34	18.57	1.056E-04
20	134000.	31.79	18.99	1.121E-04
21	138000.	32.26	19.47	1.114E-04
22	142000.	32.74	19.90	1.220E-04
23	146130.	33.24	20.44	1.303E-04
24	150180.	33.55	21.05	1.435E-04
25	154500.	34.49	21.83	1.809E-04
26	156500.	34.69	22.29	2.021E-04
27	158500.	35.05	22.89	2.204E-04
28	161000.	35.77	23.70	2.207E-04
29	163500.	36.39	24.58	2.495E-04
30	165000.	36.74	25.17	2.641E-04
31	167500.	37.15	26.23	2.831E-04
32	170220.	38.19	27.69	3.330E-04
33	171720.	38.70	28.74	3.683E-04
34	173220.	39.19	30.04	4.051E-04
35	174720.	39.82	31.30	4.619E-04
36	176220.	40.53	33.05	5.684E-04
37	177240.	41.04	34.55	7.264E-04
38	178500.	41.97	37.34	1.018E-03
39	179440.	42.81		
40	180000.	43.86		
41	180300.	44.48		

7AN1115 AF2-1DA 1200F AIR .5 CPM
R= 0.50 THICKNESS=12.700 MM
PMAX= 11.685 KN WIDTH=61.168 MM
COMPACT SPECIMEN

NO.	CYCLES	A(MM)	DEL K (MPA*√M)	DA/DN (MM/CYCLE)
1	1500.	28.92		
2	2500.	29.32		
3	3029.	29.62		
4	3222.	29.55	17.02	3.704E-04
5	4252.	29.88	17.35	3.810E-04
6	5607.	30.49	17.81	3.963E-04
7	6807.	31.15	18.25	4.009E-04
8	7607.	31.26	18.56	4.015E-04
9	8407.	31.64	18.85	3.654E-04
10	9207.	31.94	19.10	3.705E-04
11	10007.	32.29	19.42	4.151E-04
12	10407.	32.27	19.54	4.449E-04
13	11207.	32.73	19.93	5.058E-04
14	12007.	33.15	20.39	6.368E-04
15	12807.	33.80	21.06	8.469E-04
16	13207.	33.91		
17	13614.	34.46		
18	14014.	35.00		

7AN1120 AF2-1DA 800F AIR 10 CPM
R= 0.10 THICKNESS= 6.337 MM
PMAX= 5.289 KN WIDTH=61.186 MM
COMPACT SPECIMEN

NO.	CYCLES	A(MM)	DEL K (MPA*√M)	DA/DN (MM/CYCLE)
1	0.	22.71		
2	630.	22.76		
3	8040.	23.05		
4	16000.	23.58	21.36	5.787E-05
5	24310.	24.08	21.81	7.261E-05
6	32000.	24.28	22.34	9.114E-05
7	37180.	25.21	22.77	1.050E-04
8	41000.	25.52	23.18	1.090E-04
9	45000.	26.01	23.70	1.259E-04
10	49000.	26.47	24.16	1.214E-04
11	53020.	26.86	24.73	1.250E-04
12	57500.	27.72	25.35	1.298E-04
13	62500.	28.25	26.11	1.312E-04
14	64830.	28.39	26.47	1.650E-04
15	67010.	28.88	26.84	1.699E-04
16	70000.	29.23	27.57	1.897E-04
17	72000.	30.10	28.14	2.015E-04
18	74260.	30.24	28.73	2.049E-04
19	77250.	30.89	29.60	2.206E-04
20	80250.	31.48	30.47	2.442E-04
21	83000.	32.20	31.68	2.836E-04
22	85000.	32.83	32.67	2.945E-04
23	86500.	33.36	33.52	3.194E-04
24	88100.	33.84	34.51	3.394E-04
25	89500.	34.17		
26	91000.	34.88		
27	92000.	35.25		

7AN1124 AF2-1DA 1200F AIR 10MDWL
R= 0.10 THICKNESS=11.481 MM
PMAX= 9.634 KN WIDTH=60.620 MM
COMPACT SPECIMEN

NO.	CYCLES	A(MM)	DEL K (MPA*√M)	DA/DN (MM/CYCLE)
1	75.	26.69		
2	200.	26.87		
3	500.	27.01		
4	1000.	27.37	25.76	7.601E-04
5	1600.	27.93	26.26	7.180E-04
6	2000.	28.21	26.65	6.550E-04
7	2500.	28.43	27.02	6.225E-04
8	3000.	28.84	27.34	6.397E-04
9	3490.	28.88	27.76	9.786E-04
10	3700.	29.27	28.00	1.339E-03
11	3900.	29.43	28.30	1.652E-03
12	4100.	29.92	28.85	2.079E-03
13	4300.	30.34	29.54	2.002E-03
14	4476.	30.72	30.13	2.026E-03
15	4650.	31.31	30.57	2.092E-03
16	4850.	31.31		
17	5138.	31.89		
18	5300.	32.71		

7AN1125 AF2-1DA 1200F AIR 20 HZ
R= 0.10 THICKNESS= 6.325 MM
PMAX= 5.760 KN WIDTH=60.493 MM
CENTER CRACK SPECIMEN

NO.	CYCLES	A(MM)	DEL K (MPA*√M)	DA/DN (MM/CYCLE)
1	0.	15.59		
2	4000.	15.72		
3	5000.	15.81		
4	8000.	16.02	3.69	6.921E-05
5	11000.	16.23	3.75	7.802E-05
6	14000.	16.52	3.80	8.080E-05
7	17000.	16.75	3.85	9.008E-05
8	20000.	16.96	3.92	1.017E-04
9	23000.	17.27	3.99	1.180E-04
10	28000.	17.95	4.16	1.633E-04
11	30000.	18.29	4.25	1.837E-04
12	32000.	18.70	4.36	2.026E-04
13	34000.	19.11	4.49	2.354E-04
14	35000.	19.34	4.56	2.686E-04
15	36000.	19.56	4.65	3.192E-04
16	37000.	19.92	4.75	3.687E-04
17	38000.	20.44	4.88	4.502E-04
18	39000.	20.75		
19	40000.	21.32		
20	40900.	22.03		

7AN1126 AF2-1DA 1200F AIR 10 CPM
R= 0.10 THICKNESS= 6.325 MM
PMAX= 5.858 KN WIDTH=61.054 MM
COMPACT SPECIMEN

NO.	CYCLES	A(MM)	DEL K (MPA*√M)	DA/DN (MM/CYCLE)
1	0.	24.10		
2	650.	24.43		
3	1750.	24.59		
4	2950.	25.12	25.35	3.274E-04
5	4500.	25.63	25.92	3.388E-04
6	6100.	26.06	26.56	3.667E-04
7	8330.	27.09	27.51	4.033E-04
8	9030.	27.20	27.84	4.214E-04
9	10950.	28.06	28.93	4.802E-04
10	12500.	28.87	29.89	5.412E-04
11	14000.	29.68	31.15	6.312E-04
12	15000.	30.32	32.09	7.170E-04
13	16030.	31.09	33.29	8.248E-04
14	17000.	31.88	34.71	9.669E-04
15	18070.	32.98	36.81	1.133E-03
16	18580.	33.61	38.02	1.240E-03
17	19240.	34.51	39.96	1.477E-03
18	19640.	34.96	41.36	1.594E-03
19	20040.	35.64	43.01	1.841E-03
20	20440.	36.57	45.05	2.242E-03
21	20740.	36.99	47.15	2.798E-03
22	21100.	38.05	50.71	3.659E-03
23	21340.	38.98	54.04	4.850E-03
24	21460.	39.78	56.58	5.619E-03
25	21540.	40.10		
26	21640.	40.71		
27	21810.	42.01		

7AN1135 AF2-1DA 1200F AIR 20 HZ
R= 0.50 THICKNESS= 6.198 MM
PMAX= 5.667 KN WIDTH=63.607 MM
COMPACT SPECIMEN

NO.	CYCLES	A(MM)	DEL K (MPA*√M)	DA/DN (MM/CYCLE)
1	0.	20.20		
2	10000.	20.75		
3	20000.	21.04		
4	30000.	21.52	11.47	3.923E-05
5	40000.	21.87	11.61	3.763E-05
6	50000.	22.26	11.78	3.674E-05
7	60000.	22.58	11.92	3.494E-05
8	70000.	22.99	12.06	3.691E-05
9	80000.	23.26	12.22	3.875E-05
10	91000.	23.65	12.43	4.204E-05
11	102000.	24.28	12.65	4.650E-05
12	111000.	24.65	12.87	5.107E-05
13	122000.	25.20	13.17	5.531E-05
14	133000.	25.88	13.49	5.998E-05
15	143000.	26.48	13.83	6.622E-05
16	152000.	27.06	14.17	7.482E-05
17	162220.	27.85	14.64	8.353E-05
18	169000.	28.40	15.00	8.908E-05
19	175000.	29.12	15.37	9.128E-05
20	180000.	29.47	15.69	9.443E-05
21	185000.	29.97	16.02	9.755E-05
22	190000.	30.40	16.35	9.742E-05
23	195000.	30.95	16.74	1.010E-04
24	200000.	31.50	17.14	1.025E-04
25	205000.	31.98	17.53	1.127E-04
26	210000.	32.48	17.98	1.264E-04
27	215000.	33.03	18.55	1.437E-04
28	220000.	33.96	19.31	1.577E-04
29	225000.	34.87	20.18	1.918E-04
30	228000.	35.36	20.84	2.134E-04
31	231000.	35.73	21.56	2.405E-04
32	234000.	36.87	22.48	2.743E-04
33	236000.	37.33	23.28	3.055E-04
34	238000.	37.94	24.27	3.418E-04
35	240000.	38.56	25.25	3.625E-04
36	241500.	39.21	26.20	4.188E-04
37	243000.	39.90	27.37	4.553E-04
38	244000.	40.17	28.26	5.094E-04
39	245000.	40.92	29.29	5.402E-04
40	246000.	41.30	30.43	6.187E-04
41	247000.	42.08	31.91	7.490E-04
42	248000.	42.61		
43	249000.	43.66		
44	249500.	44.38		

7AN1142 AF2-1DA 1200F AIR 20 HZ
R= 0.80 THICKNESS= 6.325 MM
PMAX= 6.934 KN WIDTH=63.597 MM
COMPACT SPECIMEN

NO.	CYCLES	A(MM)	DEL K (MPA*√M)	DA/DN (MM/CYCLE)
1	35600.	20.54		
2	66600.	20.85		
3	96600.	21.23		
4	136000.	21.56	5.52	1.057E-05
5	146000.	21.60	5.54	9.647E-06
6	160000.	21.82	5.56	9.505E-06
7	180000.	22.08	5.60	9.979E-06
8	210000.	22.23	5.66	9.860E-06
9	250000.	22.68	5.74	9.762E-06
10	300500.	23.19	5.84	1.026E-05
11	402000.	24.29	6.10	1.173E-05
12	450000.	24.85	6.23	1.220E-05
13	495000.	25.42	6.37	1.231E-05
14	535000.	25.99	6.50	1.280E-05
15	575000.	26.47	6.63	1.354E-05
16	615000.	26.91	6.77	1.458E-05
17	655000.	27.55	6.94	1.592E-05
18	695000.	28.23	7.14	1.697E-05
19	725000.	28.83	7.31	1.668E-05
20	752000.	29.30	7.45	1.736E-05
21	777000.	29.66	7.59	1.741E-05
22	807000.	30.07	7.75	1.777E-05
23	852000.	31.04	8.04	2.055E-05
24	880000.	31.55	8.28	2.158E-05
25	910000.	32.26	8.55	2.311E-05
26	936000.	32.99	8.80	2.534E-05
27	956000.	33.29	9.03	2.626E-05
28	976000.	33.91	9.27	2.823E-05
29	996000.	34.59	9.54	3.093E-05
30	1010000.	34.87	9.79	3.345E-05
31	1030000.	35.63	10.15	3.642E-05
32	1043000.	36.13	10.43	3.809E-05
33	1056000.	36.63	10.76	4.119E-05
34	1077000.	37.55	11.34	3.943E-05
35	1086000.	37.89	11.57	4.832E-05
36	1095000.	38.37	11.89	5.498E-05
37	1104000.	38.47	12.22	6.339E-05
38	1115000.	39.63	12.85	7.832E-05
39	1120000.	39.96	13.21	8.607E-05
40	1126000.	40.48	13.78	9.985E-05
41	1135500.	41.39	14.70	1.109E-04
42	1141000.	42.07	15.43	1.187E-04
43	1145000.	42.70	16.01	1.258E-04
44	1150000.	43.21	16.86	1.339E-04
45	1153000.	43.59		
46	1156000.	44.07		
47	1159000.	44.53		

7AN1144 AF2 1DA 1200F AIR .5 CPM
R= 0.80 THICKNESS= 6.325 MM
PMAX= 11.734 KN WIDTH=63.619 MM
COMPACT SPECIMEN

NO.	CYCLES	A(MM)	DEL K (MPA*√M)	DA/DN (MM/CYCLE)
1	2020.	20.90		
2	3300.	21.00		
3	5010.	21.23		
4	8500.	21.28	9.29	9.520E-05
5	10680.	21.77	9.36	1.018E-04
6	14300.	22.11	9.49	1.123E-04
7	16300.	22.28	9.59	9.472E-05
8	17020.	22.37	9.59	1.022E-04
9	19190.	22.62	9.67	1.088E-04
10	21400.	22.69	9.76	1.117E-04
11	23000.	23.11	9.83	1.090E-04
12	24600.	23.25	9.89	1.189E-04
13	26240.	23.34	9.97	1.300E-04
14	28400.	23.58	10.05	1.196E-04
15	33510.	24.48	10.34	1.650E-04
16	36000.	24.67	10.51	1.963E-04
17	38700.	25.42	10.74	2.278E-04
18	40700.	25.72	10.92	2.464E-04
19	45510.	27.16		
20	47000.	27.69		
21	47450.	27.77		

7AN1148 AF2-1DA 1400F AIR 2 MDWL
R= 0.10 THICKNESS=12.700 MM
PMAX= 17.245 KN WIDTH=63.919 MM
COMPACT SPECIMEN

NO.	CYCLES	A(MM)	DEL K (MPA*√M)	DA/DN (MM/CYCLE)
1	1425.	24.92		
2	1625.	25.72		
3	1765.	26.41		
4	1857.	27.33	37.94	7.859E-03
5	1912.	28.10	38.72	7.634E-03
6	1965.	28.19	39.51	8.350E-03
7	2046.	28.83	40.49	8.029E-03
8	2110.	29.35	41.34	7.918E-03
9	2174.	29.97	42.32	9.317E-03
10	2240.	30.57	43.46	1.054E-02
11	2300.	30.95	44.71	1.248E-02
12	2360.	31.97	46.33	1.441E-02
13	2389.	32.39	47.40	1.260E-02
14	2425.	33.03	48.34	1.716E-02
15	2460.	33.49	48.92	2.184E-02
16	2505.	33.59		
17	2535.	35.97		
18	2585.	38.70		

7AN1149 AF2-1DA 1400F AIR 10 CPM
R= 0.10 THICKNESS=12.725 MM
PMAX= 13.709 KN WIDTH=63.878 MM
CENTER CRACK SPECIMEN

NO.	CYCLES	A(MM)	DEL K (MPA*√M)	DA/DN (MM/CYCLE)
1	0.	10.60		
2	600.	10.76		
3	1200.	10.86		
4	2400.	11.06	3.05	1.723E-04
5	3780.	11.46	3.09	1.714E-04
6	5000.	11.47	3.13	2.027E-04
7	6420.	11.80	3.18	2.279E-04
8	7670.	11.97	3.24	2.716E-04
9	8700.	12.49	3.29	2.911E-04
10	9600.	12.57	3.35	2.950E-04
11	10600.	13.03	3.41	3.084E-04
12	11200.	13.13	3.44	2.970E-04
13	12470.	13.50	3.52	3.580E-04
14	13500.	13.84	3.58	4.209E-04
15	14500.	14.24	3.68	5.015E-04
16	15330.	14.80	3.77	5.729E-04
17	15800.	15.09	3.83	5.527E-04
18	16200.	15.24	3.88	5.794E-04
19	16600.	15.53	3.93	5.700E-04
20	17000.	15.66	3.97	6.198E-04
21	17540.	16.08	4.04	7.878E-04
22	18130.	16.43	4.16	1.029E-03
23	18530.	16.94	4.26	1.330E-03
24	18870.	17.49	4.38	1.566E-03
25	19040.	17.63	4.46	1.567E-03
26	19300.	18.24	4.57	2.006E-03
27	19450.	18.41	4.63	2.653E-03
28	19610.	18.61	4.80	2.215E-03
29	19770.	19.38		
30	19870.	20.01		
31	20370.	20.16		

7AN1152 AF2-1DA 1200F AIR 5 MDWL
R= 0.10 THICKNESS=12.662 MM
PMAX= 14.696 KN WIDTH=60.846 MM
COMPACT SPECIMEN

NO.	CYCLES	A(MM)	DEL K (MPA*√M)	DA/DN (MM/CYCLE)
1	0.	23.23		
2	35.	23.39		
3	147.	23.48		
4	308.	23.79	30.29	1.404E-03
5	502.	24.06	30.54	1.280E-03
6	700.	24.15	30.90	1.343E-03
7	1000.	24.57	31.41	1.373E-03
8	1300.	25.20	31.96	1.510E-03
9	1602.	25.50	32.63	1.689E-03
10	2002.	26.19	33.58	1.906E-03
11	2300.	26.82	34.44	1.973E-03
12	2601.	27.45	35.41	2.337E-03
13	2873.	28.19	36.42	2.881E-03
14	3105.	28.47	37.51	3.772E-03
15	3325.	29.49	39.02	5.088E-03
16	3475.	30.32	40.46	5.793E-03
17	3577.	31.11	41.87	5.956E-03
18	3675.	31.77	43.16	6.650E-03
19	3750.	31.94	43.70	7.968E-03
20	3826.	32.54		
21	4054.	34.48		
22	4162.	38.23		

7AN1162 AF2-1DA 1200F AIR 10CPM
R= 0.80 THICKNESS= 6.350 MM
PMAX= 14.807 KN WIDTH=63.741 MM
COMPACT SPECIMEN

NO.	CYCLES	A(MM)	DEL K (MPA*√M)	DA/DN (MM/CYCLE)
1	600.	24.62		
2	1600.	24.67		
3	3600.	24.80		
4	7000.	25.38	13.45	1.305E-04
5	10500.	25.88	13.71	1.420E-04
6	14000.	26.27	14.00	1.464E-04
7	17500.	26.86	14.28	1.449E-04
8	21000.	27.42	14.60	1.378E-04
9	24500.	27.88	14.90	1.371E-04
10	28000.	28.39	15.16	1.439E-04
11	31000.	28.56	15.40	1.655E-04
12	34000.	29.14	15.73	1.925E-04
13	37000.	29.80	16.16	2.182E-04
14	39500.	30.51	16.62	2.454E-04
15	42000.	31.09	17.10	2.629E-04
16	44500.	31.67	17.59	2.833E-04
17	51500.	33.79	19.68	4.973E-04
18	52500.	34.22	20.18	7.917E-04
19	53500.	34.94	21.17	1.219E-03
20	54500.	36.08	22.58	2.329E-03
21	55000.	37.34		
22	55300.	38.58		
23	55400.	39.73		

7AN1165 AF2-1DA 1200F AIR 30SDWL
R= 0.05 THICKNESS= 7.620 MM
PMAX= 11.867 KN WIDTH=61.262 MM
COMPACT SPECIMEN

NO.	CYCLES	A(MM)	DEL K (MPA*√M)	DA/DN (MM/CYCLE)
1	0.	19.72		
2	200.	20.07		
3	500.	20.76		
4	700.	21.23	38.44	2.128E-03
5	900.	21.48	39.06	2.342E-03
6	1100.	21.98	39.73	2.724E-03
7	1106.	22.11	39.81	2.504E-03
8	1300.	22.64	40.63	2.872E-03
9	1500.	23.31	41.43	3.048E-03
10	1700.	23.62	42.51	3.422E-03
11	1900.	24.41	43.73	3.898E-03
12	2100.	25.45	45.26	4.344E-03
13	2300.	26.25	47.32	4.085E-03
14	2450.	27.06	48.66	3.790E-03
15	2600.	27.74	49.70	3.977E-03
16	2800.	27.95	51.37	5.348E-03
17	2900.	28.40	52.37	7.182E-03
18	3000.	29.43	54.08	9.286E-03
19	3050.	30.17	55.54	9.282E-03
20	3100.	30.45	57.02	9.174E-03
21	3150.	30.85	58.28	8.444E-03
22	3200.	31.37	59.33	7.815E-03
23	3250.	31.73	60.54	8.190E-03
24	3300.	32.03	61.58	9.674E-03
25	3350.	32.47	62.97	1.242E-02
26	3400.	32.97	65.08	1.850E-02
27	3450.	34.05	68.94	2.849E-02
28	3475.	34.74	71.82	3.511E-02
29	3500.	35.78	76.04	4.182E-02
30	3520.	36.73	80.44	4.564E-02
31	3530.	37.13	83.07	4.961E-02
32	3540.	37.64	85.78	5.552E-02
33	3550.	38.08	89.07	5.888E-02
34	3560.	38.83		
35	3570.	39.60		
36	3580.	40.18		

REFERENCES

1. Annis, C. G., R. M. Wallace, and D. L. Sims, "An Interpolative Model for Elevated Temperature Fatigue Crack Propagation," AFML-TR-76-176, Part I, November 1976.

2. Wallace, R. M., C. G. Annis, and D. L. Sims, "Application of Fracture Mechanics at Elevated Temperature," AFML-TR-76-176, Part II, April 1977.

3. Sims, D. L., C. G. Annis, and R. M. Wallace, "Cumulative Damage Fracture Mechanics at Elevated Temperature," AFML-TR-76-176, Part III, April 1977.

4. Miller, J. A., and G. Brodi, "Production of Powder Metallurgy Nickel Base Superalloy Turbine Disk," AFML-TR-76-101, Volume I, November 1976.

5. Hudak, S. J., A Saxena, R. J. Bucci, and R. C. Malcolm, "Development of Standard Methods of Testing and Analyzing Fatigue Crack Growth Rate Data," AFML-TR-78-40, May 1978.

6. Paris, P. C., *Fatigue — An Interdisciplinary Approach,* Proceedings 10th Sagamore Conference, Syracuse University Press, Syracuse, N. Y., 1964, p. 107.

7. Larsen, J. M. and C. G. Annis, "Cumulative Damage Fracture Mechanics Under Engine Spectra," AFML Contract F33615-77-C-5153, Pratt & Whitney Aircraft, Interim Report FR-10562, September 1978.

☆U.S.Government Printing Office: 1980 — 657-084/60

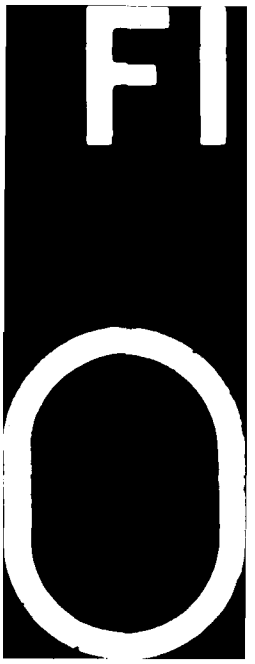
FI